

**Spatially-Periodic Turbulent Forced Convection  
in Interrupted-Plate Rectangular Ducts**

by

**Lorena Camargo**

**Department of Mechanical Engineering**

**McGill University  
Montréal, Québec, Canada**

**August, 2006**

**A thesis submitted to McGill University  
in partial fulfilment of the requirements for the degree of  
Master of Engineering**

**© Lorena Camargo, Montréal, Canada, 2006**



Library and  
Archives Canada

Bibliothèque et  
Archives Canada

Published Heritage  
Branch

Direction du  
Patrimoine de l'édition

395 Wellington Street  
Ottawa ON K1A 0N4  
Canada

395, rue Wellington  
Ottawa ON K1A 0N4  
Canada

*Your file* *Votre référence*  
*ISBN: 978-0-494-28590-9*  
*Our file* *Notre référence*  
*ISBN: 978-0-494-28590-9*

#### NOTICE:

The author has granted a non-exclusive license allowing Library and Archives Canada to reproduce, publish, archive, preserve, conserve, communicate to the public by telecommunication or on the Internet, loan, distribute and sell theses worldwide, for commercial or non-commercial purposes, in microform, paper, electronic and/or any other formats.

The author retains copyright ownership and moral rights in this thesis. Neither the thesis nor substantial extracts from it may be printed or otherwise reproduced without the author's permission.

#### AVIS:

L'auteur a accordé une licence non exclusive permettant à la Bibliothèque et Archives Canada de reproduire, publier, archiver, sauvegarder, conserver, transmettre au public par télécommunication ou par l'Internet, prêter, distribuer et vendre des thèses partout dans le monde, à des fins commerciales ou autres, sur support microforme, papier, électronique et/ou autres formats.

L'auteur conserve la propriété du droit d'auteur et des droits moraux qui protègent cette thèse. Ni la thèse ni des extraits substantiels de celle-ci ne doivent être imprimés ou autrement reproduits sans son autorisation.

---

In compliance with the Canadian Privacy Act some supporting forms may have been removed from this thesis.

Conformément à la loi canadienne sur la protection de la vie privée, quelques formulaires secondaires ont été enlevés de cette thèse.

While these forms may be included in the document page count, their removal does not represent any loss of content from the thesis.

Bien que ces formulaires aient inclus dans la pagination, il n'y aura aucun contenu manquant.

  
**Canada**

## **Abstract**

An experimental study of turbulent forced convection from the plates in the spatially-periodic fully-developed region of air flows in a straight rectangular duct fitted with interrupted-plate inserts is presented. These flows have features akin to those produced in the cores of offset-fin compact heat exchangers. A technique based on the lumped parameter analysis was proposed to determine average heat transfer coefficients on the surfaces of specially designed and instrumented test plates installed in the spatially-periodic fully-developed flow region. This technique was validated using complementary numerical simulations of unsteady three-dimensional heat conduction inside the plates. The results were obtained for Reynolds number (based on the average velocity in the minimum cross-sectional area and a hydraulic diameter) in the range 2,000 to 30,000. The main goal of this experimental research was to obtain reliable heat transfer results that could be used to check and refine corresponding mathematical models and numerical solution methods.

## Résumé

Une étude expérimentale de l'écoulement turbulent d'air spatialement périodique complètement développé à l'intérieur d'une conduite rectangulaire interrompue de plaques est présentée. Ces écoulements possèdent des caractéristiques similaires à celles produites dans un échangeur compact. Une technique basée sur l'analyse des paramètres localisés a été proposée afin de déterminer les coefficients de transfert de chaleur locaux à la surface des plaques, spécialement conçues et instrumentées, installées dans le régime d'air ci-haut mentionné. Cette technique a été validée grâce à des simulations numériques de conduction thermique tridimensionnelle dans les plaques. Des résultats ont été obtenus pour des nombres de Reynolds (basés sur le diamètre hydraulique et la vitesse moyenne dans l'air de section minimale) entre 2 000 et 30 000. L'objectif principal de ce travail était d'obtenir des résultats expérimentaux de transfert de chaleur essentiels à la vérification et au raffinement des modèles mathématiques et des méthodes numériques pour prédire ces écoulements.

## **Acknowledgements**

First and foremost I would like to thank my supervisor, Prof. B.R. Baliga, for his enthusiastic supervision. His passion for teaching and thirst for knowledge has made my past two years a great learning experience.

For their financial support, I would like to thank the Natural Science and Engineering Research Council (NSERC) of Canada for the two-year Postgraduate Scholarship and the Department of Mechanical Engineering at McGill for the top-up funding and Teaching Assistantships.

I would like to express my special thanks to Tony Micozzi, Nick Depalma, Roy Westgate, and Sam Mentor from the Machine Tool Laboratory for their exceptional help in building the experimental apparatus.

Thanks are due to Ms. Joyce Nault, Ms. Della Maharajh, Professor Meyer Nahon, and the staff of the GPSO thesis office for their help with all the paper work and constant encouragement.

Thanks also to my colleagues from the Heat Transfer group, Nima Atabaki, David Scott, Nimalakanth Jesuthasan, Alexandre Lamoureux, and Eric Duplain, for their help and friendship. I would particularly like to acknowledge the help provided by Nima Aatabaki with the data acquisition procedures and programs.

I owe my warmest thanks to my mom, Teresita, my sisters, Alexandra and Ximena: thank you very much for your encouragement and love. I could never have done this without your support. Finally, my dearest thanks to Dominic my life companion. Thank you for filling my everyday life with happiness.

# Table of Contents

Abstract.....	ii
Résumé.....	iii
Acknowledgements.....	iv
List of Figures.....	ix
List of Tables.....	xi
Nomenclature.....	xii
<b>1 Introduction.....</b>	<b>1</b>
<b>1.1 Overall Goal, Motivation, and Background.....</b>	<b>1</b>
<b>1.2 Specific Objectives.....</b>	<b>5</b>
<b>1.3 Overview of Experimental Runs and Results.....</b>	<b>6</b>
<b>1.4 Literature Review.....</b>	<b>7</b>
1.4.1 Books and Review Articles.....	8
1.4.2 Experiments and Correlations Pertaining to Full-Scale Models.....	9
1.4.2.1 <i>Classic Works (1964 – 1986)</i> .....	9
1.4.2.2 <i>Recent Investigations (1987 - present)</i> .....	10
1.4.3 Fluid Flow and Heat Transfer in Model Interrupted-Surface Ducts.....	13
1.4.3.1 Early Investigations (1977 - 1987).....	13
1.4.3.2 Recent Works (1988 – present).....	18
<b>1.5 Thesis Overview.....</b>	<b>21</b>
<b>2 Theoretical Considerations.....</b>	<b>22</b>
<b>2.1 Assumptions.....</b>	<b>22</b>
<b>2.2 Governing Equations.....</b>	<b>23</b>
<b>2.3 Turbulent Flows and the Need for Experimental Investigations.....</b>	<b>25</b>
2.3.1 Turbulence Models.....	25
2.3.2 Concluding Remarks.....	26

<b>2.4 Time-Mean Velocity, Static Pressure, and Temperature Variations</b>	
<b>in Spatially Periodic Fully Developed Flows.....</b>	<b>27</b>
2.4.1 Velocity and Static Pressure Variations.....	27
2.4.2 Temperature Variations.....	28
<b>2.5 Dimensional Analysis.....</b>	<b>29</b>
<b>3 Numerical Method.....</b>	<b>32</b>
<b>3.1 Problem Definition, Assumptions, and Assessment Strategy.....</b>	<b>32</b>
<b>3.2 Formulation of the Numerical Method.....</b>	<b>34</b>
3.2.1 Governing Equations.....	35
3.2.2 Domain Discretization.....	36
3.2.3 Interpolation Functions.....	37
3.2.4 Discretized Equations.....	39
3.2.5 Solution of the Discretized Equations.....	40
<b>3.3 Results of the Numerical Investigation and Discussion.....</b>	<b>40</b>
3.3.1 Computer Program Validation.....	40
3.3.2 Numerical Assessment of the Lumped Parameter Technique.....	50
<b>4 Experimental Apparatus and Techniques.....</b>	<b>53</b>
<b>4.1 Overview of the Experimental Apparatus.....</b>	<b>53</b>
<b>4.2 Air Inlet Section.....</b>	<b>54</b>
<b>4.3 Test Sections.....</b>	<b>55</b>
4.3.1 Geometric Configuration.....	55
4.3.2 Details Aluminium Test Section.....	57
4.3.3 Details of the Acrylic Test Section.....	57
4.3.4 Details of the Test Plates.....	60
4.3.5 Installation of the Test Plates into the Acrylic Test Section.....	62
<b>4.4 Flow Transition Section.....</b>	<b>64</b>
<b>4.5 Flow Measurement Section.....</b>	<b>65</b>
<b>4.6 Flow Generation and Control Section.....</b>	<b>65</b>
<b>4.7 Pressure Measurements.....</b>	<b>66</b>

4.8	<b>Air Flow Rate Measurements</b> .....	66
4.9	<b>Temperature Measurements</b> .....	68
4.10	<b>Data Acquisition System and Procedures</b> .....	69
4.11	<b>Summary of the Overall Experimental Procedure</b> .....	70
5	<b>Results and Discussions</b> .....	72
5.1	<b>Determination of the Average Heat Transfer Coefficient</b> .....	72
5.2	<b>Uncertainties in the Experimental Results</b> .....	73
5.3	<b>Characteristics of the Results</b> .....	74
5.3.1	Spatially-Periodic Fully-Developed Flow Regime.....	74
5.3.2	Lumped Parameter Assumption.....	75
5.3.3	Two-Dimensionality Over the Central Region.....	75
5.4	<b>Assessment of Radiation and End Losses</b> .....	77
5.4.1	Radiation Effects.....	77
5.4.2	End Losses.....	79
5.5	<b>Repeatability of the Results</b> .....	79
5.6	<b>Average Heat Transfer Coefficient</b> .....	80
5.7	<b>Correlation for Average Nusselt Number</b> .....	82
6	<b>Conclusion</b> .....	84
6.1	<b>Review and Contributions of the Thesis</b> .....	84
6.2	<b>Recommendations for Improvements and Extensions of this Work</b> .....	86
	References.....	88
	Appendix A – Correlation for the Time-Mean Average Velocity.....	99
	Appendix B – Thermocouple Calibration.....	102
	Appendix C – Radiation Effects.....	106
	Appendix D – Repeatability Checks.....	107
	Appendix E – Average Heat Transfer Coefficients: Inputs	

and Results.....	108
Appendix F – Average Nusselt Number: Inputs and Results.....	110

## List of Figures

1.1	Schematic of a portion of an offset-fin core of a compact heat exchanger.....	2
1.2	An offset strip-fin used in the core of a compact heat exchanger.....	2
1.3	Schematic of a straight duct of rectangular cross-section with spatially-periodic interrupted-plate inserts.....	4
3.1	Problem schematic, calculation domain, and coordinate system.....	32
3.2	Type-B domain discretization of the x-y cross-section of the test plate and the associate notation.....	36
3.3	Schematic of the control volume surrounding a node P and associated notation in the x-y plane of the calculation domain.....	38
3.4	Test problem schematic, calculation domain, and coordinate system.....	41
3.5	Temperature at the center for a grid of 30, 12, and 30 control volumes in x, y, and z directions, respectively, and $NSTEP$ of 500.....	49
3.6	Temperature results for unsteady, three-dimensional heat conduction in a brass bar of rectangular cross-section: grid of $60 \times 12 \times 24$ control volumes; $NSTEP = 600$ ; $q = 220 \text{ W/m}^2\text{-}^\circ\text{C}$ ; and $T_{\text{initial}} = 62^\circ\text{C}$ .....	52
3.7	Average heat transfer coefficient calculated for unsteady, three-dimensional heat conduction in a brass bar of rectangular cross-section: grid of $60 \times 12 \times 24$ control volumes; $NSTEP = 600$ ; $q = 220 \text{ W/m}^2\text{-}^\circ\text{C}$ ; and $T_{\text{initial}} = 62^\circ\text{C}$ .....	52
4.1	Schematic illustration of the experimental apparatus.....	53
4.2	Photograph of the air inlet section, the aluminium test section, and the acrylic test section of the experimental apparatus used in this work.....	54
4.3	Schematic illustration of a portion of the test section and related notation....	55
4.4	Outer casing of the acrylic test section.....	58
4.5	Acrylic side walls and jigs.....	58
4.6	Schematic of the aluminium fixtures.....	59
4.7	Photograph of the aluminium fixtures and plates.....	59
4.8	Holes in the top plate of the acrylic test section, designed to allow insertion of a jig that holds and positions the single hot-wire probe or other jigs that seal the holes; the shaded areas are top views of the interrupted-plate inserts.....	59
4.9	A photograph of the various components of a test plate with a central section made of aluminium.....	60
4.10	Technical drawing showing details and dimensions (in inches)of the central metal section and an ertalyte end section of a test plate.....	61
4.11	A test plate with a brass central section – view of components just before final assembly.....	62
4.12	Photograph of the test plates installed inside the acrylic test section.....	64
4.13	Photograph of the acrylic test section with the installed test plates mounted in the overall experimental rig.....	64

## List of Figures (continued)

5.1	Experimental data for $Re = 30\,000$ obtained using a test plate with the central section made of brass.....	75
5.2	Photograph of the test plates installed inside the acrylic test section.....	76
5.3	Average heat transfer coefficients obtained using each of the six test plates, individually, with two different temperature ranges.....	78
5.4	Percentage maximum differences between the temperature of the outer surface of the acrylic test section, above the test plates, and the ambient air temperature – sample results.....	78
5.5	Sample results of repeatability tests.....	80
5.6	Average heat transfer coefficients obtained with six different test plates, for nine different values of Reynolds number.....	81
5.7	Variation of average heat transfer coefficient with Reynolds numbers – results obtained using measurements from the first copper test plate.....	81
5.8	Comparison of the average Nusselt number values obtained from the proposed correlation, Eq. 5.4, and the corresponding experimental results....	83
A.1	Plot of $\overline{W}$ , obtained using the ten-point log-linear method versus $W_{point5}$ ...	100
B.1	Plot of the temperature reading provided by the quartz probe versus the temperature reading provided by thermocouple # 1.....	104

## List of Tables

1.1	Cross-sectional and modular dimensions of the test section.....	7
2.1	Definitions of $D_h$ and $W$ for offset-strip fin and interrupted plate ducts.....	30
3.1	First five roots, $\gamma_l$ , $l = 1 - 5$ , of the equation 3.42.....	46
3.2	Maximum absolute percentage error between the numerical solution and the corresponding analytical solution at three different positions.....	50
3.3	Results for a grid of 60x12x24 control volumes and $NSTEP = 600$ .....	52
4.1	Cross-sectional and modular dimensions of the test sections.....	56
5.1	Average heat transfer coefficient obtained individually for two successive test plates, each with a brass central section.....	74
5.2	Sample values of the average heat transfer coefficients obtained using the first and the second copper test plates.....	77
5.3	Estimates of the maximum emissivities of the central metal sections of the test plates.....	77
5.4	Comparison of the average Nusselt number values obtained from the proposed correlation, Eq. (5.4), and the corresponding experimental results.....	82
A.1	Comparison of the $\overline{W}_{10\text{-pointlog-linear}}$ and $\overline{W}_{correl}$ .....	101
B.1	Coefficients in the fifth-order polynomial calibration correlations for thermocouples 1 - 23.....	105
C.1	Average heat transfer coefficients obtained using two different temperature ranges.....	106
D.1	Repeatability checks conducted at $Re_{nominal} = 2\ 000$ ; $8\ 000$ ; and $30\ 000$ .....	107
E.1	Geometry of the test section.....	108
E.2	Effective values of (Mass * Specific Heat).....	108
E.3	Average heat transfer coefficients and Reynolds numbers.....	109
F.1	Average Nusselt number for test plates 2, 4, and 5.....	110
F.2	Average Nusselt number for test plates 1 - 6.....	111

## Nomenclature

$A_{c-s}$	Cross-sectional area of the flow
$A_{c-s-min}$	Minimum cross-sectional area for the flow
$A_{wetted}$	Total wetted solid surface area in a representative geometric module
$A_{wetted, no\ edges}$	$A_{wetted}$ minus the edge surface areas
$b$	Duct width
$b^*$	Aspect ratio or dimensionless width
$Bi$	Biot number (definition given in text)
$c_p$	Specific heat at constant pressure
$D$	Diameter of a pipe
$D_h$	Hydraulic diameter
$D_L$	Laminar equivalent diameter (Jones)
$e$	Internal energy per unit mass
$g$	Magnitude of the acceleration of gravity
$h$	Total height of a rectangular cross section duct (2H)
$h_{av}$	Average heat transfer coefficient
$H$	Duct half-height
$\bar{i}$	Unit vector in $x$ -direction
$\bar{j}$	Unit vector in $y$ -direction
$k$	Thermal conductivity
$\bar{k}$	Unit vector in $z$ -direction
$l$	Mixing length
$L$	Plate length
$L^*$	Dimensionless plate length
$L_{ch}$	Characteristic length
$L_{TS}$	Length of the test section
$\dot{m}$	Mass flow rate
$NSTEP$	Number of time steps within each characteristic time, $t_{ch}$
$Nu_{av}$	Average Nusselt number (definition given in text)
$p$	Instantaneous reduced static pressure
$P$	Time-averaged reduced static pressure
$\tilde{p}$	Local spatially periodic pressure function
$P_{atm}$	Time-averaged atmospheric pressure
$P_{dyn}$	Time-averaged dynamic pressure
$Peri_{wetted}$	Wetted perimeter of the cross-sectional area of the flow
$Pr$	Prandtl number
$P_{ref}$	Time-averaged reference pressure
$P_{stag}$	Time-averaged stagnation pressure
$P_{stat}$	Time-averaged static pressure in the flow measurement section
$p_{static}$	Instantaneous static pressure
$q''$	Heat flux
$Q$	Quantity of heat

## Nomenclature

$R$	Inner radius of a pipe
$Re$	Reynolds number (definition given in text)
$Re_D$	Reynolds number based on $D$
$s$	Spacing between plates
$s^*$	Dimensionless spacing between plates
$S$	Source term
$t$	Plate half-thickness
$t$	Time
$t_{ch}$	Characteristic time: $t_{ch} = (\rho c_p Volume) / (hA_{surf})$
$t^*$	Dimensionless plate thickness
$T$	Temperature
$u$	Instantaneous velocity component in $x$ -direction
$U$	Time-averaged velocity component in $x$ -direction
$v$	Instantaneous velocity component in $y$ -direction
$\bar{v}$	Velocity vector
$V$	Time-averaged velocity component in $y$ -direction
$w$	Instantaneous velocity component in $z$ -direction
$W$	Time-averaged velocity component in $z$ -direction
$\bar{W}$	Cross-section-average time-mean velocity
$z_{ref}$	Position of the reference tap
$ZP$	Time-averaged zero pressure reading
$\alpha$	Thermal diffusivity
$\beta$	Time-mean reduced static pressure drop per unit length
$\gamma$	Temperature gradient
$\varepsilon$	Surface roughness
$e$	Emissivity
$\varepsilon_{Rel}$	Dimensionless surface roughness
$\lambda$	Aspect ratio of duct cross-section
$\Lambda$	Spatial period
$\mu$	Dynamic viscosity
$\mu_t$	Turbulent viscosity
$\nu$	Kinematic viscosity
$\rho$	Density
$\sigma$	Stefan-Boltzmann constant
$\tau_t$	Turbulent stress
$\tau_w$	Average wall shear stress over the wetted perimeter

## Chapter 1. Introduction

### 1.1 OVERALL GOAL, MOTIVATION, AND BACKGROUND

An experimental study of turbulent forced convection from individual plates in the spatially-periodic fully-developed region of air flows in a straight rectangular duct with interrupted-plate inserts is presented in this thesis. These flows have features akin to those produced in the cores of plate-fin compact heat exchangers. The overall goal of this research was to obtain experimental data that can serve as checks on mathematical models and numerical solution methods for the simulation of fluid flow and heat transfer in the cores of compact heat exchangers. The main motivation for this research is a desire to contribute to ongoing worldwide efforts to improve the performance of heat transfer equipment.

Compact heat exchangers are characterized by cores that have a heat-transfer-area-to-volume ratio that exceeds  $700 \text{ m}^2/\text{m}^3$  [Kays and London (1964, 1984)]. In modern compact heat exchangers, this ratio could be as high as  $3000 \text{ m}^2/\text{m}^3$  [Shah et al. (2001)]. In contrast, in conventional shell-and-tube heat exchangers, this ratio usually lies between 100 to  $200 \text{ m}^2/\text{m}^3$ . Compact heat exchangers are commonly used as automobile radiators, condensers and evaporators in HVAC (heating, ventilating, and air-conditioning) systems, coolers for electronic devices, compressor intercoolers, cryogenic heat exchangers, aircraft engine oil coolers, and heat recuperators for industrial gas turbine engines [Kays and London (1964, 1984); McDonald (1972, 2000); Timmerhaus and Flynn (1989); Manglik and Bergles (1995); Shah et al. (2001); Kakaç and Liu (2002); Reay (2002)]. Newer application areas for these heat exchangers include solar and geothermal energy conversion systems [Hachemi (1999)].

The flow passages in the cores of compact heat exchangers are usually classified as follows [Kays and London (1964, 1984)]: circular and flattened circular tubes with smooth surfaces; finned tubes; and plate-fin ducts. In the plate-fin design, the fluid flow channels consist of fins sandwiched between parallel plates; these fins serve to enhance the overall rate of heat transfer, act as spacers, and supply structural support [Kays and London (1964, 1984); Hesselgreaves (2001)]. These plate-fin channels are closely packed and allow hot and cold fluids to flow in alternate layers. The fins in such plate-

fin channels may have different shapes, such as continuous, rectangular offset, zigzag, chevron, perforated, and louvered fins [Kays (1972); Kays and London (1964, 1984); Shah et al. (2001); Kakaç and Liu (2002)]. In this study, the focus is on plate-fin channels in compact heat exchangers cores with offset-fin configurations.

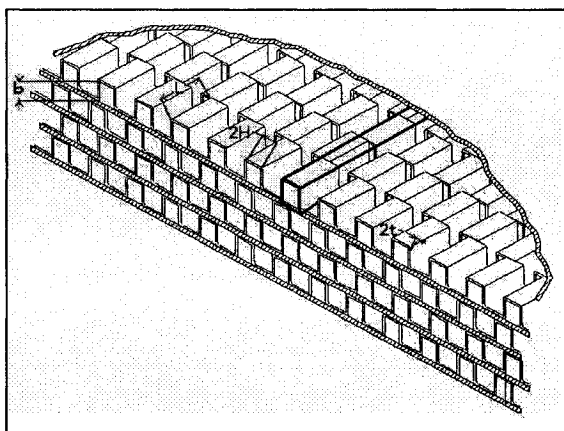


Figure 1.1: Schematic of a portion of an offset-fin core of a compact heat exchanger.

A schematic representation of a portion of an offset-fin core of a compact heat exchanger is shown Figure 1.1. Such cores are often constructed using stacks of parallel plates with an “offset strip-fin”, made from a single metal strip, sandwiched between each pair of such plates. A photograph of an offset-strip fin is shown in Figure 1.2.

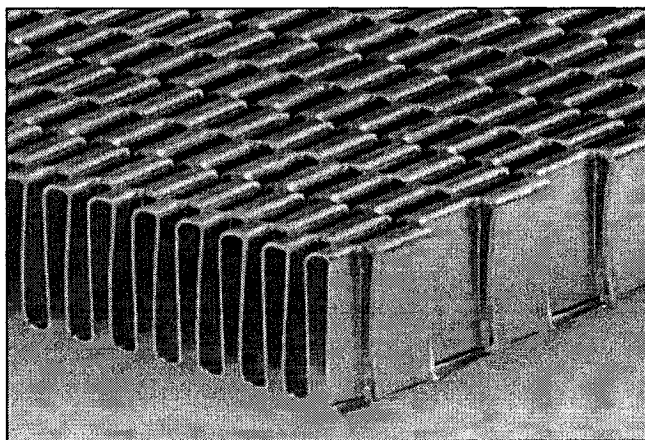


Figure 1.2: An offset strip-fin used in the core of a compact heat exchanger (Hughes-Treitler Manufacturing Corporation).

Offset-fin and other interrupted-surface cores of compact heat exchangers achieve high rates of heat transfer via the following mechanisms [London and Shah (1968); Sparrow et al. (1977); Cur and Sparrow (1978, 1979); Mullisen and Loehrke (1986); Mochizuki et al. (1987); Suzuki et al. (1994); Manglik and Bergles (1995); Zhang et al. (1997); DeJong et al. (1998); and Shah et al. (2001)]: increase in area for heat transfer; interruptions and restarts of the thermal boundary layers on the fin surfaces; and, for certain combinations of geometric parameters and Reynolds number, self-sustained flow oscillations and vortex shedding. However, for the same overall mass flow rate, these mechanisms also lead to increases in the corresponding pressure drop. Thus, the design of such interrupted-surface flow passages poses an optimization problem, in which the objective is to maximize the rate of heat transfer for a fixed pumping power, over the entire range of operating conditions.

When Newtonian fluid flow and heat transfer phenomena are involved in the laminar regime, their mathematical models are well established, and numerical simulations are an excellent tool for the solution of the aforementioned optimization problem. However, when low-Reynolds-number transitional and/or turbulent flow and heat transfer are involved, mathematical models that lend themselves to affordable numerical simulations and yet provide accurate enough solutions (in the design context) are far from well-established. In such cases, the above-mentioned optimization problem is best solved by a combination of experiments on laboratory models (that provide data that can be used check and refine the corresponding mathematical models) and numerical simulations. Such a complementary experimental-numerical research effort has been going on in the Heat Transfer Laboratory of the Department of Mechanical Engineering at McGill University for over 20 years. The experimental work reported in this thesis is a part of this ongoing research effort.

Over the last 100 years, there have been numerous experimental and numerical studies of actual heat exchangers, scaled (up or down) models of heat exchangers, and laboratory models of the flow and heat transfer in the cores of heat exchangers (a literature review is given in Section 1.4). To facilitate accurate measurements of thermofluid phenomena akin to those in the cores of offset-fin compact heat exchangers, experiments have often been conducted on model flow passages that

consist of a succession of regularly spaced (or spatially periodic) plates aligned parallel to the flow in a straight rectangular duct. Such a flow passage is shown schematically in Figure 1.3. Although relatively simple, this model duct has geometric features and generates fluid flow and heat transfer characteristics similar to those encountered in offset-fin compact heat exchanger cores, such as the following: increase in surface area, vis-à-vis plain rectangular ducts; interruptions and restarts of the velocity and thermal boundary layers; flow recirculation zones associated with the leading and trailing edges of the interrupted-plate inserts; and vortex shedding for certain combinations of the geometric parameters and Reynolds number. For these reasons, such model ducts have been used in the works of Cur and Sparrow (1978, 1979), McBrien and Baliga (1988), Sekulic (1989), Amon et al. (1992), Grosse-Gorgemann et al. (1995), Candanedo et al. (2003), and Lamoureux et al. (2005). The model duct used in the experimental work reported in this thesis is also similar to that shown schematically in Figure 1.3.

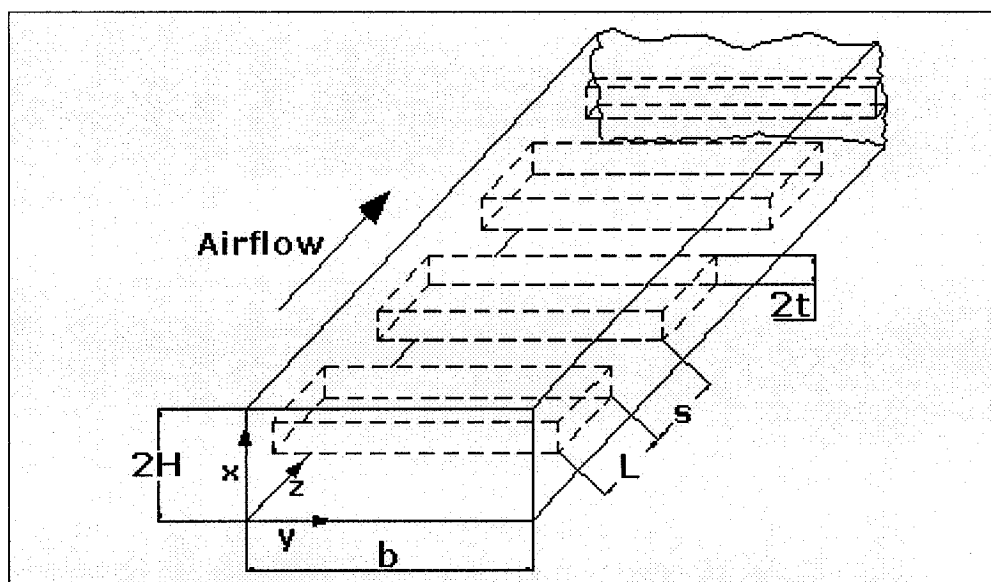


Figure 1.3: Schematic of a straight duct of rectangular cross-section with spatially-periodic interrupted-plate inserts.

The overall goal of the present study is to experimentally investigate turbulent forced convection heat transfer in the spatially-periodic fully-developed regime of air flows in an interrupted-plate rectangular duct. Again, the duct of interest is similar to that shown

schematically in Figure 1.3. In the spatially-periodic fully-developed regime in such ducts, the time-mean turbulent flow and the pressure *drop* repeat identically in successive geometrical modules [Sparrow et al. (1977); Patankar et al. (1977)]. Turbulent flows in such interrupted-plate rectangular ducts attain this spatially-periodic fully-developed behavior after a relatively short entrance region. For the range of parameters investigated in this work, this entrance region is expected to prevail over only the first two to ten geometric modules downstream of the duct inlet section [Cur and Sparrow (1978, 1979); McBrien and Baliga (1988); Candanedo (2003)].

Attention in this work is focused on measurements of time-mean and spatially-averaged heat transfer coefficients for individual plates in the spatially-periodic fully-developed regime of air flows in a rectangular interrupted-plate duct (see Figure 1.3). The geometric and fluid flow parameters investigated in this research work are relevant to heat recuperators used in industrial gas turbine engines [McDonald (2000, 2003)]. Again, the present experimental work is aimed at obtaining reliable heat transfer data that are suitable for checking and refining the mathematical models and numerical solution methods used in simulations of forced convection in the cores of offset-fin compact heat exchangers.

## 1.2 SPECIFIC OBJECTIVES

The specific objectives of this thesis are as follows:

- To redesign and modify an existing experimental set-up of a straight rectangular interrupted-plate duct, similar to that shown in Figure 1.3, with the following purposes:
  - Allow investigation of geometric and fluid flow parameters relevant to offset-fin cores of heat recuperators used in industrial gas turbine engines;
  - Allow single hot-wire measurements, in the spatially-periodic fully-developed regime, and to obtain turbulence power spectrums and vortex shedding frequencies [Lamoureux et al. (2005)];
  - Allow the study of forced convection heat transfer from individual plates in the spatially-periodic fully-developed regime

- To design and construct suitably instrumented heated plates
- To develop, numerically assess the applicability, and implement an unsteady experimental technique, based on the lumped parameter analysis, to obtain spatially-averaged time-mean heat transfer coefficients on the central region of the outer surface of each heated plate.
- To use the proposed unsteady experimental technique to obtain the aforementioned average heat transfer coefficients for individual plates in the spatially-periodic fully-developed regime, for values of the Reynolds number, based on time-mean average axial velocity in the minimum cross-sectional area and a hydraulic diameter [Kay and London (1964, 1984)], in the range 2000 – 30000.

### **1.3 OVERVIEW OF THE EXPERIMENTAL RUNS AND RESULTS**

The experimental facilities, instrumentation, and procedures for measuring overall flow rates, and also distributions of wall static pressure, in the ducts of interest have been carefully benchmarked and reported by Candanedo et al. (2003). They were also used in this work. Each of the heated plates was designed and constructed to have a central metal section and two plastic (ertalyte) sections, one on each end of the central metal section. These plastic (ertalyte) sections served to reduce end heat losses from the central metal section to negligible levels compared to the rate of heat loss to the air flowing over this section. The central metal section was constructed of two (top and bottom) parts held together by miniature machine screws. Suitable tiny groove were milled into the bottom part of the metal section and tiny holes were drilled in the ertalyte end sections to allow the insertion of thermocouples and electrical heating wires. Details of the overall experimental setup, the instrumentation, the heated plates, and the techniques that were used to measure temperatures are several locations inside the heated plates as well as the airflow rates are presented and discussed in Chapter 4 of this thesis.

The heat transfer measurements were conducted in a portion of the overall test section that was 609.6 mm (24 inches, nominal) long, with outer walls made of acrylic, as this section was also designed for surface flow visualization studies (McBrien and

Baliga (1988); Candanedo (2003)]. This portion of the test section accommodated 12 plate inserts, six of which were designed for the heat transfer measurements. It was located downstream of an aluminum part of the overall test section that was 1524 mm (60 inches, nominal) long and accommodated 30 plates, providing at least 29 geometrically identical modules in front of the portion in which the heat transfer measurements were made. The inner cross-section of the entire rectangular test section was 25.4 mm (1 inch, nominal) high and 152.4 mm (6 inches, nominal) wide. The dimensional and dimensionless geometrical details of each module of the test section are given in Table 1.1, in terms of the notations provided in Fig 1.3.

Table 1.1: Cross-sectional and modular dimensions of the test section. Uncertainties in  $b$ ,  $2H$ ,  $L$ ,  $2t$ , and  $s$  are all less than + 0.03 mm.

<b>b</b> (mm)	<b>2H</b> (mm)	<b>L</b> (mm)	<b>2t</b> (mm)	<b>s</b> (mm)
152.67	25.18	25.21	6.36	25.59

<b>D<sub>h</sub></b> (mm)	$\lambda =$ <b>b/2H</b>	$L^* =$ <b>L/2H</b>	$t^* =$ <b>2t/2H</b>	$s^* =$ <b>s/2H</b>
21.32	6.063	1.001	0.253	1.016

The values of the Reynolds number, based on the time-mean average streamwise velocity in the minimum cross-sectional area of the duct and a hydraulic diameter [Kays and London (1964, 1984)], ranged from about 2,000 to 30,000. The results obtained included Nusselt number versus Reynolds number data for individual plates in the spatially-periodic fully-developed region. These and other results of these experiments are presented, in graphical and tabular formats, and discussed in Chapter 5.

## 1.4 LITERATURE REVIEW

There has been an extensive amount of prior research on fluid flow and heat transfer in ducts and compact heat exchangers. Detail reviews and surveys of the published literature resulting from this research are already available. Therefore, a comprehensive review of publications on these topics is not intended in this section. Rather, this review

is limited to investigations which have direct relation to the research presented in this thesis. This section is organized as follows: (a) books and review articles related to fluid flow and heat transfer in ducts and heat exchangers; (b) fully-developed flows and forced convection heat transfer in straight ducts of rectangular and other non-circular cross-sections; (c) experiments and correlations pertaining to full-scale models of offset-fin compact heat exchangers; and (d) fluid flow and heat transfer in model interrupted-surface ducts.

### 1.4.1 Books and Review Articles

Basic and more advanced aspects of fluid flow and heat transfer in ducts can be found in excellent textbooks by Schlichting (1955, 1968, 1979), Kays and Crawford (1993), and White (1974, 1991). Others excellent textbooks on these subjects include the works of Rouse (1946, 1978), Streeter (1951, 1962), Landau and Lifshitz (1959, 1987), Bird et al. (1960, 2002), Batchelor (1967), Eckert and Drake (1971), Currie (1974, 2003), Incropera and DeWitt (1981, 2002), Bejan (1984, 1995), Fox and McDonald (1985, 1998), Churchill (1988), Panton (1996), Wilkes (1999), and Cebeci (2002). A comprehensive survey of studies on laminar flow and heat transfer in ducts has been presented by Shah and London (1978). In the *Handbook of Heat Transfer Fundamentals* (1985), Kays and Perkins have thoroughly covered the topics of laminar and turbulent forced convection in ducts.

The textbooks by Patankar (1980) and Anderson et al. (1984) are among the most referenced books on numerical methods for the solution of fluid flow and heat transfer problems. Books by Roache (1976, 1998), Reddy and Gartling (1994), and Ferziger and Peric (1996, 1999), among others, also treat the fundamentals of computational methods for the prediction of fluid flow and heat transfer in ducts. Detailed discussions of the modelling of turbulent flow and heat transfer in ducts are available in the works of Tennekes and Lumley (1972), Hinze (1975), Wilcox (1993), Pope (2000), and Launder and Sandham (2002). Useful coverage of various aspects of computational fluid dynamics and heat transfer can be found in the *Advances in Numerical Heat Transfer* series (Vols. 1 and 2), edited by Minkowycz and Sparrow (1997, 2000), and also in the

*Handbook of Numerical Heat Transfer* (Second Edition), edited by Minkowycz, Sparrow, and Murthy (2006).

Most of the empirical correlations for fluid flow and heat transfer in offset strip-fin heat exchangers are based on the experimental results presented in Kays and London (1964, 1984). A more recent compilation by Hesselgreaves (2001) provides in-depth coverage of the basic theoretical background for fluid flow and heat transfer in compact heat exchangers, empirical correlations, design considerations, extensive physical property data, and descriptions of several compact heat exchangers used in industrial applications. Shah et al. (2001) have presented a comprehensive review of numerical simulations of forced convection from many finned surfaces. Theoretical considerations and practical design information related to shell-and-tube heat exchangers are discussed at length in books by Saunders (1988), Frass (1989), Kakac and Liu (2002), and Mukherjee (2004).

## **1.4.2 Experiments and Correlations Pertaining to Full-Scale Models**

### **1.4.2.1 Classic Works (1964 – 1986)**

Kays and London (1964, 1984) measured heat transfer and pressure drop data for a wide variety of circular and rectangular flow passages and plate-fin ducts, including tubes, tube banks, straight fins, louvered fins, strip or lanced offset fins, wavy fins, and pin fins, using cores of commercial heat exchangers. Though it contains data that are now over 40 years old, the book by Kays and London (1964, 1984) is perhaps the most comprehensive design sourcebook.

London and Shah (1968) tested eight offset rectangular plate strip-fin surfaces from full-scale heat exchangers and obtained heat transfer and flow friction characteristics. Their paper provides overall Fanning and Colburn factors as a function of Reynolds number, all based on a hydraulic diameter, in tabulated form and also corresponding fifth-degree polynomials. Their work was a part of an extensive (20-year) empirical study of heat exchangers conducted at Stanford University under the sponsorship of the US Navy. Most of the results of that study were later published in the book by Kays and London (1964, 1984).

Kays (1972) made one of the first attempts at predicting analytically the heat transfer and friction loss in offset strip fins. He proposed a modified laminar boundary layer solution over a flat plate [Schlichting (1955, 1968, 1979)]. However, his model suffered from an oversimplification of the flow-channel geometry. Thus, comparisons of the predictions obtained from his theory to experimental data show only fair agreement, at best.

Wieting (1975) used experimental data obtained by other investigators for 22 heat exchanger geometries and developed correlations for heat transfer and flow friction in the laminar and turbulent regimes, using the multiple regression method. Correlations for the Fanning factor and the Colburn factor, as functions of the Reynolds number and geometric variables, were developed and presented in the paper. Wieting also proposed a criterion, in the form of two correlations, to estimate the Reynolds number for the transition from laminar to turbulent flow. These correlations have no theoretical basis; therefore, they are applicable only for the specific geometries of the surfaces used to develop them and only for working fluids such as air, with values of Prandtl number less than one. Also, it is not clear whether all these data were referenced to one consistent definition of hydraulic diameter. Nevertheless, Wieting's correlations are simple and practical, and they have been extensively used for design purposes.

#### **1.4.2.2 Recent Investigations (1987 – present)**

Joshi and Webb (1987) performed an experimental and analytical study of heat transfer and pressure drop phenomena in the core of an offset strip-fin heat exchanger. One of the important contributions of this study is the development of analytical models that predicts the friction factor and the heat transfer coefficient. In the laminar regime, the model was based on the numerical data from Sparrow and Liu (1979), with corrections to incorporate the heat transfer from the ends of the fins, the form drag due to the finite fin thickness, and heat transfer and friction loss from the parting plates. In the turbulent regime, a semi-empirical method partially based on earlier experimental works, mainly those reported by Kays and London (1964, 1984), was used. Their models predicts the overall Fanning and Colburn factors to within  $\pm 20\%$  of data on scale-up cores [Webb and Joshi (1982)] and actual cores [Joyner (1943); London and

Shah (1968); Kays and London (1984)]. The authors suggested that burred edges and wall roughness are responsible for discrepancies between the predicted and measured values. It should be noted, however, that these models are quite cumbersome. So, these authors re-evaluated the empirical equations of Wieting (1975) and offered them as a more practical tool than their models.

In the experimental part of the work of Joshi and Webb (1987), aqueous ethylene glycol flows through an offset-strip channel having five rows of fifteen collinear fins aligned in the flow direction were studied. The plate thickness, length, and perpendicular separation distance between parallel plates were varied for a total of eight core configurations, and a set of plain fins without interruptions were also investigated. The Reynolds number, based on average velocity in the minimum cross-sectional area, and hydraulic diameter, ranged from 200 to 4000. The Fanning friction factor was determined using measurements of the pressure drops. Flow visualization experiments for three scaled-up geometries were also performed to investigate the flow structure. Using flow visualization, they were able to divide the flow into four different regimes. In the first regime, the flow was steady and laminar. In the second regime, oscillations in the transverse direction were visible near the upstream stagnation point of each fin. In the third regime, oscillations encompassed the entire gap between the upstream and downstream plates. In the fourth regime, vortices were shed. Their laminar flow correlations for Fanning and Colburn factors under-predict the data at the onset of the flow oscillations. Therefore, they designated the Reynolds number at this point as the critical  $Re$  for transition from laminar to turbulent flow. Based on their analytical and experimental work, they also developed correlations to predict this transition from laminar to turbulent flow.

Manglik and Bergles (1995) provided a thorough review of available fluid flow and heat transfer correlations for offset strip-fin surfaces. They pointed out some weaknesses in the correlations of Wieting (1975), Joshi and Webb (1987), Mochizuki and Yagi (1987), and Dubrovsky and Vasiliev (1988). One of shortcomings of these correlations is that they pertain to laminar or turbulent flow, and ignore the transition region, while evidence in the data for actual cores shows that it is important to account for the transition region too. The authors also state that most of the available

correlations are a reworking of the Wieting (1975) equations and that little attempt has been made to extend their validity. They also note that there appears to be no consensus in the literature over the definition of the hydraulic (or equivalent) diameter. Experimental data for 18 different cores given by Kays and London (1964, 1984), Walters (1969), and London and Shah (1968) were examined to develop equations that describe the asymptotic behaviour of the data in the laminar and fully turbulent regions. These equations are functionally related to the Reynolds number and three geometric parameters, involving the thickness, the length, the width, and the spacing of the plates. The asymptote-matching technique of Churchill was employed to combine these equations to form single predictive correlations for the Fanning and Colburn factors. These improved design correlations represent the data continuously in the laminar, transition, and turbulent flow regimes, obviating the need for determining the specific flow regime for any given operating condition.

Mochizuki et al. (1988) conducted an experimental study to determine the flow patterns and turbulence intensity in stacks of interrupted parallel-plate surfaces, using flow visualisation, pressure measurements, and hot-wire measurements. The authors observed that for a fixed pressure drop, the offset-strip surface yield higher flow rates and higher turbulence intensity than the in-line arrangement. They also noted that the flow patterns may change significantly between the core inlet and the exit, and the extent of each flow pattern within the core may vary with the Reynolds number. Thus, they suggest that if a model core is to be used to determine the flow patterns in an actual heat exchanger, then the model must have the same number of rows of fins in the flow direction as the actual unit.

Muzychka and Yovanovich (2001) performed a thorough review of correlations already available in the literature and notice that the correlations proposed by Wieting (1975), and also those put forward by Manglik and Bergles (1990, 1995), depart from the theoretical behaviour as the Reynolds numbers tends to zero and infinity. Consequently, the Fanning and Colburn factors are underpredicted outside the  $200 < Re < 10\,000$  range. The new models proposed by these authors overcome this limitation, just as the correlations of Joshi and Webb (1987), but they have the advantage of being simpler. The predictions obtained with these new models are within  $\pm 20\%$  for 96% of

the Fanning friction factor data and 82% of the Colburn j-factor data presented by Kays and London (1984). Finally, these authors have also discussed extensions of their new models for offset strip-fins having non-rectangular sub-channels.

### **1.4.3 Fluid Flow and Heat Transfer in Model Interrupted-Surface Ducts**

#### **1.4.3.1 Early Investigations (1977 – 1987)**

Sparrow, Baliga, and Patankar (1977) conducted one of the first numerical investigations of flow in offset-fin passages. They assumed infinitesimally thin plates, and steady, laminar, two-dimensional flows. Detailed velocity and temperature distributions, heat transfer coefficients, and pressure drop data were obtained for Reynolds number ranging from 200 to 1600 and several values of a dimensionless geometrical parameter characterizing the streamwise length of the interrupted plates. The Prandtl number was maintained constant at 0.7 in all computations. One of the important findings of this investigation was the observation that at sufficiently large downstream distances, typically after the fifth row of plates, the velocity and dimensionless temperature profiles are identical in successive modules, and the modular pressure drop and an average modular heat transfer coefficient take on constant values. They called this type of flow pattern periodically fully developed. The authors also found that for conditions of equal heat transfer surface area and equal pumping power, the heat transfer rates improved by approximately 80% in the interrupted-wall channel for a wide range of operating conditions. Later, Sparrow and Liu (1979) extended the numerical study of Sparrow, Baliga and Patankar (1977) to obtain heat transfer, pressure drop, and performance relations for two-dimensional flows through arrays of inline and staggered plate segments. They also included the entrance and exit effects.

Patankar, Liu and Sparrow (1977), conducted a numerical analysis of the heat transfer and fluid flow in channels whose walls are periodically interrupted along the streamwise direction. They proposed the first mathematical model and numerical solution procedure that are capable of accounting for flow recirculation regions in the spatially-periodic fully-developed regime. The governing equations were solved in the context of the assumptions that the fluid properties remain constant and the viscous

dissipation and compression work are negligible. The plates were assumed to be of negligible thickness, smooth edged, and isothermal. The spatially-periodic fully-developed regime was found to be a characteristic phenomenon of all long-enough flow passages having streamwise periodic variations in their cross sections. Under fully-developed conditions, the velocity components are periodic and the pressure can be reduced to a periodic function after subtraction of a term that varies linearly with main streamwise distance. For the temperature field, the periodicity conditions are of a different nature depending on the thermal boundary conditions. For constant wall temperature, profiles of similar shape recur periodically. On the other hand, for constant heat flux, the temperature field is periodic provided that a linear term related to the bulk temperature change is subtracted.

Cur and Sparrow (1978) performed an experimental study to determine heat transfer and pressure drop characteristics for a two-plate collinear array. Plate thickness and inter-plate spacing were varied parametrically. The Reynolds number, based on the nominal hydraulic diameter, ranged from 1000 to 14000. Measurements of the heat transfer coefficients, using the naphthalene sublimation technique, demonstrated that the Nusselt number increases substantially with plate thickness at higher values of Reynolds number, but decreases moderately at lower values of Reynolds number. Curves of Nusselt number versus inter-plate spacing attain a local maximum at a value other than the conventional spacing-to-length ratio of unity. The pressure drop increase caused by increasing plate thickness is greater than the Nusselt number increase obtained. On the other hand, the inter-plate gap was found to have little effect on the pressure drop in the range of parameters investigated.

Cur and Sparrow (1979) have also extended their previous study by analysing an array of eight collinear plates. They focused their efforts on the periodic fully-developed region, attained in the regime prior to the eighth plate, in contrast to their entrance-region study of 1978. Again using the naphthalene sublimation technique, they found the Nusselt number to increase with plate thickness, up to about 40% at higher Reynolds number and even higher increases at lower Reynolds number due to the laminar-turbulent transition. The presence of the interruptions increased the Nusselt number by about a factor of two compared to a continuous-walled duct. The pressure

drop was also found to increase with plate thickness, this increase being greater at higher flow rates.

Sparrow and Hajiloo (1980) studied heat transfer and pressure drop characteristics of an array of five columns of staggered interrupted plates. The naphthalene sublimation technique and the mass-heat transfer analogy were used to obtain heat transfer coefficients. The values of Reynolds number, based on the hydraulic diameter, ranged from 1000 to 9000. Their measurements again confirmed the existence of a spatially-periodic fully-developed regime: The per-plate Nusselt number was essentially the same for the second and all subsequent rows. The fully-developed heat transfer coefficient was found to increase with Reynolds number and with plate thickness, especially at the larger Reynolds numbers. However, more than 20% difference was found between their measured heat transfer coefficients and those obtained using the correlations of Wieting (1975). Differences in geometry, thermal boundary conditions, and calculation of averages were mentioned as possible reasons for these discrepancies. The friction factor was found to increase with plate thickness. For the thickest plates, the friction factor was essentially independent of the Reynolds number, indicating the dominance of inertial losses associated with separation and mixing. For thin plates, on the other hand, frictional losses were found to be the primary cause of the corresponding pressure losses. The agreement of the measured pressure drops with those obtained using the correlations of Wieting (1975) is remarkably good. However, the measured friction factors tends to achieve an essentially constant value at higher Reynolds numbers, as is to be expected, while those predicted by Wieting's correlation show a slope in the same range.

Patankar and Prakash (1981) analysed the effect of plate thickness on the laminar flow field and heat transfer in an interrupted staggered-plate passage, using numerical solutions of the governing equations. They assumed stable laminar wakes, which is contrary to the results of flow visualization studies. The constant-heat-flux boundary condition was studied in addition to another thermal boundary condition in which each row of fins was kept at a fixed temperature. Their calculations showed that the finite-thickness plates give rise to a complex flow pattern involving impingement and recirculation zones and flow deflection. It was observed that only when the plate is

sufficiently thick, the recirculation zones extend to the next plate. Patankar and Prakash (1981) compared their computed results with the experimental data of Kays and London (1964) and paid special attention to the definition of hydraulic diameter. For  $t/H = 0.05$  and a nondimensional plate length ( $L/H$ ) of 1.14, the friction factor was in good agreement. However, there were significant discrepancies between the numerical predictions and experimental values of the Colburn factors, and, unfortunately, these discrepancies were not explained. From their investigations, it was concluded that compared to the case of zero-thickness plates, the thick-plate situation leads to significantly higher pressure drop, while the heat transfer does not sufficiently improve, despite the increased surface area and increased mean velocity.

Zelenka and Loehrke (1983) studied the effects of leading edge bluntness, plate spacing distance, and Reynolds number on the leading and trailing plate average heat transfer, using two plates aligned with the flow direction in a wind tunnel. Steady laminar and transitional flow regimes, typical of those in compact heat exchangers, were investigated. An internal resistance heating strip was used to heat the plates. Average plate heat transfer coefficients were calculated using the total power dissipated, total plate surface area, and the difference between temperatures of upstream air and the plate centre. Their experiments supported the following conclusions: (1) the average heat transfer coefficient depends on both the plate length and plate thickness; (2) the heat transfer rate from a single blunt plate may be inhibited compared to that from a single rounded plate at low Reynolds numbers and enhanced at high Reynolds numbers; (3) the leading-edge shape of the first plate has an effect on the heat transfer from the second plate for small inter-plate spacing, when the wake behind the first plate is steady; (4) the leading-edge configuration of the second plate is important only at large values of plate spacing; and (5) the heat transfer from the second plate was often found to be greater than that of the first plate. Furthermore, the measured heat transfer rate from the leading plate agrees well with laminar theory for thin plates when the leading edge is rounded.

Roadman and Loehrke (1983) focused their work on the region of transition from steady to unsteady laminar flow between pairs of flat collinear plates at low Reynolds numbers. They used dye and hydrogen bubbles to visualize the flow in a water tunnel

and hot-wire and hot-film anemometers to measure the vortex shedding frequency in a wind tunnel. They determined that the critical flow velocity depends strongly on geometric parameters and weakly on flow disturbance level. The downstream plate was found to have a pronounced upstream influence on the critical velocity.

Suzuki et al. (1985) carried out a combined numerical and experimental study of a two-dimensional system with a staggered array of vertical plates in free-forced mixed convection at low Reynolds numbers (under 1 000). They analyzed the effect of fin thickness and free-stream turbulence. Similar results were obtained using two different numerical schemes. The numerical computations take account of the finite thickness of the plates and the free-stream turbulence. There was excellent agreement between the numerical predictions and the experimental values of local Nusselt numbers. Based on their results, they concluded that plate thickness has a minor effect on the heat transfer rates for the range of Reynolds number and the geometric parameters considered.

Mullisen and Loehrke (1986) studied the flow mechanisms (boundary layer interruptions and restarts, and vortex shedding) that enhance heat transfer in interrupted-plate ducts, in perpendicular, in-line, and staggered interrupted-plate arrays, for a range of Reynolds numbers from 100 to 10 000. They used the Schlieren technique to visualize the flow and a transient heating technique to analyze heat transfer. Steady, general unsteady, and periodic unsteady flow regimes were observed in the in-line arrangement. The periodic unsteady flow was characterized by periodic, synchronized, vortex shedding from the trailing edges of upstream plates, and it was accompanied by a strong acoustic tone. No periodic vortex-shedding regime was detected for the perpendicular-plate array. They found that the transition from steady to unsteady flow occurs at a critical value of Reynolds number that decreases with increasing streamwise spacing between plates and with increasing plate thickness. This transition is best correlated by a Reynolds number based on plate-wake width rather than by a Reynolds number based on passage hydraulic diameter. They also reported that enhancement of over 100 percent in the average heat transfer coefficient in a parallel-plate core may be realized by interrupting the surface.

#### 1.4.3.2 Recent Works (1988 – present)

McBrien and Baliga (1988) carried out measurements of wall static pressure for turbulent flows in straight rectangular ducts with spatially-periodic interrupted plates aligned parallel to the flow direction and mounted along the centre, as shown schematically in Figure 1.3. The Reynolds number based on the module hydraulic diameter and average velocity ranged between 5 000 and 45 000. Detailed time-mean intramodular wall static pressure distributions confirmed the existence of the spatially-periodic fully-developed flow regime. Their results show that the friction factor decreases with increasing Reynolds number. At low Reynolds numbers, the contribution of the wall friction to the overall pressure drop is significant, while at high Reynolds numbers, the inertial losses become dominant, and the friction factor becomes less sensitive to variations in Reynolds numbers. They also obtained surface flow visualization data, using paints made by suspending titanium dioxide and DayGlo pigments in kerosene. The main objective of their study was to enhance the available data and knowledge of local flow and pressure distributions within each periodic geometric module of the duct. Their data is reliable, detailed, and accurate enough for the testing mathematical models and numerical predictions.

Kelkar and Patankar (1989) numerically predicted laminar heat transfer and fluid flow in interrupted-plate ducts. They considered both the spatially-periodic fully-developed regime and the developing region with a fully three-dimensional elliptic mathematical model. A parametric study was made for various values of the cross-sectional aspect ratio and a fin-length parameter, and the results were compared to experimental data.

Sebben (1996) presented a numerical investigation of steady, spatially-periodic, fully-developed turbulent flows in channels with arrays of interrupted-plates. The intermediate Reynolds number turbulent regime was studied with different turbulence models. Comparison of the numerical friction factor values with experimental data of McBrien and Baliga (1988) showed qualitatively good results. In quantitative terms, however, none of the numerical predictions compared well with the experimental results, casting doubts on the suitability of the turbulence models used for the simulations of the flows investigated in this study.

Zhang et al. (1997) employed numerical simulations to explore the fluid flow and heat transfer in parallel-plate fin heat exchangers. They studied the time-dependent flow behaviour due to vortex shedding, usually overlooked in earlier studies, by solving two-dimensional and three-dimensional unsteady equations. Zhang et al. (1997) were the first to consider both the unsteadiness and the three-dimensionality of the flow within interrupted-plate ducts. Their inclusion of the unsteady terms in the governing equations greatly improves the agreement of the predicted values of the Fanning and Colburn factors with the corresponding experimental results of Mullisen and Loehrke (1986), especially for moderate Reynolds numbers. Good agreement is reported with previous experimental works [Okajima (1982)] concerning the dependence of the Strouhal number on the Reynolds number. Finally, the authors concluded that previous two-dimensional models slightly over-predicted both the friction and Colburn factors for relatively high Reynolds number values.

Dejong and Jacobi (1997) conducted flow visualization and local, row-by-row, and spatially averaged mass transfer experiments to determine the relative impact of boundary-layer restarting and vortex shedding on heat transfer performance in parallel-plate arrays. They showed a direct link between vortex shedding and mass transfer enhancement and found this contributions to depend strongly on the Reynolds number. Spatially-periodic fully-developed flow was not attained even though as many as 92 plates arranged in seven rows were used.

Dejong et al. (1998) presented a detailed analysis of experimental and numerical results for flow and heat transfer in similar offset strip-fin geometries. The experimental apparatus used was the same as that used by Dejong and Jacobi (1997). For the numerical simulations, they approximated the array as a periodic repetition of a basic unit. Thus, it has been assumed that the flow is both hydrodynamically and thermally fully developed in the fin array, and the effects of entrance and exit have been neglected. Their results showed that in steady laminar flow, heat transfer behaviour is determined mainly by boundary layer growth while at higher Reynolds numbers, vortex shedding is also important. They also establish that inclusion of flow unsteadiness plays a very important role in the accurate prediction of heat transfer. Both the numerical and the experimental results agreed quite well with the correlations of Wieting (1975), Joshi

and Webb (1987), and Manglik and Bergles (1995). The authors emphasize the need for additional complementary experimental and numerical investigations using identical geometries and boundary conditions.

Candanedo (2003) performed an experimental study of spatially-periodic fully-developed flows in straight rectangular ducts with interrupted-plate inserts. His work is an extension of the work of McBrien and Baliga (1988) and Candanedo et al. (2003). Values of the Reynolds number, based on the Kays and London definition of hydraulic diameter and the maximum average streamwise velocity, ranged from about 2 000 to 65 000. The results included graphical and tabular presentations of time-mean static pressure distributions along the axial centreline of the top wall of the duct, and also module friction factor versus Reynolds number data, for a range of values of the Reynolds number and some geometric parameters, all in the spatially-periodic fully-developed region.

Michna et al. (2005) undertook experiments to measure the heat transfer and pressure drop characteristics of an offset-strip fin array at much higher Reynolds numbers than had been previously investigated,  $5\,000 < \text{Re} < 120\,000$ . They determined that both the pressure and the convection coefficients are approximately twice those predicted by correlations developed using data from low-Reynolds number conditions.

Lamoureux, Camargo, and Baliga (2005) presented detailed turbulence measurements in the spatially-periodic regions of flows in a rectangular interrupted-plate duct akin to that shown in Figure 1.3. Their results were based on single hot-wire measurements, and included ensemble-averaged power spectrums and Strouhal number distributions. The Reynolds number, based on average velocity at the minimum cross-sectional area and the hydraulic diameter, ranged from 2 000 to 30 000. Their measurements showed repeatability, vertical and lateral symmetry at corresponding points in the central region of the duct cross-section, and spatial periodicity in successive geometrical modules.

Beside the aforementioned studies, much research has been done on flow and heat transfer interrupted-surface ducts, yielding useful data and results, but do not contribute any fundamentally new theories or concepts in this area. Such papers include the works of Lee and Kwon (1992), Tinaut et al. (1992), Cowell et al. (1995), Dubrovsky (1995),

Fehle and Klas (1995), Hu and Herold (1995a, 1995b), Stasiak et al. (1996), Ranganayakulu et al. (1997), Acharya et al. (1997, 1998), Wang et al. (1998), Hwang (1998), Kilicastalian and Sarac (1998), Ali et al. (1998), Atkinson et al. (1998), Olsson and Sunden (1998), Sara et al. (2001), Wang et al. (2001), and Lyman et al. (2002).

In the published literature, there are also numerous studies on self-sustained oscillatory flows. Examples include the works of Amon et al. (1992), Suzuki et al. (1994), Gorgemann et al. (1995), Valencia (1999), and Saidi and Sundén (2001).

## **1.5 THESIS OVERVIEW**

The motivation for this thesis, its objectives, an overview of the experimental runs and results, and a synopsis of published investigations directly relevant to this research have already been presented in the earlier sections of this chapter (Chapter 1). In Chapter 2, the theoretical considerations related to this work are presented and discussed concisely. In Chapter 3, a synopsis of the numerical method that was used to assess the applicability of the proposed unsteady experimental technique based on the lumped parameter analysis is presented. The experimental apparatus, instrumentation, and procedures are given in Chapter 4. The results of this work are presented and discussed in Chapter 5. In the concluding chapter, Chapter 6, the contributions of this thesis are summarized, and some suggestions for improvements and extensions of this work are presented.

## Chapter 2. Theoretical Considerations

The theoretical considerations employed in the planning of the experiments and in the interpretation and presentation of the results are presented in this chapter.

### 2.1 ASSUMPTIONS

As was mentioned in Chapter 1, an experimental study of forced convection heat transfer from individual plates in the spatially-periodic region of flows of air through a straight rectangular duct with interrupted-plate inserts (see Figure 1.3) was undertaken in this work. The air temperature at the inlet of this duct in all of the experiments was essentially constant ( $299.6 \pm 1\text{K}$ ). Moreover, the values of the total static pressure drop across the whole test section were less than 7 kPa [Candanedo, 2003]; the inlet absolute static pressure was close to the atmospheric pressure in the laboratory (mean value of about 101.3 kPa); and the time-mean average flow velocities in the minimum cross-sectional area of the duct were less than 22 m/s for all the experiments undertaken here. Based on these statements and observations, the following assumptions were made.

- The continuum hypothesis applies and the fluid is Newtonian.
- The air in the test section is incompressible and has constant thermophysical properties during each experimental run at values corresponding to the mean values of temperature and pressure.
- The Reynolds number, based on the hydraulic diameter and the time-mean average velocity in the minimum cross-sectional area of the duct [Kays and London (1964, 1984)], ranged from 2,000 to 30,000. Thus, the flow is assumed to be turbulent. The exact definition of the Reynolds number and hydraulic diameter used in this work are given later in this chapter.
- Spatially-periodic fully-developed flow prevails over geometrically similar modules in the acrylic portion of the test section in which the heat transfer measurements were conducted. This assumption is justified as the acrylic portion of the test section is located downstream of its aluminum portion which contains 29 geometrically similar modules (full details of the experimental setup are given in Chapter 4); and the works of McBrien and

Baliga (1988), Candanedo et al. (2003), and Lamoureux, Camargo and Baliga (2005) have conclusively demonstrated that time-mean spatially-periodic fully-developed flow conditions are established even over the last 12 geometric modules of the aluminum portion of the test section.

- The viscous dissipation and the  $Dp_{static} / Dt$  terms in the energy equation are negligible; here, it should be noted that the Eckert number [Incropera and DeWitt (2002)] is much less than one in the problems of interest.
- The Mach number in the problems of interest is less than 0.1 for all cases considered in this work, thus compressibility effects are negligible.

The above assumptions apply implicitly throughout the remainder of this thesis.

## 2.2 GOVERNING EQUATIONS

The fluid flow and heat transfer in the problems of interest are govern by differential equations that express the conservation of mass, momentum, and energy, and they can be cast in the following forms [Rouse (1946), Schlichting (1955), Batchelor (1967) and White (1974)]:

Conservation of Mass:

$$\frac{D\rho}{Dt} + \rho \frac{\partial u_i}{\partial x_i} = 0 \quad (2.1)$$

Conservation of Momentum:

$$\rho \frac{Du_i}{Dt} = -\frac{\partial p}{\partial x_i} + \frac{\partial \tau_{ij}^{VIS}}{\partial x_j} \quad (2.2)$$

Conservation of Energy:

$$\rho \left( \frac{De}{Dt} + p \frac{Dv}{Dt} \right) = \frac{\partial}{\partial x_j} k \frac{\partial T}{\partial x_j} + \Phi \quad (2.3)$$

Here,  $p$  represents the reduced static pressure, and accounts for the gravitational body force:

$$p = p_{static} + \rho g(y - y_{datum}) \quad (2.4)$$

For Newtonian fluids, invoking the Stokes hypothesis, the viscous stress term can be expressed as follows [Batchelor (1967); White (1974)]:

$$\tau_{ij}^{VIS} = \mu \left( \frac{\partial u_i}{\partial x_j} + \frac{\partial u_j}{\partial x_i} \right) - \frac{2}{3} \mu \left( \frac{\partial u_k}{\partial x_k} \right) \delta_{ij} \quad (2.5)$$

Here,  $\delta_{ij}$  is the Kronecker delta function:

$$\delta_{ij} = \begin{cases} 1, & \text{if } i = j \\ 0, & \text{if } i \neq j \end{cases} \quad (2.6)$$

In Eq. (2.3),  $\Phi$  is the viscous dissipation function:

$$\Phi = \tau_{ij}^{VIS} \frac{\partial u_i}{\partial x_j} \quad (2.7)$$

For compactness, the above equations have been written using the Einstein summation notation: thus,  $u_i = (u_1, u_2, u_3) = (u, v, w)$ , and a repeated subscript index implies summation over all possible values of that index.

For Newtonian fluids whose thermofluid properties remain essentially constant in the operating range of interest, as is the case in this investigation, the above-mentioned governing equations reduce to the following forms [Batchelor (1967); White (1974)]:

$$\frac{\partial u_i}{\partial x_i} = 0 \quad (2.8)$$

$$\rho \frac{Du_i}{Dt} = -\frac{\partial p}{\partial x_i} + \mu \left( \frac{\partial}{\partial x_j} \left( \frac{\partial u_i}{\partial x_j} \right) \right) \quad (2.9)$$

The governing equation for the temperature field is the energy equation (2.3) with the viscous dissipation neglected:

$$\rho c_p \frac{DT}{Dt} = k \frac{\partial}{\partial x_j} \left( \frac{\partial T}{\partial x_j} \right) \quad (2.10)$$

Exact analytical solutions of these equations for the spatially-periodic fully-developed flows and heat transfer in interrupted-plate rectangular ducts of interest here are not possible. For laminar flows and heat transfer in such geometries, the mathematical models are well established and numerical techniques can be used to obtain solution, as seen, for example, in the works of Sparrow et al. (1977), Patankar et al. (1977), Kelkar et al. (1989), Sebben (1996), and Zhang et al. (1997). However, with regard to turbulent flows and heat transfer in spatially-periodic interrupted-surface ducts, though many attempts have been made at proposing suitable models of

turbulence and solving the corresponding mathematical models of these problems numerically, for example, in the works of Sebben (1996) and Shah et al. (2001), many difficulties continue to plague the turbulence models, especially in the low-Reynolds-number transitional and turbulent flows. Thus, experimental data are critically needed for such flow and heat transfer problems, and this work is an effort towards fulfilling a part of this need. These points are elaborated further in the next section.

## **2.3 TURBULENT FLOWS AND THE NEED FOR EXPERIMENTAL INVESTIGATIONS**

### **2.3.1 Turbulence Models**

Turbulence is a random three-dimensional rotational time-dependent motion [Schlichting (1955); Tennekes and (1972); Hinze (1975)]. The Navier-Stokes equations accurately describe turbulent flows of Newtonian fluids [Wilcox (1993), Launder and Sandham (2002)]. One approach to the numerical simulation of turbulent flows is referred to as direct numerical simulation (DNS). In DNS, the full unsteady, three-dimensional, Navier-Stokes equations are solved numerically; therefore, it does not involve approximations other than those due to numerical discretization and yields detailed information concerning the flow field. However, the random fluctuations of the velocity and pressure fields about some mean value that are intrinsic to turbulent flows occur over wide ranges of time and length scales (with the largest scale typically at least three orders of magnitude greater than the smallest scales). Furthermore, these ranges increase with increasing Reynolds number, leading to corresponding increases in computer time and storage requirements. In consequence, DNS is limited to turbulent flows in relative simple geometries and at relative low Reynolds numbers; and to undertake such simulations even at moderately high Reynolds numbers is too expensive and impractical, even with the most powerful computers available today [Wilcox (1993); Launder and Sandham (2002)].

For the turbulent flows encountered in most practical applications, full details of the fluctuations of velocity, pressure, and temperature are not necessary, as suitably averaged (mean) values of these fields are often sufficient for effective designs. A broad range of averaging procedures have been used to describe turbulent flow fields:

examples include time-averaging, volume-averaging with weighting functions or filters, density-weighted- or Favre-averaging, and ensemble-averaging, each having its own pros and cons. For an in-depth discussion of these averaging procedures and their implications, the reader is referred to the work of Wilcox (1993). In comparison to the instantaneous values of the flow fields, the averaged (or mean) fields vary relatively smoothly (if at all) in position and time, and the equations that govern them can be obtained by suitable manipulation and corresponding averaging of the Navier-Stokes equations. However, by averaging these equations, unknown correlations of the fluctuations of the dependent variables about their mean values are introduced. Derivation of differential equations that describe the evolution, advection, diffusion, and generation of such correlations is possible, but these equations contain additional (and higher order) unknown correlations of the fluctuations. This process leads to the so-called “closure problem” in such analytical treatments of turbulence [Launder and Spalding (1972); Tennekes and Lumley (1972); Wilcox (1993); Launder and Sandham (2002)].

To resolve the closure problem, many turbulence models have been proposed over the last 80 years. The turbulence models estimate the correlations of the fluctuations in terms of the averaged values of the dependent variables and their derivatives. Without exception, experimental inputs are needed to determine unknown constants and/or functions in these corrections. Different categories of turbulence models are available: these include zero-equation (or algebraic) models, Reynolds-stress and turbulent-flux models, algebraic stress and flux models, and the so-called large eddy simulation (LES) models. A detailed review of these turbulent models goes well beyond the scope of this thesis. Rather, the interested reader is referred to such reviews in the works of Tennekes and Lumley (1972), Hinze (1975), Wilcox (1993), Deissler (1998), and Launder and Sandham (2002).

### **2.3.2 Concluding Remarks**

Despite more than a century of work on turbulent flows and turbulence modelling, computer predictions in this area have some serious restrictions. The rapid development of computational power opens up more flows to direct numerical simulation (DNS).

However, such progress is likely to be rather slow since the computer time and storage requirements for DNS increases rapidly with Reynolds numbers. Thus, DNS is certain to be limited to simple geometries and relatively low Reynolds numbers for some years to come. Turbulence models offer an alternative for the prediction of a wide range of turbulent flows. However, key elements of these models are constants and functions that are determined by comparing numerical predictions to experimental measurements. Thus, there is a critical need for laboratory experiments, complementary to numerical simulations, for studying turbulence, and for checking and refining turbulence models. The experimental investigation presented in this thesis is a small effort to contribute to the world-wide research efforts aimed at fulfilling this need.

## **2.4 TIME-MEAN VELOCITY, STATIC PRESSURE, AND TEMPERATURE VARIATIONS IN SPATIALLY-PERIODIC FULLY-DEVELOPED FLOWS**

### **2.4.1 Velocity and Static Pressure Variations**

The time-mean velocity and static pressure fields in interrupted-plate rectangular ducts, akin to that shown in Figure 1.3, change in the streamwise ( $z$ ) direction. However, for the range of Reynolds number and geometric parameters investigated in this work, after five to ten geometric modules downstream of the inlet plane, a spatially-periodic fully-developed flow regime is attained for both laminar and statistically steady turbulent flows.

A numerical study by Sparrow et al. (1977) first introduced the concept of spatially-periodic fully-developed flow in interrupted-surface ducts. Later, other numerical studies, for example, those of Patankar et al. (1977), Patankar and Prakash (1981), Kelkar et al. (1989), and also experimental investigations, for example, those of Sparrow and Hajiloo (1980), Mullisen and Loehrke (1986), McBrien and Baliga (1988), Candanedo (2003), and Lamoureux et al. (2005), confirmed the existence of such a fully-developed region.

Spatially-periodic fully-developed flows in the interrupted-plate ducts considered in this work (Figure 1.3) are characterised by time-mean  $x$ -,  $y$ -, and  $z$ -direction velocity components (denoted as  $U$ ,  $V$ , and  $W$ , respectively) that repeat identically in each

successive geometric module (height =  $2H$ , width =  $b$ , and length =  $L + s$ ); and the differences in values of time-mean reduced static pressure at adjacent  $(x,y)$  points, located one spatial period  $(L + s)$  apart in the axial  $(z)$  direction, are the same throughout. Therefore, denoting the spatial period by  $\Lambda = (L + s)$ , the following equation applies to the time-mean velocity components:

$$\begin{aligned} U(x, y, z) &= U(x, y, z + \Lambda) = U(x, y, z + 2\Lambda) = \dots \\ V(x, y, z) &= V(x, y, z + \Lambda) = V(x, y, z + 2\Lambda) = \dots \\ W(x, y, z) &= W(x, y, z + \Lambda) = W(x, y, z + 2\Lambda) = \dots \end{aligned} \quad (2.11)$$

Following Patankar et al (1977), for spatially-periodic fully-developed flows, the variation of the time-mean reduced static pressure can be expressed as follows:

$$P(x, y, z) = -\beta z + \tilde{P}(x, y, z) \quad (2.12)$$

where  $\tilde{P}(x, y, z)$  is spatially periodic in the  $z$  direction, and  $\beta$  denotes the time-mean reduced static pressure drop per unit axial ( $z$ -direction) length over each geometric module:

$$\beta = \frac{P(x, y, z) - P(x, y, z + \Lambda)}{\Lambda} \quad (2.13)$$

Thus,  $\tilde{P}(x, y, z) = \tilde{P}(x, y, z + \Lambda) = \tilde{P}(x, y, z + 2\Lambda) = \tilde{P}(x, y, z + 3\Lambda) = \dots$  is a spatially periodic function.

#### 2.4.2 Temperature Variations

The rate of heat transfer from the interrupted-plate array depends on the thermal boundary condition. The corresponding mathematical model and laminar forced convection solutions for the following two thermal boundary conditions on the surfaces of the plates have been presented by Patankar et al. (1977): (i) prescribed rate of heat transfer per plate with each plate at an essentially uniform temperature, that increases with each successive plate in the main flow direction; and (ii) all plates at a uniform wall temperature. The analysis for the first of these thermal boundary conditions is presented in this section, and the readers are referred to the paper by Patankar et al. (1977) for the analysis pertaining to the latter boundary conditions.

For the purpose of this analysis, consider an array of plates with an electric heater of power output,  $Q$ , embedded in each plate, and the spacing between the plates,  $s$ , equal to the plate length,  $L$  (see Figure 1.3). The plate at a given streamwise location,  $z$ , is at uniform temperature,  $T_w$ , and the next downstream plate is at  $T_w + \Delta T$ , and so on. If a thermally-periodic state prevails, each plate transfers the same amount of heat  $Q$  to the fluid and the time-mean fluid temperature also rises by  $\Delta T$  from one module to the next module in the flow direction. Thus,

$$T(x, y, z + L) - T(x, y, z) = T(x, y, z + 2L) - T(x, y, z + L) = \dots \quad (2.14)$$

Following Patankar et al. (1977), we define

$$\gamma = \frac{T(x, y, z + L) - T(x, y, z)}{L} \quad (2.15)$$

It then follows from an overall steady-state energy balance that,

$$\gamma = \frac{Q}{m c_p L} \quad (2.16)$$

Furthermore, the temperature field can be expressed as follows:

$$T(x, y, z) = \gamma z + \tilde{T}(x, y, z) \quad (2.17)$$

where  $\tilde{T}(x, y, z)$  is spatially periodic in the  $z$  direction. In view of this spatial periodicity, the solution domain can be limited to the streamwise length  $z^+ \leq z \leq (z^+ + L)$ , where  $z^+$  is any convenient location. Then,

$$\tilde{T}(x, y, z^+) = \tilde{T}(x, y, z^+ + L) \quad (2.18)$$

## 2.5 DIMENSIONAL ANALYSIS

The dimensionless parameters that characterize the turbulent convection from each plate in the spatially-periodic fully-developed flow region of the rectangular interrupted-plate duct investigated here (see Figure 1.3) are the following:

$$\begin{aligned} \text{Re} &= \rho \bar{W} D_h / \mu; \quad b^* = b / (2H); \quad L^* = L / (2H); \quad s^* = s / (2H); \\ t^* &= 2t / (2H) = t / H; \quad \varepsilon_{\text{Rel}} = \varepsilon / D_h; \quad \text{Pr} = (\mu c_p / k)_{\text{fluid}} \end{aligned} \quad (2.19)$$

In this work, air at an essentially uniform inlet temperature of about 300 K was used in all experimental runs, and the maximum plate temperature was limited to less than 65

°C in all case. Thus, the Prandtl number remained pretty much constant at  $(Pr)_{fluid} = 0.7$ . The rms roughness,  $\varepsilon$ , of the wetted surfaces of the aluminium and acrylic test sections were well below the viscous sub-layer thickness on these surfaces in all experimental runs. Thus, these surfaces could be referred to as smooth, and the effect of  $\varepsilon/D_h$  on the flow could be considered negligible. Several different definitions of the hydraulic diameter and average time-mean axial (z-direction) velocity for spatially-periodic turbulent flows in offset-strip fin ducts and related geometries are used in the literature. Examples of some of these definitions are listed in Table 2.1.

Table 2.1: Definitions of  $D_h$  and  $\bar{W}$  for offset-strip fin and interrupted plate ducts

Investigations	$D_h$	$\bar{W}$
Kays and London (1964, 1984)	$\frac{4A_{c-s-min} \Lambda}{A_{wetted}}$	$\frac{\dot{m}}{\rho A_{c-s-min}}$
McBrien and Baliga (1988)	$\frac{4A_{c-s-min} \Lambda}{A_{wetted, no edges}}$	$\frac{\dot{m}}{\rho A_{c-s-min}}$
Wieting (1976) and Mochizuki et al. (1987)	$\frac{4A_{c-s}}{Peri_{wetted}}$	$\frac{\dot{m}}{\rho A_{c-s}}$

In this table, the terms  $\Lambda$ ,  $A_{c-s-min}$ ,  $A_{c-s}$ ,  $A_{wetted}$ ,  $A_{wetted, no edges}$ , and  $Peri_{wetted}$  denote, respectively, the following: the spatial period in the axial (z) direction; minimum cross-sectional area for the flow; the nominal cross-sectional area of the duct as if there were no interrupted-plate inserts; the total wetted solid surface area in a representative geometric module,  $A_{wetted}$ , minus the edge surface areas (normal to the axial z-direction); and the wetted perimeter of the nominal cross-sectional area. With respect to the notation given in Figure 1.3, the above terms are:

$$\begin{aligned}
 \Lambda &= L + s; \quad A_{c-s-min} = 2b(H - t); \quad A_{c-s} = 2Hb; \\
 A_{wetted} &= 2 \left[ (2L + s)b + 2 \{ L(H - t) + Hs \} + 2bt \right]; \\
 A_{wetted, no edges} &= A_{wetted} - 4bt; \quad Peri_{wetted} = 2(2H + b)
 \end{aligned} \tag{2.20}$$

In the present work, the Kays and London (1964, 1984) definitions of  $D_h$  and  $\bar{W}$  were preferred for the following reasons:

- The definitions of Kays and London are used in the most referenced correlations [Joshi and Webb (1987); Manglik and Bergles (1995)].
- In the literature on compact heat exchangers, the definitions of Kays and London (1964, 1984) are most often used.
- The definitions of Kays and London (1964, 1984) reduce to the classical definition of hydraulic diameter  $\left( D_h = 4A_{c-s} / Perimeter_{wetted} \right)$  and average time-mean axial velocity  $\left( \bar{W} = \dot{m} / \rho A_{c-s} \right)$  for plates of negligible thickness and for ducts without plates.

The average heat transfer coefficient is often presented in the literature in terms of the Colburn  $j$  factor:

$$j = \frac{Nu_{av}}{Re Pr^{1/3}} \quad (2.21)$$

In this equation, the average Nusselt number per plate in the spatially-periodic fully developed regime is defined as follows:

$$Nu_{av} = h_{av} D_h / k_{fluid} \quad (2.22)$$

In this work, the average heat transfer coefficient for each individual plate,  $h_{avg}$ , in the spatially-periodic fully-developed flow region was determined experimentally: the experimental apparatus and procedures are described in Chapter 4 of this thesis.

## Chapter 3. Numerical Method

As was mentioned in Chapter 1, in the proposed experimental technique for obtaining the average heat transfer coefficients on individual plates in the spatially-periodic fully-developed flows in an interrupted-plate rectangular duct (see Figure 1.3), a lumped parameter analysis is used to process the data. Furthermore, each test plate consists of a central metal section with two plastic (ertalyte) sections, one on each end, to reduce end losses. Full details of the experimental setup and these test plates are given in Chapter 4, and the lumped parameter is presented in Chapter 5. In this chapter, a numerical method that was formulated, implemented, tested, and used to assess the applicability of the aforementioned lumped parameter analysis is described concisely.

### 3.1 PROBLEM DEFINITION, ASSUMPTIONS, AND ASSESSMENT STRATEGY

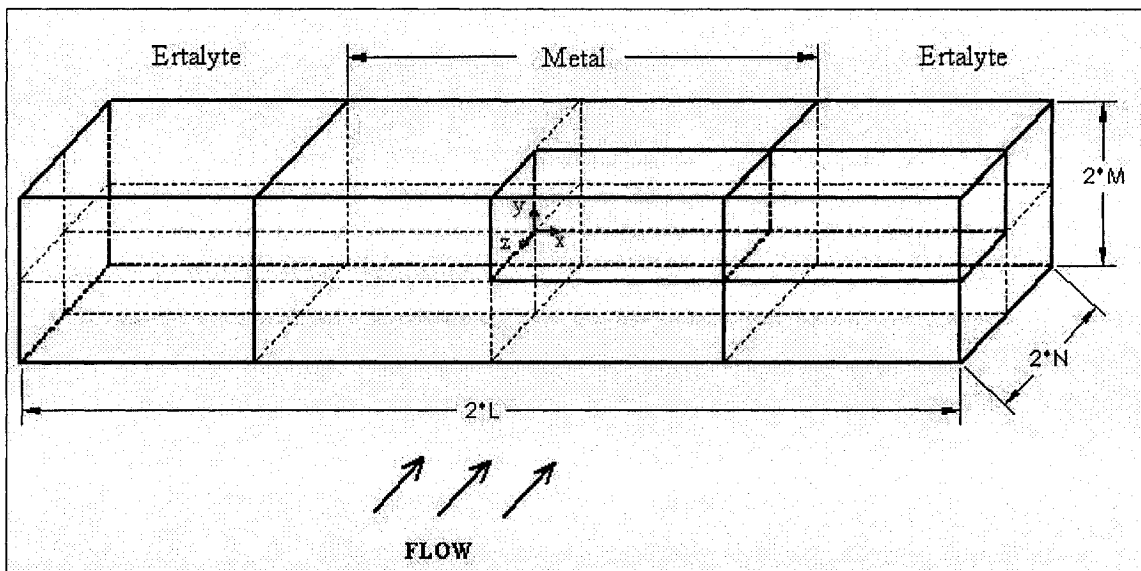


Figure 3.1: Problem schematic, calculation domain, and coordinate system.

The problem considered is that of three-dimensional unsteady heat conduction in the test plates used in the experimental investigation. These test plates are solid parallelepiped bars, each consisting of a central metal section with two plastic (ertalyte) end sections. The entire bar is initially at a uniform temperature,  $T_i$ , and suddenly

exposed to convective heat transfer on its lateral surfaces, with the fluid at a uniform (constant) ambient temperature of  $T_\infty < T_i$ . The problem of interest is schematically illustrated in Figure 3.1.

The metal and plastic portions of the solid bar were assumed to have constant thermophysical properties. In the numerical simulations, the ambient fluid temperature was maintained constant, and the heat transfer coefficient was set equal to a value somewhat greater than the maximum value expected in the experiments, using guidance from the earlier work of [Cur and Sparrow (1979)]. At the interfaces between the metal and plastic portions of the solid bar, excellent thermal contact (zero thermal contact resistance) was assumed: this allowed the assessment of the proposed lumped parameter technique under the worst possible conditions with respect to end losses. The outer end surfaces of the plastic pieces ( $x = \pm L$  in Figure 3.1) were assumed to be adiabatic, as, in the experiments, the rate of heat loss from these surface was expected to be negligible compared to that due to the forced convection on the lateral surfaces of the solid bar. With these assumptions and prescriptions, the calculation domain could be limited to one-eighth of the solid bar, as shown in Figure 3.1:  $0 \leq x \leq L$ ,  $0 \leq y \leq M$ , and  $0 \leq z \leq N$ .

In each experimental run, for the central metal portion of each of the test plates in the spatially-periodic fully-developed regime of the air flows in the straight rectangular interrupted-plate ducts, the Biot number ( $Bi = h_{av} L_{ch} / k_{solid}$ ;  $L_{ch} = Vol / A_{surface}$ ) is expected to be less than 0.1: thus, the lumped parameter analysis would be expected to be valid [Incropera and DeWitt (2002)]. However, in the experimental setup, the central metal portion of each test plate has plastic portions on each side (see Figure 3.1), and for these plastic portions, the Biot number is not less than 0.1 in all cases. Thus, to establish the applicability of the lumped parameter analysis even under these circumstances, the proposed method was used to simulate unsteady *three-dimensional* heat conduction within the entire test plate, the central metal portion plus the plastic end portions.

The strategy for the above-mentioned numerical assessment of the applicability of the lumped parameter analysis is the following: 1) with the highest expected value of

the average heat transfer coefficient ( $h_{av,specified}$ ) in the experiments, the effective density, the effective thermal conductivity, the effective specific heat at constant pressure, the dimensions of both the metal and the plastic portions, the uniform initial temperature of these portions, and the temperature of the flowing air as inputs, conduct a fully three-dimensional unsteady simulation of the heat conduction inside the test plate.(with the electrical power switched off and cooling under the influence of the convection to the flowing air); 2) using the effective density, the effective thermal conductivity, the effective specific heat at constant pressure, the dimensions of the metal portion, the temperature of the flowing air, and the time-varying temperature of the center of the metal portion of the test plate as inputs to the proposed lumped parameter analysis, calculate the average heat transfer coefficient on the surface of the metal portion ( $h_{av,calculated}$ ); 3) compare the specified and calculated average heat transfer coefficients; and 4) if the percentage difference  $\{|h_{av,specified} - h_{av,calculated}| / h_{av,specified}\} \times 100 < 1 \%$ , the lumped parameter analysis is considered to be applicable.

### 3.2 FORMULATION OF THE NUMERICAL METHOD

A control-volume-based finite difference method was used to simulate the unsteady three-dimensional conduction inside the test plate for the conditions described in the last section. This numerical method is a slightly modified version of a similar method described in detail by Patankar (1980) and Baliga and Atabaki (2006). Thus, only a concise description of this method is given in this section, in terms of the following key steps in its formulation: 1) governing equations; 2) domain discretization; 3) interpolation functions; 4) derivation of the discretized equations; and 5) solution of the discretized equations. For a more detailed description of this method, the reader is referred to Patankar (1980) and Baliga and Atabaki (2006).

### 3.2.1 Governing Equations

With respect to the Cartesian coordinate system shown in Figure 3.1, three-dimensional unsteady heat conduction inside the test plate is governed by the following differential equation [Incropera and DeWitt (2002)]:

$$\rho c_p \frac{\partial T}{\partial t} = \frac{\partial}{\partial x} \left( k \frac{\partial T}{\partial x} \right) + \frac{\partial}{\partial y} \left( k \frac{\partial T}{\partial y} \right) + \frac{\partial}{\partial z} \left( k \frac{\partial T}{\partial z} \right) + S \quad (3.1)$$

In this equation,  $\rho$ ,  $c_p$ , and  $k$  are the mass density, the specific heat at constant pressure, and the thermal conductivity of the material, respectively; in the simulations, they are assigned suitable effective values that pertain to the metal and plastic portions of the test plates. Provision is also made for a volumetric rate of heat generation, or source, term,  $S$ , though in the problem of interest (with the electrical heating of the test plates shut off), this term is zero.

On surfaces that are exposed to the convective heat loss to the flowing air, the following boundary condition applies:

$$-k \partial T / \partial n |_{\text{surface,local}} = h_{\text{av,specified}} (T |_{\text{surface,local}} - T_{\text{air}}) \quad (3.2)$$

Here,  $n$  is a coordinate normal to the surface pointing out of the test plate, and  $k$  is the thermal conductivity of the plate material at the location being considered. At the interfaces between the central metal portion and the plastic (ertalyte) end portions, perfect thermal contact is assumed in the simulations (in order to assess the influence of maximum possible end effects on the central metal portion): thus, the temperature and the heat flux within the metal and the plastic portions at each point on these surfaces are assumed to be identical [Incropera and DeWitt (2002)]. The other ends of the plastic portions are assumed to be adiabatic, as the rates of heat loss from these surfaces are expected to be negligible compared to those from the surfaces exposed to the air flow.

The initial condition is a specified uniform temperature within the entire (metal and plastic portions) of the test plate; the electrical power input to the test plate is assumed to be shut off, and the entire lateral plate surface is exposed to the convective heat loss to the flowing air, whose temperature is assumed to remain essentially constant at  $T_{\text{air}}$  far enough away from the plate.

### 3.2.2 Domain Discretization

The so-called type-B domain discretization of Patankar (1980) was used in the formulation of the finite volume method. Thus, the calculation domain is first divided into rectangular parallelepiped control volumes, and then the grid points (or nodes) are placed at the geometric centre of each control volume. This discretization is shown in Figure 3.2 for a two-dimensional  $x$ - $y$  cross-section of the calculation domain; a given internal grid-point,  $P$ , is connected to four neighbouring grid points (denoted by  $N$ ,  $S$ ,  $E$  and  $W$ ) by grid lines, passing through the four faces of the associated control volume (denoted by  $n$ ,  $s$ ,  $e$ ,  $w$ ). Similar discretization arrangements apply to the  $x$ - $z$  and  $y$ - $z$  cross-sections of the calculation domain. In this arrangement, nodes on the boundary of the calculation domain have zero-thickness control volumes.

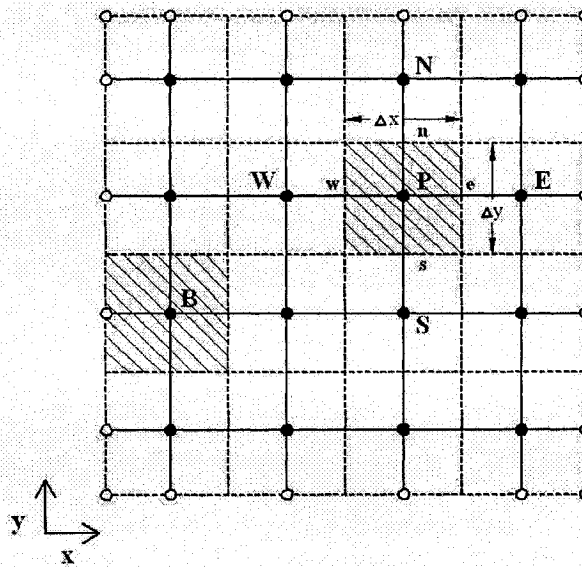


Figure 3.2: Type-B domain discretization [Patankar (1980)] of the  $x$ - $y$  cross-section of the test plate and the associated notation.

In all simulations, the domain discretization was done in way that locates a control volume face at the interfaces between that central metal portion and the plastic (ertalyte) end portions of the test plate. Thus, none of the control volumes contained *both* the metal and the plastic materials. A grid-independence and time-step independence study

was performed before the final simulations were conducted: the details are given in Sections 3.3.1 and 3.3.2, respectively.

### 3.2.3 Interpolation Functions

The nodal value of density at each internal grid point is assumed to prevail over the corresponding control volume. The source term is linearized, if need, following the procedure described in Patankar (1980):  $S = S_C + S_p T_p$ . The nodal values of  $S_C$  and  $S_p$  at each grid point are assumed to prevail over the corresponding control volume.

The thermal conductivity,  $k$ , of the metal and plastic portions of the test plate is stored at the nodes at the centres of the control volumes, but its values are needed, as will be seen in a subsequent subsection, at the faces of the control volume. For example, with reference to the node P and its control volume shown in Figure 3.3 in the  $x$ - $y$  plane, the value of the thermal conductivity at the east face of the control volume,  $k_e$ , is needed; and similarly, the values of thermal conductivity at the west, north, south, front, and back faces of this control volume,  $k_w$ ,  $k_n$ ,  $k_s$ ,  $k_f$ ,  $k_b$ , respectively, would be needed. Following the recommendation of Patankar (1980), the value of the thermal conductivity at each control volume face is obtained by solving a locally one-dimensional conduction problem along the grid line joining the nodes on either side of this face. Thus, the value of  $k_e$  is obtained from the values of  $k_P$  and  $k_E$  and the distances  $(\delta x)_{e^-}$ ,  $(\delta x)_{e^+}$ , and  $(\delta x)_e$  shown in Figure 3.3 as follows:

$$k_e = \frac{(\delta x)_e k_E k_P}{k_E (\delta x)_{e^-} + k_P (\delta x)_{e^+}} \quad (3.3)$$

The values of  $k_w$ ,  $k_n$ ,  $k_s$ ,  $k_f$ , and  $k_b$  are obtained in a similar manner [Patankar (1980)].

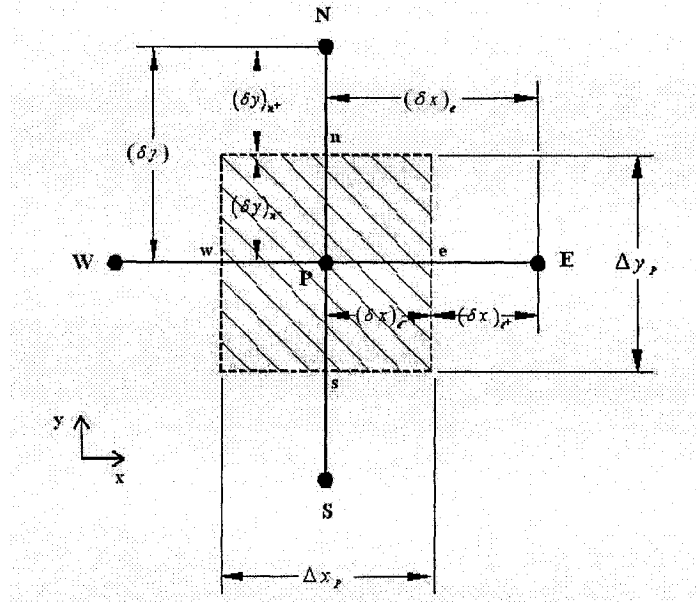


Figure 3.3: Schematic of the control volume surrounding a node P and associated notation in the  $x$ - $y$  plane of the calculation domain.

The nodal values of  $T$  are interpolated linearly along the  $x$ ,  $y$ , and  $z$  grid lines when approximating the values of the corresponding components of the gradients of temperature at the points where these grid lines intersect the control volume faces inside the calculation domain: with regard to the gradients, this formulation is equivalent to using second-order accurate approximations of the functions when the control-volume faces intersect the grids lines at midway locations in between the nodes [Patankar (1980)], as is the case when uniform grids are used in the proposed finite volume method. However, at the boundaries of the calculation domain, the boundary nodes and the control-volume faces coincide (see Figure 3.2): thus, in order to obtain second-order approximations of the values of the temperature gradients at such nodes and control-volume faces, quadratic interpolation of the temperature is used [Baliga and Atabaki (2006)].

With regard to the unsteady aspects of the problem, the fully-implicit scheme is used: thus, when the spatial terms are integrated with respect to time, the values at the end of the time step are assumed to prevail over the time step [Patankar (1980)]. It is well-known that the fully-implicit scheme is only first-order accurate. However, this scheme is very easy to implement, is unconditionally stable, and is particularly well-

suit to the modelling of processes which vary exponentially in time. Furthermore, during the unsteady cooling of the test plates (with the electrical power input shut off), the temperatures at points inside the plates are expected to decay exponentially with time, and eventually reach the temperature of the flowing air. Thus, the fully implicit scheme was chosen for incorporation in the proposed finite volume method.

### 3.2.4 Discretized Equations

The discretized equations are obtained by using the above-mentioned interpolation functions to derive algebraic approximations to integral energy conservation equations applied to the control volumes in the calculation domain. For a particular node, P, which is not adjacent to or on the boundaries of the calculation domain, this procedure leads to the following discretized equation [Patankar (1980)]:

$$a_P T_P = a_N T_N + a_S T_S + a_E T_E + a_W T_W + a_F T_F + a_B T_B + b \quad (3.4)$$

Where

$$a_N = \frac{k_n \Delta z \Delta x}{(\delta y)_n} \quad (3.5a)$$

$$a_S = \frac{k_s \Delta z \Delta x}{(\delta y)_s} \quad (3.5b)$$

$$a_E = \frac{k_e \Delta y \Delta z}{(\delta x)_e} \quad (3.5c)$$

$$a_W = \frac{k_w \Delta y \Delta z}{(\delta x)_w} \quad (3.5d)$$

$$a_F = \frac{k_f \Delta x \Delta y}{(\delta z)_f} \quad (3.5e)$$

$$a_B = \frac{k_b \Delta x \Delta y}{(\delta z)_b} \quad (3.5f)$$

$$a_P^o = \frac{\rho c_p \Delta x \Delta y \Delta z}{\Delta t} \quad (3.5g)$$

$$b = S_c \Delta x \Delta y \Delta z + a_P^o T_P^o \quad (3.5h)$$

$$a_p = a_N + a_S + a_E + a_W + a_F + a_B + a_p^o - S_p \Delta x \Delta y \Delta z \quad (3.5i)$$

In this equation,  $a_p^o$  is the coefficient associated with the temperature of the “time neighbour”,  $T_p^o$  (old value of  $T_p$ ).

The discretized equations for the nodes that are adjacent to the boundaries of the calculation domain have the same form as that of Eq. (3.4), but the expressions for the coefficients not as simple as those given in Eqs. (3.5 a – i). This is because the aforementioned quadratic interpolation is used to approximate the temperature gradients at the boundary nodes and also because of the implementation of the appropriate boundary conditions. In the problem of interest, the boundary conditions are the convective loss condition given by Eq. (3.2) on the surface exposed to the air flow, and the adiabatic condition on the outer ends of the plastic portions of the test plates. The full derivation of the discretization equations for nodes adjacent to the boundaries of the calculation domain is available in the recent work of Baliga and Atabaki (2006), so it is not repeated here.

### 3.2.5 Solution of the Discretized Equations

At each time step, the discretized equations were solved using an iterative plane-by-plane-cum-line-by-line Gauss-Seidel method [Patankar (1980)]. Furthermore, at each time step, this iterative method was considered to have converged when the absolute values of suitably normalized residues at all internal nodes were all less than  $10^{-8}$ .

## 3.3 RESULTS OF THE NUMERICAL INVESTIGATION AND DISCUSSION

### 3.3.1 Computer Program Validation

The computer program incorporating the numerical method described in Section 3.2 was validated by applying it to a three-dimensional test problem for which an analytical solution could be obtained. This test problem involves unsteady three-dimensional heat conduction in a bar of rectangular cross-section. A schematic description of this problem is given in Figure 3.4.

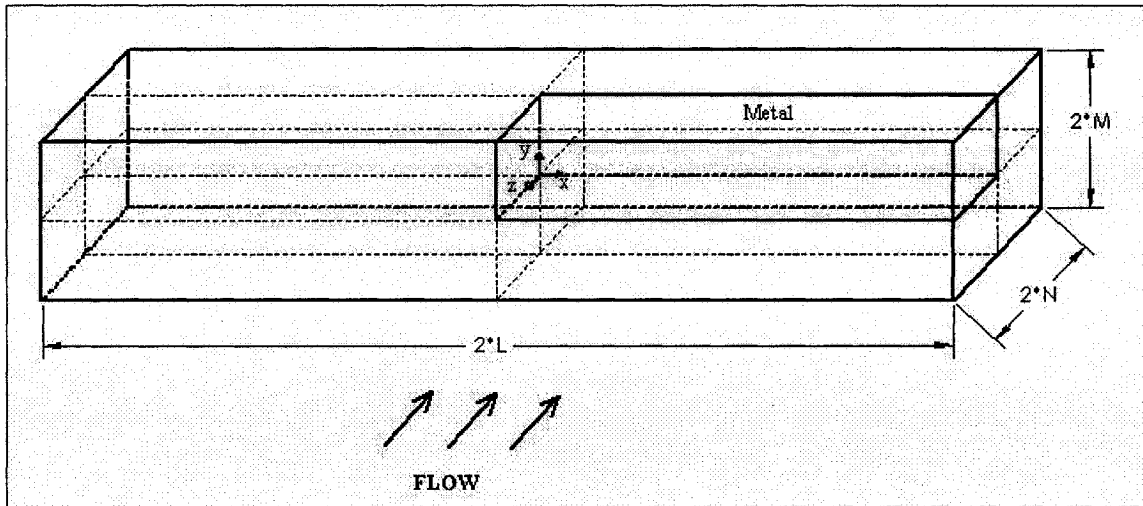


Figure 3.4: Test problem schematic, calculation domain, and coordinate system.

The bar shown in Figure 3.4 is initially at a uniform temperature,  $T_i$ . At time  $t = 0$ , it is suddenly exposed to convection heat loss with a constant heat transfer coefficient,  $h = \text{constant}$ , and a constant ambient fluid temperature,  $T_\infty = \text{constant}$ . The bar is made of a material that is isotropic and has constant properties: thermal conductivity  $k = \text{constant}$ ; density  $\rho = \text{constant}$ ; and specific heat at constant pressure  $c_p = \text{constant}$ .

The differential equation that governs the temperature of the bar is the following:

$$\frac{\partial^2 T}{\partial x^2} + \frac{\partial^2 T}{\partial y^2} + \frac{\partial^2 T}{\partial z^2} = \frac{1}{\alpha} \frac{\partial T}{\partial t} \quad (3.6)$$

In this equation,

$$\alpha = \frac{k}{\rho \cdot c_p} \quad (3.7)$$

At the boundary surfaces of the bar, at  $x = L$ ,  $y = M$ , and  $z = N$ , the heat flux to the surface by conduction through the bar is lost by convection to the ambient fluid:

$q''_{\text{conducted}} = q''_{\text{convected}}$ . Thus, at  $x = L$ :

$$-k \left. \frac{\partial T}{\partial x} \right|_{x=L} = h(T_{x=L} - T_\infty) \quad (3.8)$$

Similarly, at  $y = M$  and at  $z = N$ , respectively:

$$-k \frac{\partial T}{\partial y} \Big|_{y=M} = h(T_{y=M} - T_{\infty}) \quad (3.9)$$

$$-k \frac{\partial T}{\partial z} \Big|_{z=N} = h(T_{z=N} - T_{\infty}) \quad (3.10)$$

The symmetry-surface (adiabatic) condition applies at  $x = 0$ ,  $y = 0$ , and  $z = 0$ :

$$\frac{\partial T}{\partial x} \Big|_{x=0} = 0 \quad (3.11)$$

$$\frac{\partial T}{\partial y} \Big|_{y=0} = 0 \quad (3.12)$$

$$\frac{\partial T}{\partial z} \Big|_{z=0} = 0 \quad (3.13)$$

The initial condition (at  $t = 0$ ) is the following:

$$T|_{t=0} = T_i \quad (3.14)$$

This mathematical model is first recast in terms of the following dimensionless temperature:

$$\theta(x, y, z, t) = \left( \frac{T - T_{\infty}}{T_i - T_{\infty}} \right) \quad (3.15)$$

The governing equation then becomes

$$\frac{\partial^2 \theta}{\partial x^2} + \frac{\partial^2 \theta}{\partial y^2} + \frac{\partial^2 \theta}{\partial z^2} = \frac{1}{\alpha} \frac{\partial \theta}{\partial t} \quad (3.16)$$

The corresponding boundary conditions become:

$$\text{at } x = 0, \frac{\partial \theta}{\partial x} \Big|_{x=0} = 0 \quad (3.17)$$

$$\text{at } x = L, \frac{\partial \theta}{\partial x} \Big|_{x=L} = -\frac{h}{k} \cdot \theta \Big|_{x=L} \quad (3.18)$$

$$\text{at } y = 0, \frac{\partial \theta}{\partial y} \Big|_{y=0} = 0 \quad (3.19)$$

$$\text{at } y = M, \frac{\partial \theta}{\partial y} \Big|_{y=M} = -\frac{h}{k} \cdot \theta \Big|_{y=M} \quad (3.20)$$

$$\text{at } z = 0, \left. \frac{\partial \theta}{\partial z} \right|_{z=0} = 0 \quad (3.21)$$

$$\text{at } z = N, \left. \frac{\partial \theta}{\partial z} \right|_{z=N} = -\frac{h}{k} \cdot \theta \Big|_{z=N} \quad (3.22)$$

The initial condition takes on the following form:

$$\text{at } t = 0, \theta = 1 \quad (3.23)$$

The solution to Eq. (3.16) with the aforementioned boundary and initial conditions may be found by the method of separation of variables. First, the following product solution is proposed:

$$\theta(x, y, z, t) = X(x, t) \cdot Y(y, t) \cdot Z(z, t) \quad (3.24)$$

Substituting this assumed form into Equation (3.16) gives

$$YZ \frac{\partial^2 X}{\partial x^2} + XZ \frac{\partial^2 Y}{\partial y^2} + XY \frac{\partial^2 Z}{\partial z^2} = \frac{1}{\alpha} \left[ YZ \frac{\partial X}{\partial t} + XZ \frac{\partial Y}{\partial t} + XY \frac{\partial Z}{\partial t} \right] \quad (3.25)$$

For this equation to be valid for all  $x, y, z$  and  $t$ , we must have

$$\frac{\partial^2 X}{\partial x^2} = \frac{1}{\alpha} \cdot \frac{\partial X}{\partial t} \quad (3.26)$$

With boundary conditions

$$\text{at } x = 0, \left. \frac{\partial X}{\partial x} \right|_{x=0} = 0 \quad (3.27)$$

$$\text{at } x = L, \left. \frac{\partial X}{\partial x} \right|_{x=L} = -\frac{h}{k} \cdot X \Big|_{x=L} \quad (3.28)$$

Also

$$\frac{\partial^2 Y}{\partial y^2} = \frac{1}{\alpha} \cdot \frac{\partial Y}{\partial t} \quad (3.29)$$

With boundary conditions

$$\text{at } y = 0, \left. \frac{\partial Y}{\partial y} \right|_{y=0} = 0 \quad (3.30)$$

$$\text{at } y = M, \left. \frac{\partial Y}{\partial y} \right|_{y=M} = -\frac{h}{k} \cdot Y \Big|_{y=M} \quad (3.31)$$

and

$$\frac{\partial^2 Z}{\partial z^2} = \frac{1}{\alpha} \cdot \frac{\partial Z}{\partial t} \quad (3.32)$$

With boundary conditions

$$\text{at } z=0, \left. \frac{\partial Z}{\partial z} \right|_{z=0} = 0 \quad (3.33)$$

$$\text{at } z=N, \left. \frac{\partial Z}{\partial z} \right|_{z=N} = -\frac{h}{k} \cdot Z|_{z=N} \quad (3.34)$$

The separation of variables technique is now used to solve for  $X(x, t)$ . Thus,  $X(x, t) = \Psi(x) \cdot \Gamma(t)$ , and Eq. (3.26) becomes

$$\Gamma \cdot \frac{d^2 \Psi}{dx^2} = \frac{1}{\alpha} \cdot \Psi \cdot \frac{d\Gamma}{dt} \quad (3.35)$$

This equation is recast as follows:

$$\frac{1}{\Psi} \cdot \frac{d^2 \Psi}{dx^2} = \frac{1}{\alpha} \cdot \frac{1}{\Gamma} \cdot \frac{d\Gamma}{dt} \quad (3.36)$$

For a function of  $x$  to be identical to a function of  $t$  for all  $x$  and  $t$ , both sides of Eq. (3.36) must be equal to a constant, and this constant must be negative as  $\theta$  must decay to zero with  $t$ . Let this constant be  $-\beta^2$ . Then, Eq. (3.36) is separated into two ordinary differential equations.

$$\frac{d^2 \Psi}{dx^2} + \beta^2 \Psi = 0 \quad (3.37)$$

$$\frac{d\Gamma}{dt} + \alpha \cdot \beta^2 \cdot \Gamma = 0 \quad (3.38)$$

The solution to Eq. (3.37) can be obtained via the corresponding characteristic equation:

$$\lambda^2 + \beta^2 = 0 \quad (3.39)$$

The roots of Eq. (3.39) are  $\lambda = \pm i\beta$ . Therefore, the general solution for  $\Psi(x)$  is

$$\Psi(x) = A \sin(\beta x) + B \cos(\beta x) \quad (3.40)$$

Applying the boundary conditions we get

$$\text{i) } \frac{d\Psi(0)}{dx} = 0,$$

$$\frac{d\Psi(x)}{dx} = A\beta \cos(\beta x) - B\beta \sin(\beta x) \Rightarrow$$

$$0 = A\beta \cos(0) - B\beta \sin(0) = A\beta \Rightarrow A = 0$$

$$\text{ii) } k \cdot \frac{d\Psi(L)}{dx} + h \cdot \psi(L) = 0,$$

$$-k \cdot B\beta \sin(\beta L) + h \cdot B \cos(\beta L) = 0 \Rightarrow$$

$$k \cdot \beta \sin(\beta L) = h \cdot \cos(\beta L) \Rightarrow \beta \tan(\beta L) = \frac{h}{k}$$

Let  $\gamma = \beta \cdot L$ , then

$$\gamma \cdot \tan(\gamma) = \frac{h L}{k} = Bi_L \quad (3.41)$$

Here,  $Bi_L$  is a Biot number based on  $L$ . Eq. (3.41) can be satisfied by multiple values of  $\gamma$ ,  $\gamma_l$ , and

$$\gamma_l \cdot \tan(\gamma_l) = Bi_L \quad (3.42)$$

Where  $\gamma_l$  is the positive  $l^{\text{th}}$  root of Eq. (3.42): the first five root of this equation for a range of  $Bi_L$  are given in Table 3.1. In this context, it should be noted that the corresponding infinite series solutions, as given later in Eqs. (3.50), (3.51), (3.54), and (3.57), converge very rapidly, and the results obtained with the summation of the first five terms in these series are within 0.01% of the exact values.

Table 3.1: First five roots,  $\gamma_l$ ,  $l=1-5$ , of the equation 3.42.

$B_i$	$\gamma_1$	$\gamma_2$	$\gamma_3$	$\gamma_4$	$\gamma_5$
0.000	0.0000	3.1416	6.2832	9.4248	12.5664
0.002	0.0447	3.1422	6.2835	9.4250	12.5665
0.004	0.0632	3.1429	6.2838	9.4252	12.5667
0.006	0.0774	3.1435	6.2841	9.4254	12.5668
0.008	0.0893	3.1441	6.2845	9.4256	12.5670
0.010	0.0998	3.1448	6.2848	9.4258	12.5672
0.020	0.1410	3.1479	6.2864	9.4269	12.5680
0.040	0.1987	3.1543	6.2895	9.4290	12.5696
0.060	0.2425	3.1606	6.2927	9.4311	12.5711
0.080	0.2791	3.1668	6.2959	9.4333	12.5727
0.100	0.3111	3.1731	6.2991	9.4354	12.5743
0.200	0.4328	3.2039	6.3148	9.4459	12.5823
0.300	0.5218	3.2341	6.3305	9.4565	12.5902
0.400	0.5932	3.2636	6.3461	9.4670	12.5981
0.500	0.6533	3.2923	6.3616	9.4775	12.6060
0.600	0.7051	3.3204	6.3770	9.4979	12.6139
0.700	0.7506	3.3477	6.3923	9.4983	12.6218
0.800	0.7910	3.3744	6.4074	9.5087	12.6296
0.900	0.8274	3.4003	6.4224	9.5190	12.6375
1.000	0.8603	3.4256	6.4373	9.5293	12.6453
1.500	0.9882	3.5422	6.5097	9.5801	12.6841
2.000	1.0769	3.6436	6.5783	9.6296	12.7223
3.000	1.1925	3.8088	6.7040	9.7240	12.7966
4.000	1.2646	3.9352	6.8140	9.8119	12.8678
5.000	1.3138	4.0336	6.9096	9.8928	12.9352
6.000	1.3496	4.1116	6.9924	9.9667	12.9988
7.000	1.3766	4.1746	7.0640	10.0339	13.0584
8.000	1.3978	4.2264	7.1263	10.0949	13.1141
9.000	1.4149	4.2694	7.1806	10.1502	13.1660
10.000	1.4289	4.3058	7.2281	10.2003	13.2142
15.000	1.4729	4.4255	7.3959	10.3998	13.4078
20.000	1.4961	4.4915	7.4954	10.5117	13.5420
30.000	1.5202	4.5615	7.6057	10.6543	13.7085
40.000	1.5325	4.5979	7.6647	10.7334	13.8048
50.000	1.5400	4.6202	7.7012	10.7832	13.8666
100.000	1.5552	4.6658	7.7764	10.8871	13.9981

In terms of  $\gamma_l$ , the solution for  $\Psi(x)$  is

$$\Psi(x) = B_l \cos\left(\frac{\gamma_l \cdot x}{L}\right) \quad (3.43)$$

At this stage, the solution for  $\Gamma(t)$  is obtained. Equation (3.38) is first rearranged in the following form:

$$\frac{1}{\Gamma} d\Gamma = -\alpha\beta^2 dt \quad (3.44)$$

Integration of both sides of this equation gives

$$\Gamma(t) = Ce^{-\alpha\beta^2 t} \quad (3.45)$$

This solution ensures that  $\Gamma(t)$  decays to zero as  $t \rightarrow \infty$ . Recombining these solutions, the multiple solutions to  $X(x,t)$  are obtained:

$$X(x,t) = C_l \cos\left(\frac{\gamma_l \cdot x}{L}\right) \cdot e^{-\alpha\left(\frac{\gamma_l}{L}\right)^2 t} \quad (3.46)$$

Since every linear combination of these solutions is also a solution, the following linear combination gives a general solution to  $X(x,t)$ :

$$X(x,t) = \sum_{l=1}^{\infty} C_l \cos\left(\frac{\gamma_l \cdot x}{L}\right) \cdot e^{-\alpha\left(\frac{\gamma_l}{L}\right)^2 t} \quad (3.47)$$

This general expression for  $X(x,t)$  satisfies Eq. (3.26) and the corresponding boundary conditions. To determine the constants  $C_l$ , the initial condition is used:

$$\text{at } t = 0, X=1 \Rightarrow 1 = \sum_{l=1}^{\infty} C_l \cos\left(\frac{\gamma_l \cdot x}{L}\right) \quad (3.48)$$

Multiplying this equation by  $\cos\left(\frac{\gamma_m x}{L}\right)$  and integrating the results from 0 to L gives:

$$\int_0^L \cos\left(\frac{\gamma_m x}{L}\right) dx = \sum_{l=1}^{\infty} C_l \int_0^L \cos\left(\frac{\gamma_m x}{L}\right) \cdot \cos\left(\frac{\gamma_l x}{L}\right) dx$$

The right-hand side of this equation is non-zero only when  $m = l$ , as the cosine function is orthogonal. Thus,

$$\begin{aligned} \Rightarrow \int_0^L \cos\left(\frac{\gamma_l x}{L}\right) dx &= C_l \int_0^L \cos^2\left(\frac{\gamma_l x}{L}\right) dx \\ \Rightarrow \frac{L}{\gamma_l} \sin\left(\frac{\gamma_l x}{L}\right) \Big|_0^L &= C_l \left( \frac{L}{2 \cdot \gamma_l} \left(\frac{\gamma_l x}{L}\right)^L + \frac{1}{2 \cdot \gamma_l} \left(\sin \frac{2 \cdot \gamma_l x}{L}\right)^L \right) \\ \Rightarrow \frac{1}{\gamma_l} \sin(\gamma_l) &= C_l \left( \frac{\gamma_l}{2 \cdot \gamma_l} + \frac{1}{2 \cdot \gamma_l} \sin(2 \cdot \gamma_l) \right) \end{aligned}$$

$$\Rightarrow \frac{1}{\gamma_l} \sin(\gamma_l) = \frac{C_l}{\gamma_l} \left( \frac{\gamma_l}{2} + \frac{1}{2} \sin(2 \cdot \gamma_l) \right)$$

Thus,

$$C_l = \frac{4 \sin(\gamma_l)}{2 \cdot \gamma_l + \sin(2 \cdot \gamma_l)} \quad (3.49)$$

Therefore, the solution for  $X(x,t)$  is

$$X(x,t) = \sum_{l=1}^{\infty} C_l \cdot e^{-\alpha \left( \frac{\gamma_l}{L} \right)^2 t} \cdot \cos\left( \frac{\gamma_l x}{L} \right) \quad (3.50)$$

In this equation,  $\gamma_l$  and  $C_l$  are given by Eqs. (3.42) and (3.49), respectively.

Similarly, the solution for  $Y(y,t)$  is

$$Y(y,t) = \sum_{m=1}^{\infty} C_m \cdot e^{-\alpha \left( \frac{\gamma_m}{M} \right)^2 t} \cdot \cos\left( \frac{\gamma_m y}{M} \right) \quad (3.51)$$

Where  $\gamma_m$  and  $C_m$  are given by, respectively:

$$\gamma_m \cdot \tan(\gamma_m) = Bi_M = \frac{h \cdot M}{k} \quad (3.52)$$

$$C_m = \frac{4 \sin(\gamma_m)}{2 \cdot \gamma_m + \sin(2 \cdot \gamma_m)} \quad (3.53)$$

Similarly, the solution for  $Z(z,t)$  is

$$Z(z,t) = \sum_{n=1}^{\infty} C_n \cdot e^{-\alpha \left( \frac{\gamma_n}{N} \right)^2 t} \cdot \cos\left( \frac{\gamma_n z}{N} \right) \quad (3.54)$$

Where  $\gamma_n$  and  $C_n$  are given by, respectively:

$$\gamma_n \cdot \tan(\gamma_n) = Bi_N = \frac{h \cdot N}{k} \quad (3.55)$$

And  $C_n$  by

$$C_n = \frac{4 \sin(\gamma_n)}{2 \cdot \gamma_n + \sin(2 \cdot \gamma_n)} \quad (3.56)$$

Finally, substitution of Eqs. (3.50), (3.51) and (3.54) into Eq. (3.24) gives:

$$\theta(x,y,z,t) = \left[ \sum_{l=1}^{\infty} C_l e^{-\alpha \left( \frac{\gamma_l}{L} \right)^2 t} \cos\left( \frac{\gamma_l x}{L} \right) \right] \left[ \sum_{m=1}^{\infty} C_m e^{-\alpha \left( \frac{\gamma_m}{M} \right)^2 t} \cos\left( \frac{\gamma_m y}{M} \right) \right] \left[ \sum_{n=1}^{\infty} C_n e^{-\alpha \left( \frac{\gamma_n}{N} \right)^2 t} \cos\left( \frac{\gamma_n z}{N} \right) \right] \quad (3.57)$$

Where  $\gamma_l, C_l, \gamma_m, C_m, \gamma_n,$  and  $C_n$  are given by Eqs. (3.42), (3.49), (3.52), (3.53), (3.55) and (3.56), respectively. This is the analytical solution to the test problem.

The finite volume method described in Section 3.2 was used to solve this test problem, and the numerical results obtained were checked against the analytical solution given in Eq. (3.57). Results were obtained for copper ( $k = 399 \text{ W/m}^2\text{-}^\circ\text{C}$ ;  $\rho = 8933 \text{ Kg/m}^3$ ;  $c_p = 383 \text{ J/kg-}^\circ\text{C}$ ) with extents of  $0 \leq x \leq 0.0381 \text{ m}$ ,  $0 \leq y \leq 0.003175 \text{ m}$ , and  $0 \leq z \leq 0.0127 \text{ m}$ , and several different values of the Biot number,  $Bi_{L_{ch}}$ , ranging from 0.002 to 10.0. Checks were done with several different spatial grids and time steps. Sample results obtained for  $h_{av,specified} = 350 \text{ W/m}^2\text{-}^\circ\text{C}$ , which yields  $Bi_{L_{ch}} = 0.002$ , with the following spatial grids and time steps are shown in Figure 3.5: 10 and 30 control volumes in the  $x$  direction; 4 and 12 control volumes in the  $y$  direction; 10 and 30 control volumes in the  $z$  direction; and  $\Delta t = t_{ch} / NSTEP$ , with  $NSTEP$  equal to 100, 200, 300, 400, and 500. Here,  $t_{ch} = (\rho c_p Volume) / (h A_{surf})$ .

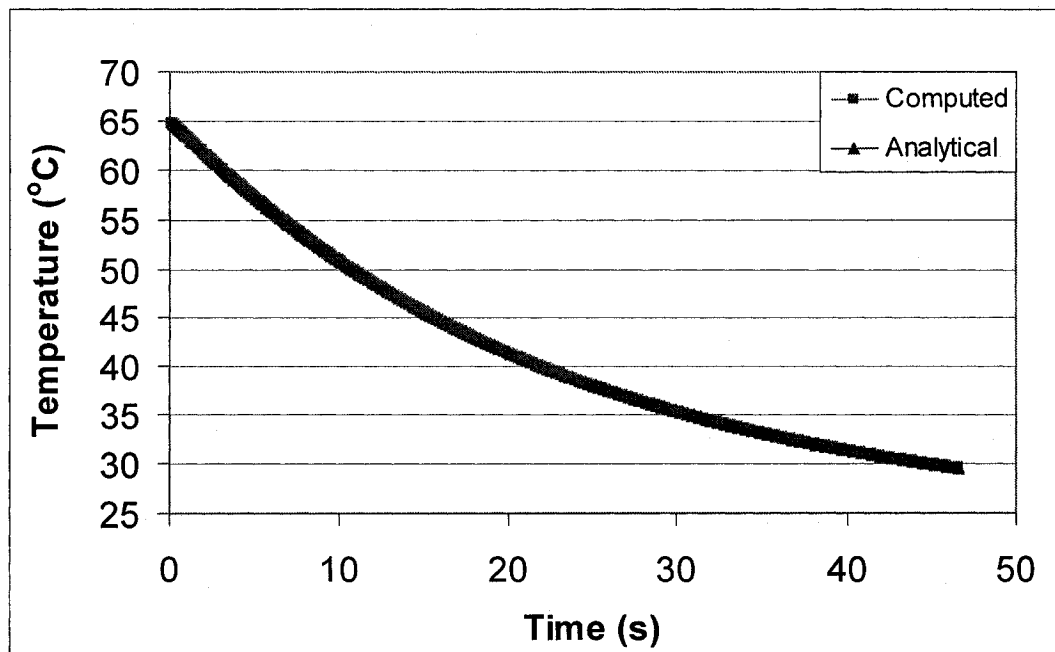


Figure 3.5: Temperature at the center for a grid of 30, 12, and 30 control volumes in the  $x$ ,  $y$ , and  $z$  directions, respectively, and  $NSTEP$  of 500.

The maximum temperature errors at three different points (one at the center, PT1; one at the top right corner, PT2; and one at the bottom left corner, PT3) are presented in Table 3.2. These results show that with a grid of 30, 12, and 30 control volumes in the  $x$ ,  $y$ , and  $z$  directions, respectively, and  $NSTEP$  of 500, the errors (absolute percentage difference between the numerical solution and the corresponding analytical solution obtained with the first five roots to Eqs. (3.42), (3.52), and (3.55)) are less than 0.05 %.

Table 3.2: Maximum absolute percentage error between the numerical solution and the corresponding analytical solution at three different positions.

Grid	NSTEP	Max % Error @ PT1	Max % Error @ PT2	Max % Error @ PT3
10x4x10	100	0.207	0.206	0.204
10x4x10	200	0.104	0.103	0.102
10x4x10	300	0.069	0.069	0.068
10x4x10	400	0.052	0.052	0.051
10x4x10	500	0.041	0.041	0.041
30x12x30	100	0.208	0.207	0.205
30x12x30	200	0.104	0.104	0.102
30x12x30	300	0.069	0.069	0.068
30x12x30	400	0.052	0.052	0.051
30x12x30	500	0.042	0.042	0.041

### 3.3.2 Numerical Assessment of the Lumped Parameter Technique

As was stated earlier in this chapter, in each experimental run, for the central metal portion of each of the test plates, the Biot number ( $Bi = h_{av} L_{ch} / k_{solid}$ ;  $L_{ch} = Vol / A_{surface}$ ) is expected to be less than 0.1: thus, the lumped parameter analysis (details are provided in Chapter 5) would be expected to be valid [Incropera and DeWitt (2002)]. However, the central metal portion of each test plate has plastic portions on each side (see Figure 3.1), and for these plastic portions, the Biot number is not less than 0.1 in all cases. Thus, to establish the applicability of the lumped parameter analysis even under these

circumstances, the strategy described in Section 3.1 (last paragraph) was used with  $h_{av,specified} = 220 \text{ W/m}^2\text{-}^\circ\text{C}$  (the highest expected value of the average heat transfer coefficient in the experiments), the effective density, the effective thermal conductivity, the effective specific heat at constant pressure, the dimensions of both the metal and the plastic portions, the uniform initial temperature of these portions, and the temperature of the flowing air as inputs.

The numerical simulations were done with a calculation domain that includes half of central metal section and one of the two ertalyte end-sections of the test plates: with respect to the notation in Figure 3.1,  $0 \leq x \leq 0.0762 \text{ m}$ ;  $0 \leq y \leq 0.003175 \text{ m}$ ;  $0 \leq z \leq 0.0127 \text{ m}$ . Based on the discussions in Section 3.3.1 of the validation of the computer program, this calculation domain was discretized using the following grid, which had uniform control volume extents in the  $x$ ,  $y$ , and  $z$  directions: 60 control volumes in the  $x$  direction; 12 control volumes in the  $y$  direction; and 24 control volumes in the  $z$  direction. The assessment was done with brass ( $k \approx 100 \text{ W/m-}^\circ\text{C}$ ;  $\rho \approx 8530 \text{ kg/m}^3$ ; and  $c_p \approx 0.380 \text{ J/kg-}^\circ\text{C}$ ), the central metal section with lowest thermal conductivity, in comparison to the other two, made of aluminium and copper: this was done in order to work with the highest value of Biot number ( $Bi_{L_{ch}}$ ). The effective properties of the ertalyte were set to the following values, based on inputs provided by the supplier:  $k \approx 0.29 \text{ W/m-}^\circ\text{C}$ ;  $\rho \approx 1410 \text{ kg/m}^3$ ; and  $c_p \approx 1.208 \text{ J/kg-}^\circ\text{C}$ .

The results of this numerical assessment of the applicability of the lumped parameter analysis are given in Figures 3.6, and 3.7, and in Tables 3.3. These results show that it is indeed valid to use the lumped parameter analysis to process the experimental data and obtain the time-mean average heat transfer coefficients on the central metal portions of the test plates.

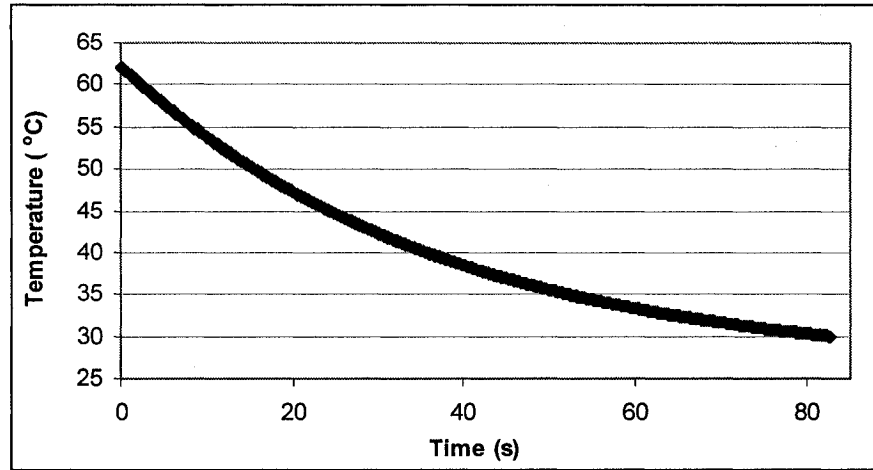


Figure 3.6: Temperature results for unsteady, three-dimensional heat conduction in a brass bar of rectangular cross-section: grid of 60x12x24 control volumes;  $NSTEP = 600$ ;  $h_{av,specified} = 220 \text{ W/m}^2\text{-}^\circ\text{C}$ ; and  $T_{initial} = 62^\circ\text{C}$ .

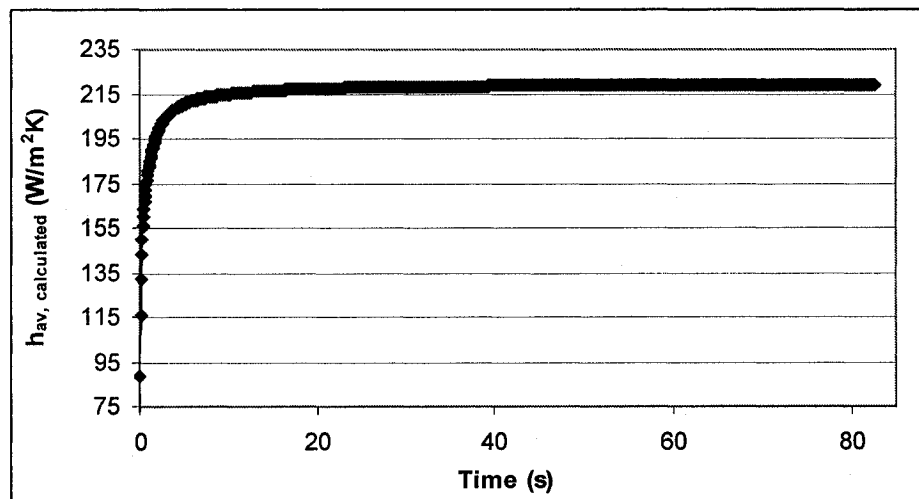


Figure 3.7: Average heat transfer coefficient calculated for unsteady, three-dimensional heat conduction in a brass bar of rectangular cross-section: grid of 60x12x24 control volumes;  $NSTEP = 600$ ;  $h_{av,specified} = 220 \text{ W/m}^2\text{-}^\circ\text{C}$ ; and  $T_{initial} = 62^\circ\text{C}$ .

Table 3.3: Results for a grid of 60x12x24 control volumes and  $NSTEP = 600$ .

Material	Bi	$h_{av, specified} \text{ (W /m}^2 \text{ K)}$	$h_{av, calculated} \text{ (W /m}^2 \text{ K)}$	%diff
Brass	5.080E-03	220.000	218.916	0.49

## Chapter 4. Experimental Apparatus and Techniques

The majority of the experimental apparatus used in this work was originally designed and built by McBrien (1986) and then modified by Candanedo (2003). However, for completeness, a description of the entire experimental set-up is provided in this chapter: descriptions of the sections designed and constructed by McBrien (1986) and Candanedo (2003) are provided, but kept very concise; the parts of the setup and the techniques specific to this research are described in detail.

### 4.1 OVERVIEW OF THE EXPERIMENTAL APPARATUS

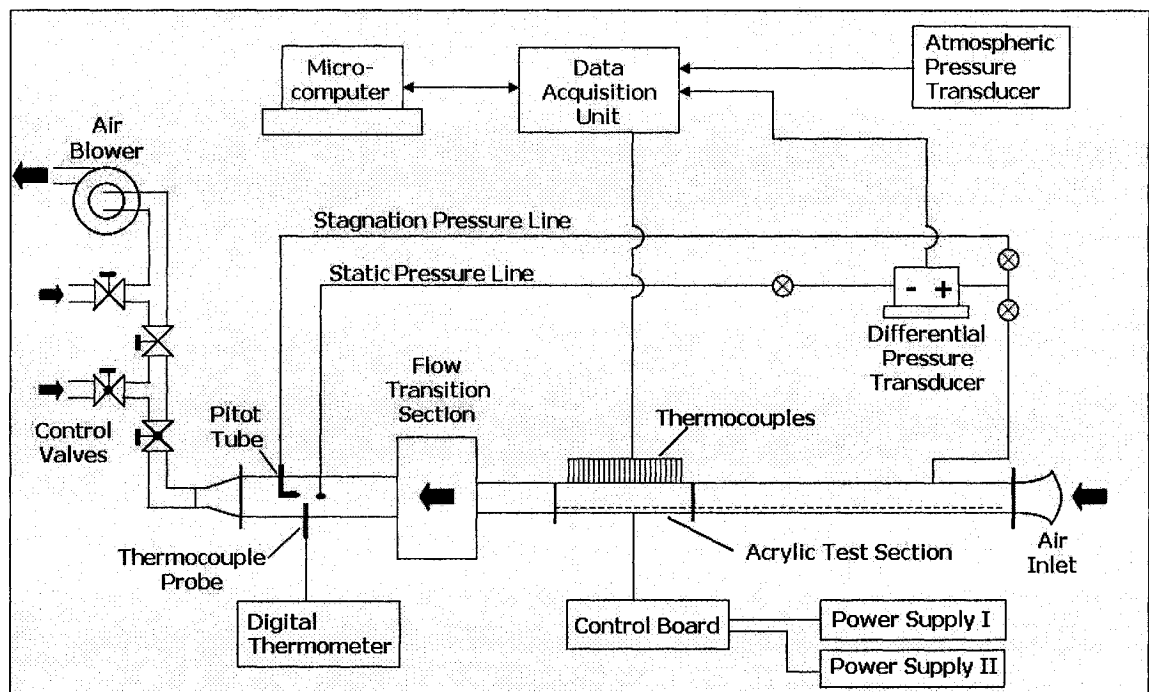


Figure 4.1: Schematic illustration of the experimental apparatus.

The experimental apparatus used in this work is schematically presented in Figure 4.1. It consists of the following main sections: (i) an air inlet section; (ii) an aluminum test section in which wall static pressure distributions can be measured; (iii) an acrylic test section, designed and constructed in this work for determining the average heat transfer coefficients from heated plates in the spatially-periodic fully-developed flow regime; (iv) a flow transition section; (v) a flow metering section; (vi) a flow control,

generation, and exhaust section; and (vii) data acquisition and processing system. Details of these elements and procedures are concisely presented in this chapter.

## 4.2 AIR INLET SECTION

As was mentioned in Chapter 1, this work is focused on heat transfer measurements with individual plates in the spatially-periodic fully-developed flow regime. Therefore, the air inlet section is not a critical element with respect to the experimental results of interest in this study. Nevertheless, in the interest of possible extensions of this work to developing flows and heat transfer, it is noted here that McBrien (1986) designed the air inlet section by scaling down the dimensions of the air inlet section of a low-speed wind tunnel designed and constructed by the late Professor Barry G. Newman and used in the Aerodynamics Laboratory of the Department of Mechanical Engineering at McGill University. A photograph of the air inlet section of the experimental apparatus used in this work is given in Figure 4.2.

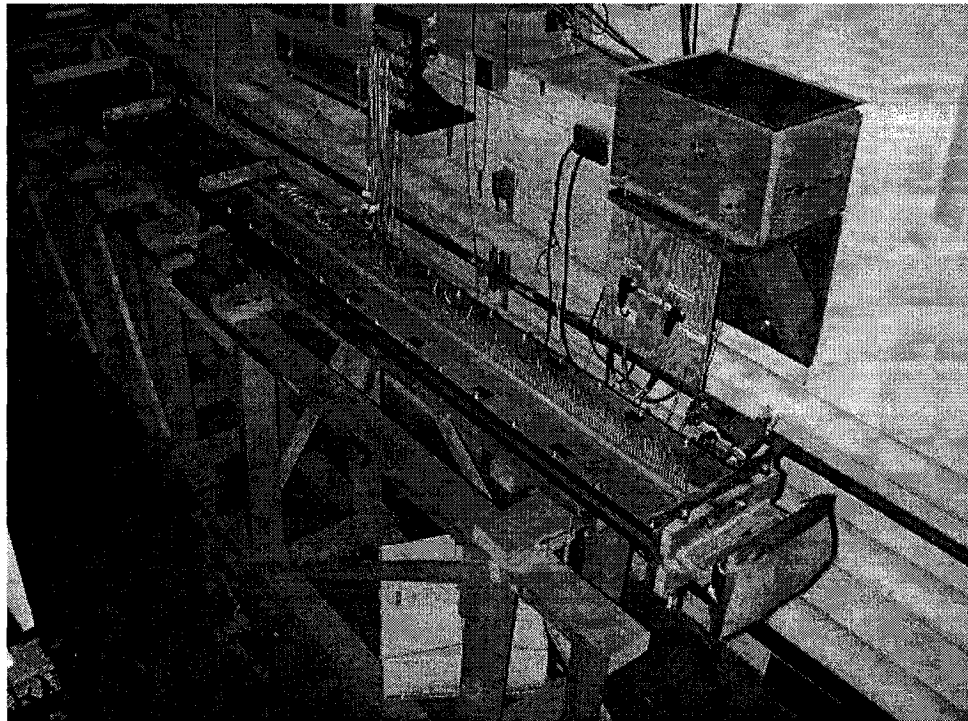


Figure 4.2: Photograph of the air inlet section, the aluminium test section, and the acrylic test section of the experimental apparatus used in this work.

## 4.3 TEST SECTIONS

### 4.3.1 Geometric Configuration

The two test sections, one made of aluminum and the other of acrylic, are straight rectangular cross-section ducts that can be configured with interrupted-plate inserts, as shown schematically in Figure 4.3, or without these inserts. The walls of the first test section are made of aluminium and instrumented for wall static pressure measurements. The walls of the subsequent test section are made of clear acrylic (Lexan). The dimensional and dimensionless geometrical details of these sections are given in Table 4.1, in terms of the notations provided in Figure 4.3.

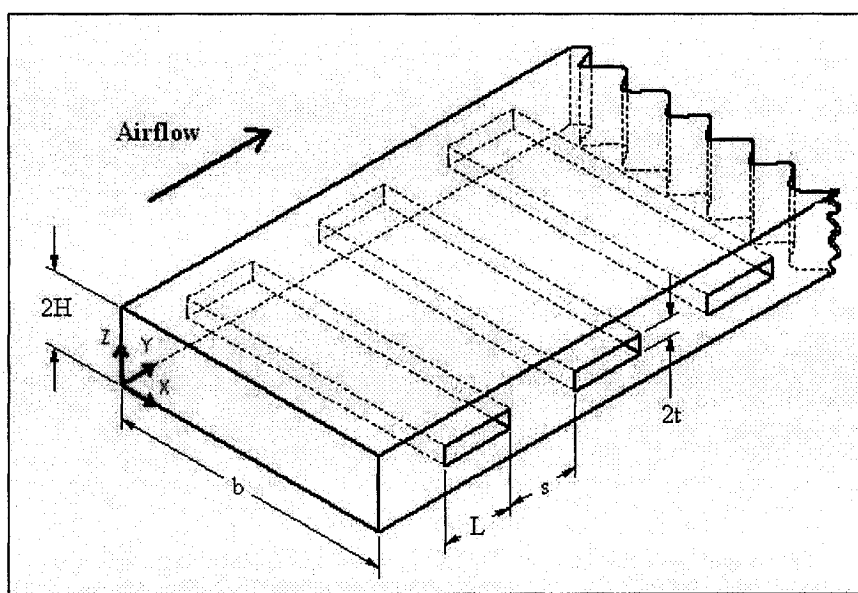


Figure 4.3: Schematic illustration of a portion of the test section and related notation.

The uncertainties in the measured lengths reported in Table 4.1 are all less than  $\pm 0.10$  mm. The aspect ratio,  $\lambda$ , used in this work ensures essentially two-dimensional flow over the central region 80% (at least) of the duct cross-section, as established by the surface flow visualization studies of McBrien (1986). The values of the geometric parameters  $L^*$  and  $s^*$  presented in this table, are representative of those found in the cores of compact heat exchangers [Kays and London (1984)]. However, the value of  $t^*$  used here is more than double that typically used in compact heat exchangers [Kays and London (1984)]. This value of  $t^*$  was used in this work as thinner heated plates could

not be machined and instrumented using the facilities available in the Mechanical Engineering Department of McGill University. Furthermore, the goal in this work is not to obtain data directly applicable to the design of compact heat exchangers, but rather to obtain accurate data on turbulent forced convection heat transfer phenomena that are akin to those encountered in the cores of offset-fin heat exchangers, at least qualitatively. If this objective is met, then this data would be useful in testing and refining mathematical models and numerical solution methods for computer simulations of such heat transfer phenomena: these computational methods could then be used to simulate turbulent forced convection heat transfer over thinner plates than those employed in this study, and also aid in the design of actual heat exchanger cores.

Table 4.1: Cross-sectional and modular dimensions of the test sections.

<b>b</b> (mm)	<b>2H</b> (mm)	<b>L</b> (mm)	<b>2t</b> (mm)	<b>s</b> (mm)
152.67	25.18	25.21	6.36	25.59

<b>D<sub>h</sub></b> (mm)	<b>λ</b> (mm)	<b>L*</b> (mm)	<b>t*</b> (mm)	<b>s*</b> (mm)
152.67	25.18	25.21	6.36	25.59

The rectangular interrupted-plate duct geometry is uniformly (or faithfully) maintained from the first plate of the aluminium test section through to the last plate in the acrylic test section. The total length of the aluminium test section is 1 524 mm, which allowed this portion of the flow passage to be configured with 30 geometrically similar modules in the main flow direction. The length of the acrylic test section is 609.6mm, which allowed another 12 geometrically similar modules. This ensures that spatially-periodic fully-developed flow prevails over the last 18 modules of the aluminium test section, as was established in the earlier experimental works of McBrien and Baliga (1988) and Candanedo et al. (2003), and all modules of the acrylic test section for the parameters investigated in this work. The interrupted-plates were made of precision-ground steel, except for the six instrumented plates that were used in the heat transfer studies; details of these six instrumented plates are given later in this chapter. All plates had sharp square edges.

### **4.3.2 Details of the Aluminium Test Section**

The aluminium test section is a straight rectangular duct with interrupted-plate inserts, akin to those schematically illustrated in Figure 4.3, and with a total of 221 static pressure taps along the axial centreline of its top plate. Brass mating tubes attached to the static pressure taps on the outside surface of the top plate were connected by vinyl tubes (Scanivalve model # Vinl-063) to a mechanical multiplexor (Scanivalve model # 48D9) with a solenoid drive and controller (Scanivalve model # CTRLR10(P)/S2-26).

Flanges and rubber gaskets at the upstream and downstream ends of this section allow it to be mated appropriately to the air inlet section and the acrylic test section, respectively. Black vinyl electrical tape (10 mm wide), the variety that is commonly sold in electrical stores, was used on the outer surface of this test section to seal the edges along which its outer component plates mate. This design proved to be effective and convenient in making these edges of the test section air-tight: the black electrical tape can be applied and taken off quite easily, and it leaves almost no residue on the outside surfaces of the plates.

For additional details related to the design and construction of this test section, the reader is referred to the work of Candanedo (2003).

### **4.3.3 Details of the Acrylic Test Section**

The acrylic test section is mated to the downstream end of the aluminium test section and these two sections together create a uniform interrupted-plate rectangular duct. The acrylic test section consists of a 609.6 mm (24 inch nominal) long Plexiglas (Lexan) outer casing of rectangular cross-section. The top surface of this casing includes a lid that can be removed after the entire duct has been assembled and connected to the flow circuit: this removable lid facilitates the removal and insertion of the plates used in the heat transfer experiments. The Plexiglas sidewalls were designed with a total of six holes each to allow the insertion of specially designed jigs that allow the insertion of thermocouples and heating wire (see Figures 4.4 and 4.5).

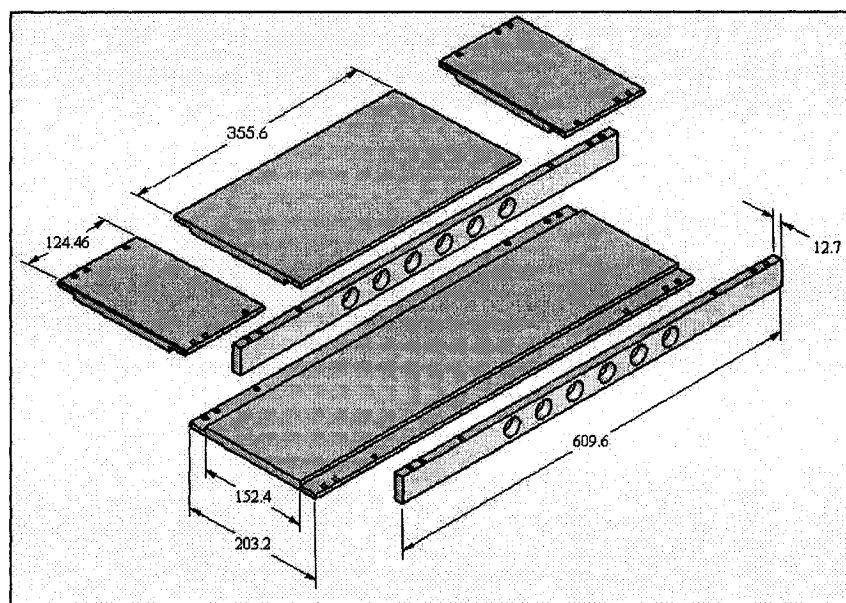


Figure 4.4: Outer casing of the acrylic test section.

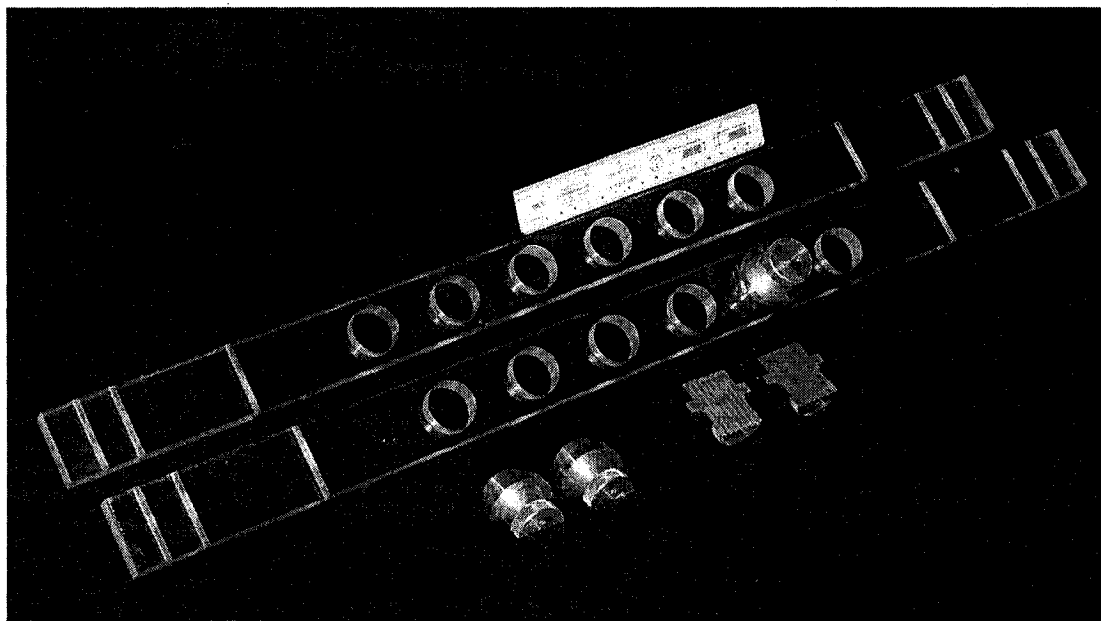


Figure 4.5: Acrylic side walls and jigs.

The inner side walls of the acrylic test section, labelled here as aluminium fixtures, were made up of upper and lower parts, as shown in Figure 4.6, and designed to allow the insertion of the interrupted plate array within the Plexiglas frame, as shown in

Figure 4.7. Three pairs of such aluminium fixtures were installed in the acrylic test section. Together, these fixtures allowed the insertion of twelve interrupted-plates.

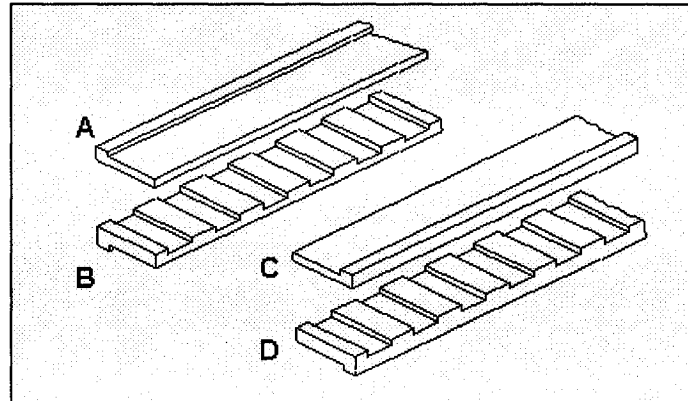


Figure 4.6: Schematic of the aluminium fixtures.



Figure 4.7: Photograph of the aluminium fixtures and plates.

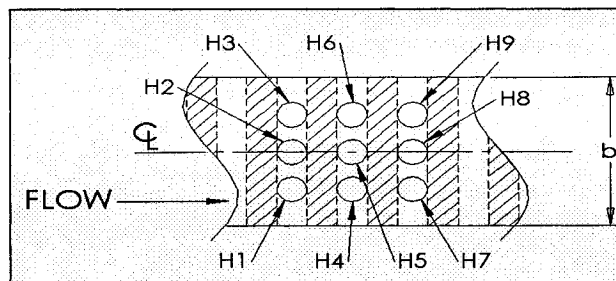


Figure 4.8: Holes in the top plate of the acrylic test section, designed to allow insertion of a jig that holds and positions the single hot-wire probe or other jigs that seal the holes; the shaded areas are top views of the interrupted-plate inserts.

Hot wire measurements were also performed in this section as a part of research work [Lamoureux, Camargo, and Baliga (2005)] that complements the work undertaken in this thesis. In this complementary research work, another removable lid was designed with a total of nine holes through which a special jig for holding the single hot-wire probe could be inserted, as shown in Figure 4.8. Full details of these single hot-wire measurements are available in Lamoureux, Camargo, and Baliga (2005).

#### 4.3.4 Details of the Test Plates

The test plates were designed, fabricated, instrumented, assembled, and used for the heat transfer measurements. A total of six such test plates were installed in the acrylic test section. Each of these plates is made up of three sections: a central metal section that is an assembly of two thinner plates held together with miniature screws; and two end sections were made out of ertalyte, a low thermal conductivity plastic that is easy to machine. The central metal sections of two of these test plates were made of brass; those of another two were made of aluminum; and those of the remaining two were made of copper. The ertalyte plates are used to render the heat losses from the ends of the central metal section negligible compared to that from its lateral surfaces to the flowing air. In the bottom plate of the central metal section, seven grooves, each 1/16" wide and 1/32" deep, were milled, and the ertalyte end plates had corresponding holes drilled into them, to accommodate the thermocouples and the electrical heating wire. The ertalyte end plates were connected to the assembled central metal section using six 1/32" diameter, 1/4" long precision stainless steel dowel pins.

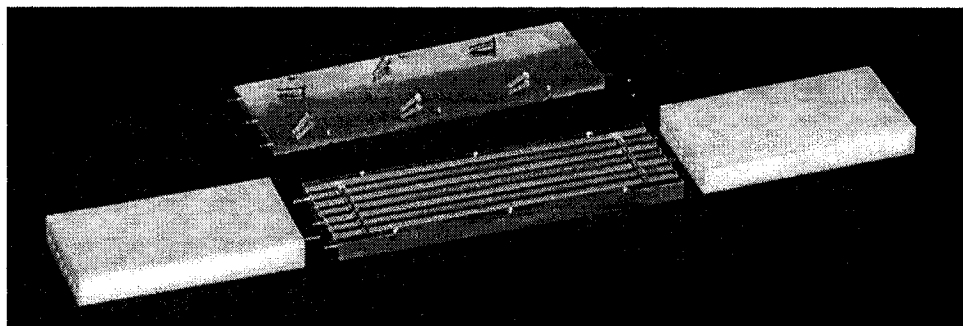


Figure 4.9: A photograph of the various components of a test plate with a central section made of aluminium.

A photograph showing the various parts of a test plate with an aluminum central section is given in Figure 4.9. A technical drawing showing the details and precise dimensions of an ertalyte end plate and the central metal section of the test plates is given in Figure 4.10. These details and dimensions apply to all six test plates.

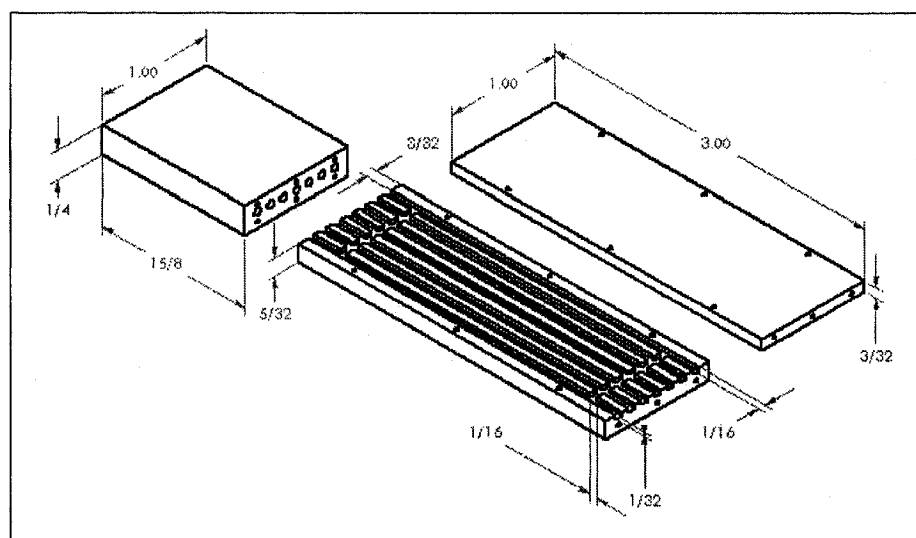


Figure 4.10: Technical drawing showing details and dimensions (in inches) of the central metal section and an ertalyte end section of a test plate.

Each of the six test plates was instrumented and assembled as follows: a 30-gage nickel-chromium resistance heating wire was threaded through a flexible woven Fiberglas sleeve tubing and then inserted into four of the seven grooves in the bottom plate of the central metal section; the ends of this heating wires were soldered to two copper wires (hook-up wire 22 AWG); in the remaining three grooves in the bottom plate of the central metal section, 30-gage chromel-constantan type-E thermocouples were installed, at distances of  $\frac{1}{4}$ ,  $\frac{1}{2}$  and  $\frac{3}{4}$  of the metal plate length; a small piece of the Fiberglas sleeve ( $\sim 5$  mm long) was positioned over the thermocouple wire immediately adjacent to the bead, to ensure that the thermocouple wires exposed during the construction of the bead did not contact the metal plate; several small amounts (pools or dots) of epoxy (Omegabond 101) were used to hold the thermocouples in place in the grooves; once the thermocouples and the heating wires were in place; a high-thermal conductivity silicone paste (Omegatherm 201) was applied in the remaining open

spaces in the grooves; and finally, the central metal portion was put together using six miniature machine screws, and the ertalyte end plates were attached to the central metal section, using six miniature dowel pins on each end. A photograph of a test plate with the brass central section just before final assembly is shown in Figure 4.11.

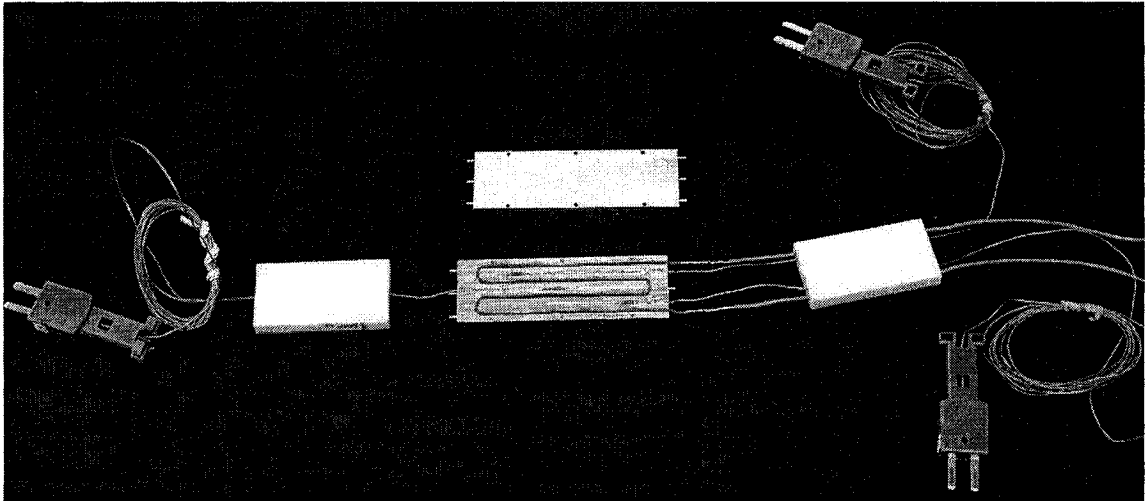


Figure 4.11: A test plate with a brass central section – view of components just before final assembly.

#### 4.3.5 Installation of Test Plates into the Acrylic Test Section

The above-mentioned test plates had to be installed with special care into the acrylic test section in order to obtain reliable and repeatable results. The following procedure was used for this task.

1. The acrylic test section was separated from the rest of the experimental set-up, by loosening and removing the bolts and nuts from the flanges at each end of this test section.
2. The bolts on the longitudinal sides of the acrylic test section were removed, to free the walls of its outer acrylic casing.
3. The acrylic walls were removed leaving only the aluminium fixtures and the precision-ground steel plates [Candanedo (2003)].
4. The screws holding the aluminium fixtures together were loosened in stages and then removed, in a sequence to avoid distortions. Six precision-ground steel plates in the central region of the aluminum fixtures were then removed.

5. The six test plates were then placed in the six slots of the lower fixture that were left open after the removal of the precision-ground steel plates.
6. The acrylic walls were then remounted carefully, passing the thermocouples and heating wire through the holes in the sidewalls (see Figures 4.4 and 4.5). A small steel block was used to properly align the acrylic walls with the aluminium fixtures.
7. Twelve special aluminum jigs, each of a split-cylinder design with milled grooves in one half of the split cylinder, were then used to pass and support the thermocouples and heating wires through the holes in the longitudinal sidewalls of the acrylic test section.
8. To prevent possible air leaks between the inside of the duct and the external ambient, the aforementioned jigs and the lid on the top wall of the acrylic test section were sealed with a removable transparent sealant. This sealant was left to dry overnight (at least 12 hours). A photograph of the test plates installed in the acrylic test section is shown in Figure 4.12
9. Once the aforementioned sealant was dry, the acrylic test section with the installed test plates was reattached to the rest of the experimental rig.
10. The black vinyl electrical tape mentioned in Section 4.3.2 was then used to refresh the airtight seals around all edges of the aluminium test section. The mounted acrylic test section with the installed test plates can be seen in the photograph given in Figure 4.13.

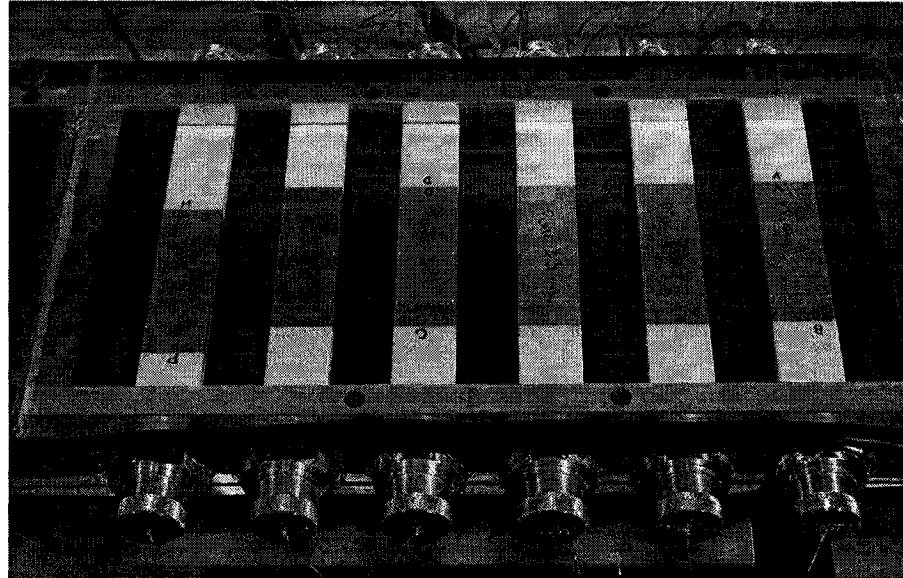


Figure 4.12: Photograph of the test plates installed inside the acrylic test section.

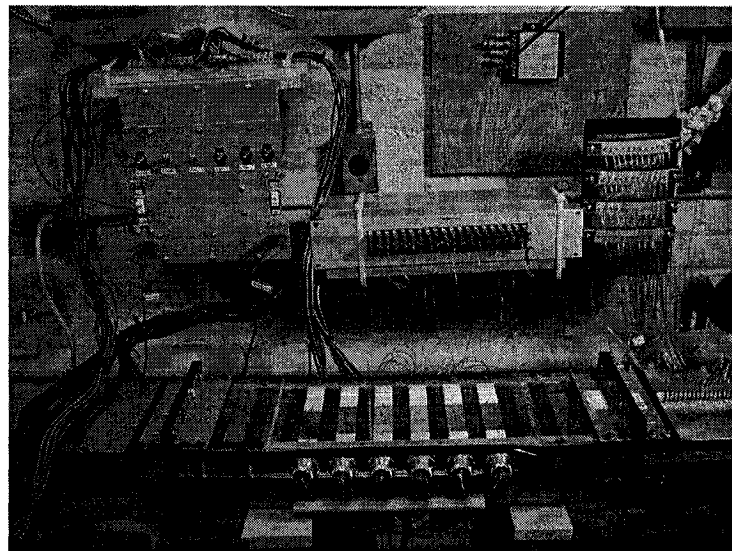


Figure 4.13: Photograph of the acrylic test section with the installed test plates mounted in the overall experimental rig.

#### 4.4 FLOW TRANSITION SECTION

The flow transition section allows the air leaving the test sections of rectangular cross-section and the interrupted plates to adjust to essentially fully-developed turbulent flow in the circular cross-section of the flow measuring section.

As can be seen in Figure 4.1, the flow transition section is attached to the end of the interrupted-plate rectangular duct test section on one side and to the upstream end of the flow metering section on the other side. This section consists of two parts: (i) a flow development section, and (ii) a diffuser box. The flow development section is a continuation of the straight rectangular test section, but without the interrupted-plate inserts. This flow development section reduces the effects of the interrupted plates in the test sections.

The diffuser box is a hard wood (mahogany) box of the following nominal dimensions: 0.61 m. length, 0.3 m. height, and 0.3 m. width. The function of the diffuser box is to redistribute the air leaving the rectangular redevelopment duct to enter the circular cross-section flow metering tube axisymmetrically. Additional design and construction details of the flow transition section are given in McBrien (1986).

#### **4.5 FLOW MEASUREMENT SECTION**

The flow measurement section is a 63.22 mm internal diameter and 1320.8 mm long straight acrylic pipe. This section is attached at its upstream end to the diffuser box of the flow transition section, and at its downstream end to a flexible tube that is a part of the flow generation and control section.

The airflow rate was obtained using measurements from a traversing pitot tube and static pressure measurements from two taps located on the wall of the acrylic tube. The pitot tube was installed 854 mm (roughly 13.5 acrylic tube diameters) downstream from the inlet of the acrylic pipe. A vernier calliper attached to the pitot tube allows the vertical position to be determined to an accuracy of  $\pm 0.02$  mm.

#### **4.6 FLOW GENERATION AND CONTROL SECTION**

The flow generation and control section is schematically illustrated in Figure 4.1. A centrifugal-type, constant speed, blower (Regenair R7100A) driven by a 10 HP AC motor at a rotor speed of 3450 rpm was used in suction mode to generate the air flow in the apparatus. This air blower is connected to the downstream end of the flow measurement section by a flexible, steel spiral reinforced, rubber tube with one control

valve and a one shut-off-valve (a ball valve). For the flow control, a gate valve was preferred to a globe valve in order to avoid large pressure drops. A by-pass duct fitted with a second flow-control valve and shut-off valve were used for improving airflow control and also to allow complete airflow shut-off in the test sections with out starving the air blower of air. The complete airflow shut-off in the test sections permitted the removal and reassembly of the interrupted-plates, and also the insertion and removal of the hot-wire probe in the above-mentioned complementary research work, without altering settings of the airflow-control valves.

#### **4.7 PRESSURE MEASUREMENTS**

Measurements of the atmospheric, static, and dynamic pressures were required in this investigation.

An electronic barometer (Vaisala PTA 427), accurate to  $\pm 0.1\%$ , was used to measured the atmospheric pressure. Static gauge pressures in the flow metering section and all other differential pressures less than 1 kPa were measured using an integral Barocel (capacitance type) pressure transducer (Datametrics, Model 590-D-1kPa-2Q8-VIX-4D), accurate to  $\pm 0.3$  Pa. Both instruments were connected to a laboratory-grade D.C. power supply. The output voltage was measured with an accuracy of  $\pm 3 \mu V$ , using a data acquisition system described in Section 4.10. An inclinable reservoir-type manometer (Airflow Developments, Type 5) with resolution of 0.01 kPa, and accuracy of  $\pm 1\%$ , was used for measurements of differential pressures grater than 1 kPa.

#### **4.8 AIR FLOW RATE MEASUREMENTS**

The air flow rates in this work were determined from measurements of time-mean stagnation pressures, static pressure, and temperature measured in the flow metering section.

The ten-point log-linear rule [Winternitz and Fischl (1957)] was first used to obtain a correlation for the air flow rate in the particular experimental rig used in this work. Using this ten-point log-linear rule, for each air flow rate of interest, the average time-mean axial velocity in the flow-tube cross-section,  $\overline{W}$ , was first obtained as follows: (i)

determining the time-mean dynamic pressure (stagnation pressure – static pressure) at ten specific points (picked in accordance with the ten-point log-linear technique) in the cross-section of the flow tube; (ii) calculating the values of  $W$ , the time-mean-velocity component normal to the cross-section of the flow tube, at the aforementioned ten specific points; and (iii) taking the arithmetic-mean of these 10 individual values of  $W$ .

Local values of time-mean dynamic pressure,  $P_{dyn}$ , were determined from measurements of time-mean average wall static pressure,  $P_{static}$ , and time-mean stagnation pressure,  $P_{stag}$ , at the point of interest.

$$P_{dyn} = P_{stag} - P_{static} \quad (4.1)$$

The ten-point log-linear rule of Winternitz and Fischl (1957) was used to determine the location of the  $P_{stag}$  measurements points. The  $y^*$  coordinates (distance along a diameter from the flow-tube inner surface) of these measuring points are given below:

$$\begin{aligned} y_1^* &= 0.019D & y_6^* &= 0.639D \\ y_2^* &= 0.077D & y_7^* &= 0.783D \\ y_3^* &= 0.153D & y_8^* &= 0.847D \\ y_4^* &= 0.217D & y_9^* &= 0.924D \\ y_5^* &= 0.361D & y_{10}^* &= 0.981D \end{aligned} \quad (4.2)$$

The individual values of  $W$  were calculated from:

$$W = \left( \frac{2P_{dyn}}{\rho} \right)^{1/2} \quad (4.3)$$

In accordance with the ten-point log-linear technique, the cross-sectional average value,  $\bar{W}$ , in the flow tube is obtained by taking the arithmetic-mean of the individual values of  $W$  measured at the ten  $y^*$  locations given in Eq. (4.2). The measured values of air temperature and time-mean average wall static pressure in the flow-metering cross-section were used with standard air tables [Eckert and Drake (1972)] to obtain the corresponding time-mean density and dynamic viscosity of air.

The values of  $W$  and  $\bar{W}$  obtained using the ten-point log-linear rule at flow rates corresponding to several Reynolds numbers of interest were then used to develop a calibration curve relating  $\bar{W}$  to the value of  $W$  at only one specific point. Details of this

correlation can be found in Appendix A. The errors in the air flow rates determined using this calibration curve with reference to those obtained using the full ten-point-log-linear technique were all less than 0.35%. Thus, throughout all of the remaining experiments, the dynamic pressure measurement was measured at only the one aforementioned specific point in the flow-tube cross-section, the corresponding value of  $W$  was determined using Eq. (4.3), and the  $\bar{W}$  vs.  $W$  calibration curve was used to determine  $\bar{W}$  and the air flow rate.

For each experimental run, the values of  $\bar{W}$  and the air density were used to calculate the time-mean mass flow rate through the entire length of the flow circuit:

$$\dot{m} = \rho * \bar{W} * A_f \quad (4.4)$$

where  $A_f$  is the cross-sectional area of the flow metering section.

The Reynolds number in the test section (Kays & London definition) was calculated from:

$$Re = \frac{\bar{W}_{min-cs} \cdot D_H \cdot \rho}{\mu} \quad (4.5)$$

where,

$$D_H = \frac{4A_{c-s-min} \Lambda}{A_{wetted}} \quad (4.6)$$

and,  $\Lambda$ ,  $A_{c-s-min}$  and  $A_{wetted}$  are given by Equation (2.20), and  $\bar{W}_{min-cs}$  is the time-mean average axial velocity in the test section in its minimum cross-sectional area.

#### 4.9 TEMPERATURE MEASUREMENTS

The air temperature inside the flow metering section was measured using a 30-gage chromel-constantan (type-E) thermocouple with Teflon insulation (made from Omega TT-E-30 thermocouple wire). This thermocouple was connected to an electronic digital thermometer (Omega Model 410A) with an internal electronic reference junction and a temperature resolution of 0.1°C.

Twenty-three chromel-constantan type-E 36-gage prefabricated thermocouples (obtained from Omega Ltd.) were calibrated and used in this work. Eighteen of these

thermocouples (three per plate) were used to monitor the temperature inside the test plates; one was placed at the flow entrance; one was used to monitor the laboratory ambient temperature; and three were placed on the acrylic lid on the top wall of the acrylic test section. These thermocouples were calibrated in the temperature range of  $5^{\circ}\text{C} - 75^{\circ}\text{C}$  using a constant-temperature bath (Neslab RTE 221) and a quartz thermometer (Hewlett-Packard 2804A; precision calibrated to  $\pm 0.005^{\circ}\text{C}$  over the temperature range from  $0^{\circ}\text{C}$  to  $95^{\circ}\text{C}$ , using a platinum resistance thermometer as a secondary standard, at the Physics Division of the National Research Council in Ottawa). The uncertainties in the temperature readings provided by the calibrated thermocouples were determined to be less than  $\pm 0.02^{\circ}\text{C}$ . The procedure used for the calibration of the thermocouples is presented and discussed in Appendix B of this thesis.

#### **4.10 DATA ACQUISITION SYSTEM AND PROCEDURES**

The thermocouples were connected to a data acquisition unit (Hewlett-Packard, Model 3497A). This system was connected to a personal computer. The data acquisition was realized with a computer program written using the VEE OneLab (Agilent Technologies) software.

Once the measurements of the temperatures were initiated for each test plate (just after the electrical power to the test plate is shut off and the plate starts cooling), data from all thermocouples were acquired and saved periodically, at a 6.5-second time interval, on the hard disk of the personal computer. The input voltage and current supplied to the electrical heater inserted inside the test plate were measured using suitable multimeters (HP 3478A). These voltages and current measurements were also acquired and saved using the aforementioned data acquisition system, and time-mean values of these measurements were used later to calculate the corresponding power inputs to the test plate *prior* to the aforementioned cooling phase (when there is no power input to the test plate).

The above-mentioned temperature data, acquired and stored during the cooling of the test plate in each experimental run, are used in a lumped parameter analysis to obtain the time-mean average convection heat transfer coefficient on the outer surface of the

central metal portion of plate. This analysis and the results are presented and discussed in Chapter 5.

#### 4.11 SUMMARY OF THE OVERALL EXPERIMENTAL PROCEDURE

This section presents a step-by-step summary of the procedure that was used to run the final experiments for each desired flow rate.

1. Power-up all electrical systems, turn on the blower, and allow all systems to warm up at least two hours, in order to ensure their stable operation.
2. Zero the Barocel pressure sensor.
3. Place the traversing pitot tube in the flow measurement section at a distance equal to 96.054 mm. Using the calibration curve given in Appendix A, and the local stagnation pressure at this point, the average velocity in the flow-tube cross-section coincident with this measurement location can be obtained with an accuracy of  $\pm 0.35\%$ .
4. Using the above-mentioned HP-VEE computer software that was written/modified for these experiments, obtain an estimate of the dynamic (stagnation minus static) pressure needed to achieve the desired Reynolds number in the test section. Adjust the flow control valves so that the voltage output of Barocel pressure sensor is within  $\pm 0.001V$  of the value corresponding to this estimated pressure difference value.
5. Using that same software, record measurements of the atmospheric pressure. Also, measure, average, and record (save) 30 different “zero pressure” (ZP) readings of the Barocel.
6. Using the Barocel and the computer software, measure the difference between the atmospheric pressure ( $P_{atm}$ ) and the pressure at the reference static pressure tap ( $P_{ref}$ ), and also the difference between  $P_{ref}$  and the static pressure at the flow measurement section ( $P_{stat}$ ). Then, correct the recorded  $P_{ref}$  and  $P_{stat}$  value by subtracting ZP. When exceeding 1kPa, the differential pressures are measured manually using an inclinable alcohol-in-glass manometer, as discussed earlier in this chapter, and entered into the computer code.

7. Record the ambient air temperature and also the temperature of the air in the flow metering section. Note: The variations in air flow temperature observed during the individual experiments were negligibly small (all less than  $\pm 0.2$  °C).
8. Turn on the electrical power to one of the test plates (the one chosen for the particular experimental run), and adjust/set the level of the power needed to attain a desired steady-state temperature.
9. Wait for steady-state (about 50 minutes): when the temperature variation at the center of the plate is less than  $\pm 0.05$ °C over a period of 10 minutes, it is assumed that steady-state conditions prevail.
10. Turn off the electrical power supply to the test plate and acquire/record the temperatures of the test plate as it cools, using the above-mentioned HP-VEE OneLab computer software.
11. Feed the recorded experimental data as inputs to a lumped parameter analysis and calculate the corresponding time-mean average convection heat transfer coefficient on the outer surface of the central metal section of the test plate. This analysis and the related calculations were done using Excel (a spreadsheet computer program). The results are presented in Chapter 5.

## Chapter 5. Results and Discussions

The results of the experimental investigation of turbulent forced convection from individual plates in the spatially-periodic region of air flows in a straight rectangular duct with interrupted-plate inserts (see Figures 1.3 and 4.3, and also Table 4.1) are presented in this chapter.

### 5.1 DETERMINATION OF AVERAGE HEAT TRANSFER COEFFICIENT

For each of the final experimental runs, the average heat transfer coefficients on the outer surface of the central metal section of the chosen test plate (located in the spatially-periodic fully-developed air flow) was determined using a lumped parameter analysis (LPA). In this LPA, the spatial variation of temperature inside the central metal portion of the test plate is considered negligible; so the test-plate temperature varies only with time. The inputs to this LPA were the time-varying temperatures recorded by the central thermocouple embedded in the metal section of the test plate as it cooled under the influence of the air flow over it. This LPA is based on the following assumptions:

1. The Biot number is less than 0.1:  $Bi = h_{av} L_{ch} / k_{metal} < 0.1$ , with  $L_{ch} =$   
(Volume/Surface Area)<sub>metal section</sub>

2.  $q_{edge\ surfaces} \ll q_{conv.\ lateral\ surface}$

$$\text{where } q_{conv.\ lateral\ surface} = A_{metal\ lateral\ surface} h_{av} [T_{plate} - T_{air}]$$

3.  $q_{surface\ radiation} \ll q_{surface\ conv.}$

$$\text{where } q_{surface\ radiation\ max} = \epsilon_{max} \sigma A_{metal\ lateral\ surface} \left[ T_{plate\ abs}^4 - T_{duct\ wall\ abs}^4 \right]$$

4.  $T_{duct\ wall} \approx T_{air}$

Based on these assumptions, the LPA give the following solution:

$$\Phi = \frac{T_{plate} - T_{air}}{T_{plate, t=0} - T_{air}} = \exp \left\{ - \left( \frac{A_{metal\ lateral\ surface} h_{av}}{(\rho_{metal} c_{p, metal})_{effective} Volume_{metal}} \right) t \right\} \quad (5.1)$$

This equation can be recast as follows:

$$\Phi = \exp \left\{ - \left( \frac{A_{metal\ lateral\ surface} h_{av}}{\sum (m \cdot c_p)_{constituents, metal}} \right) t \right\} \quad (5.2)$$

For each experimental run, the measured (temperature versus time) data were first converted to  $(-\ln(\Phi))$  versus time) data. Then the average heat transfer coefficient on the outer surface of the central metal section of the chosen test plate was determined by using the slope of a least-squares fitted straight line passing through the origin and the  $(-\ln(\Phi))$  versus time) data points in the following equation:

$$h_{av} = \frac{slope * \sum (m \cdot c_p)_{constituents, metal}}{A_{metal\ lateral\ surface}} \quad (5.3)$$

Experimental results that support the validity of the LPA and some of the aforementioned assumptions, demonstrate the repeatability of the measured data, and establish the spatial periodicity of  $h_{av}$  in the acrylic test section are presented in the following sections, along with the final  $Nu_{av}$  vs.  $Re$  results.

## 5.2 UNCERTAINTIES IN THE EXPERIMENTAL RESULTS

The uncertainties in the experimental results were estimated using the methods elaborated by Kline and McClintock (1953) and Moffat (1985). A detailed description of the uncertainty analysis for flows similar to those investigated in this work is given in the work of McBrien (1989); thus, it is not repeated here. The uncertainties in the reported values of Reynolds number, as defined in Eq. (4.5), were estimated to be less than  $\pm 2\%$  in all of the experimental runs undertaken in this work.

The flow measurements were performed several times during the course of each experimental run, following the procedure outlined in Section 4.11. The deviation in the Reynolds number from the average value for any particular nominal value was determined to be less than  $\pm 2\%$  for all the flow rates considered in the experiments. For the average heat transfer coefficients and the corresponding Nusselt numbers, as defined

in Eq. (2.22), the uncertainties were estimated to be less than  $\pm 4\%$  of the reported values.

### 5.3 CHARACTERISTICS OF THE RESULTS

#### 5.3.1 Spatially-Periodic Fully-Developed Flow Regime

As was mentioned earlier, spatially-periodic fully-developed flow was expected to prevail over at least the last 15 geometric modules in the aluminium test section and all of the geometric modules in the acrylic test section (in which the heat transfer experiments were conducted). Initial tests confirmed that this expectation was indeed met, as shown by the sample results presented in Table 5.1.

Table 5.1: Average heat transfer coefficient obtained individually for two successive test plates, each with a brass central section.

Re	$h_{av}$ (W/m <sup>2</sup> K)		% Difference in $h_{av}$ values
	1st Brass Plate	2nd Brass Plate	
2054.01 $\pm 1.74\%$	37.30	37.46	-0.43
7965.74 $\pm 0.48\%$	83.58	84.14	-0.67
29282.11 $\pm 1.19\%$	211.77	213.92	-1.018

Previous experimental works have also confirmed the existence of the spatially-periodic fully-developed regime for flows in interrupted-surface ducts, based on time-mean heat transfer data, wall static pressure measurements, and surface flow visualization studies: examples, include the works of Cur and Sparrow (1979), Joshi and Webb (1987), McBrien and Baliga (1988), and Candanedo et al. (2003). In addition, the recent experimental work of Lamoureux, Camargo and Baliga (2005) demonstrated, for the first time, that turbulence statistics, such as ensemble-averaged power spectral densities, also display spatially-periodic behaviour in such fully-developed flows.

### 5.3.2 Lumped Parameter Assumption

The applicability of the lumped parameter analysis (LPA) was numerically assessed by simulating three-dimensional unsteady heat conduction inside the test plate using a finite-volume method, as was described in Chapter 3. The *maximum* absolute percentage difference between the prescribed average heat transfer coefficient and the average heat transfer coefficient calculated was less than 1%. As expected, the test plates with the central section made of copper are the ones for which the LPA is most applicable, since they have the lowest values of Biot number. Furthermore, if the LPA applies, the ( $-\ln(\Phi)$  versus time) experimental data points would fall on a straight line. In Figure 5.1, this data for an experimental run done using a test plate with the central section made of brass and for  $Re = 30,000$  (highest Biot number) are plotted: as can be seen, they fall very well on a straight line and thus confirm the applicability of the LPA.

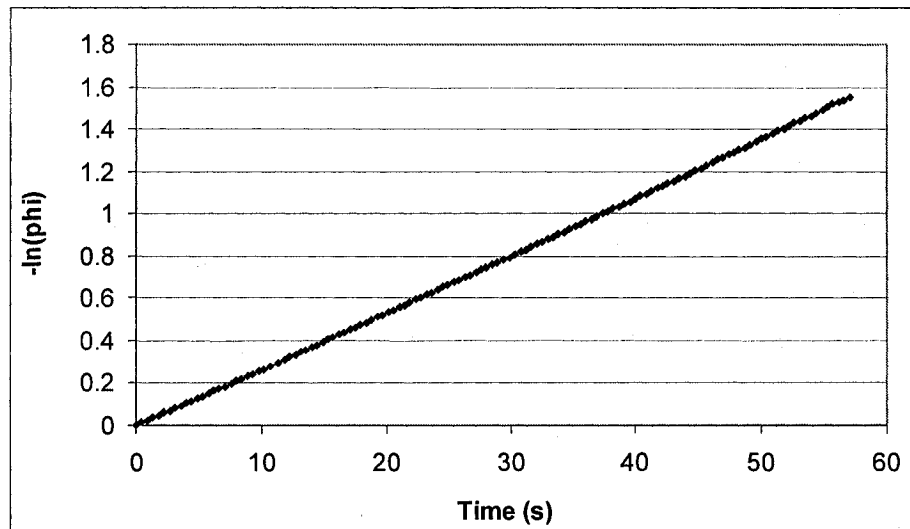


Figure 5.1: Experimental data for  $Re = 30\ 000$  obtained using a test plate with the central section made of brass.

### 5.3.3 Two-Dimensionality Over the Central Region

The average heat transfer coefficient obtained over the surface of the central metal sections of the test plates is also representative of the average value of the heat transfer coefficient over the cross-sectional perimeter of these section, over at least the entire length of these sections: in other words, the time-mean fluid flow and heat transfer over

the test plates is essentially two dimensional (with reference to Figure, 1.3, varying with  $x$  and  $z$ , but essentially insensitive to  $y$ ) over at least the length (76.2 mm) of the central metal section of the test plates. This statement is supported by the results of a surface flow visualization study by McBrien (1990) and also by the results of hot-wire measurements conducted by Lamoureux Camargo and Baliga (2005). Furthermore, the second copper test plate is shifted laterally by  $\frac{1}{2}$  inch (12.7 mm) in relation to the other test plates (see Figure 5.2); however, the average heat transfer coefficients obtained with this second copper test plate were essentially the same as those obtained with the other test plates for corresponding values of the Reynolds number: sample values of the average heat transfer coefficient obtained with the first and the second copper test plates are presented in Table 5.2.

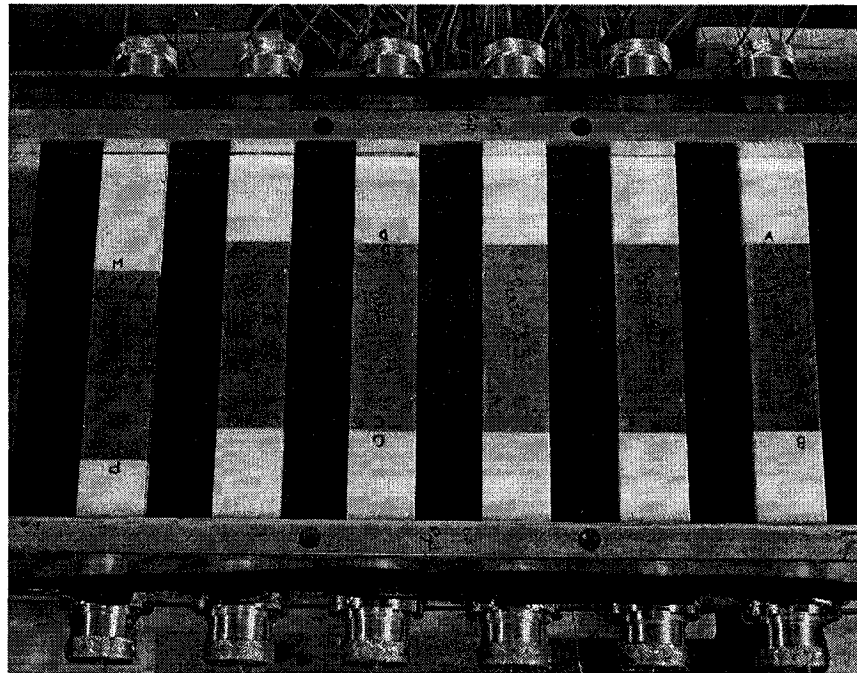


Figure 5.2: Photograph of the test plates installed inside the acrylic test section.

Table 5.2: Sample values of the average heat transfer coefficients obtained using the first and the second copper test plates.

Re	$h_{av}$ (W/m <sup>2</sup> K)		% Difference in $h_{av}$ values
	1 <sup>st</sup> Copper plate	2 <sup>nd</sup> Copper plate	
2039.58 ± 1.40%	37.52	37.52	-8.6E-06
7924.00 ± 0.57%	86.04	86.00	0.041
29282.11 ± 1.19%	217.33	217.48	-0.069

## 5.4 ASSESSMENT OF RADIATION AND END LOSSES

### 5.4.1 Radiation Effects

The maximum difference between the rate of surface radiation heat loss,  $q_{surface, radiation}$ , evaluated with the emissivities given in Table 5.3, and the total power input to the test plates was less than 2.2 % in all of the experimental runs. On the basis of this result, it was assumed that the radiation effects in this investigation were negligible.

Table 5.3: Estimates of the maximum emissivities of the central metal sections of the test plates.

<b>Brass</b>	0.10
<b>Al</b>	0.09
<b>Copper</b>	0.12

Further evidence of the negligible effects of radiation heat losses in this investigation is provided by the results presented in Figure 5.3: the square symbols represent values of the average heat transfer coefficient obtained with recorded temperatures of the test plate in the range 45°C to 30 °C; and the dots represent these values obtained for the same experimental run but with recorded test-plate temperatures in the range 62 °C to 28 °C. The corresponding results from each of the six test plates (two with brass central sections; two with aluminum central sections; and two with copper central sections) are also shown in Figure 5.3. These results show that the average heat transfer coefficient is

essentially insensitive to differences in the aforementioned ranges of test-plate temperatures (percentage difference less than  $\pm 0.44\%$ ), and also independent, for all practical purposes, of the material of the central metal section of the test plates used in this work (emissivities given in Table 5.3). Tabular presentations of the results shown graphically in Figure 5.3 are provided in Appendix C.

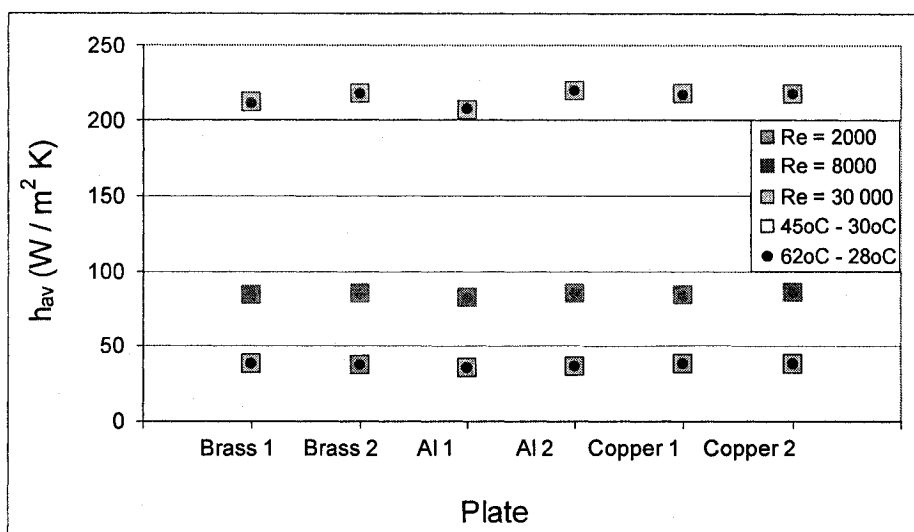


Figure 5.3: Average heat transfer coefficients obtained using each of the six test plates, individually, with two different temperature ranges.

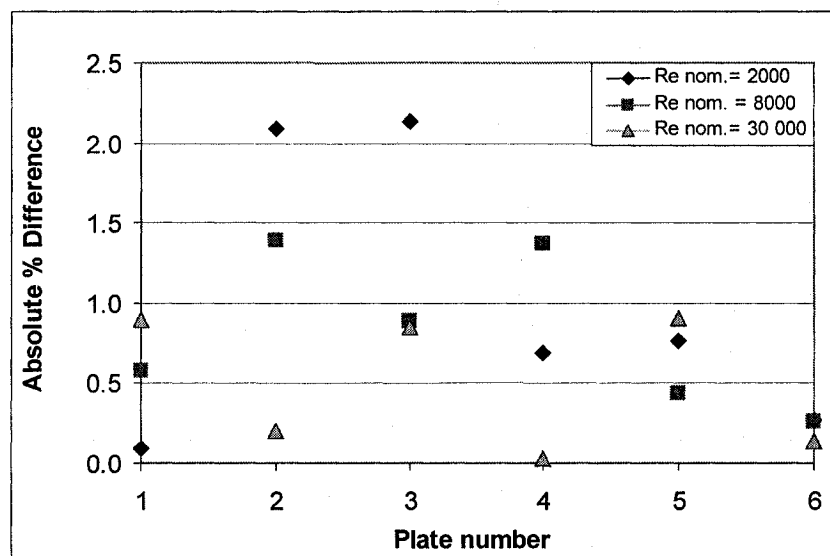


Figure 5.4: Percentage maximum differences between the temperature of the outer surface of the acrylic test section, above the test plates, and the ambient air temperature – sample results.

It should also be noted that numerous tests were undertaken over the course of this investigation to determine the difference between the temperature of the outer surface of the acrylic test section, above the test plates, and the ambient air temperature. A sample of the results of these tests is presented in Figure 5.4. In all cases the absolute difference between the air temperature and the top wall temperature is less than 2.5%.

#### **5.4.2 End Losses**

The graphs presented in Figure 5.3 also show that either the end losses from the electrolyte sections of the test plates are negligible or that they are almost the same for all the plates. To establish that the end losses are indeed negligible, numerical simulations of three-dimensional heat conduction inside the full test plates were performed using the finite volume method and the assessment strategy presented in Chapter 3. These simulations were run with perfect thermal contact and also with infinite thermal contact resistance at the interfaces between central metal section and the electrolyte end sections of the test plates: the maximum absolute difference between the calculated values of the average heat transfer coefficient was found to be less than 1.2%, clearly establishing that the end effects are negligible.

### **5.5 REPEATABILITY OF THE RESULTS**

At least two repeatability tests were performed for the  $h_{av}$  values over each of the six test plates, at three different nominal values of the Reynolds number: 2 000, 8 000 and 30 000. The results are shown in Figure 5.5. The agreement between corresponding results is excellent in all cases: the maximum absolute deviation of the  $h_{av}$  value for any experimental run from that for its repeated run is less than 3.5%. A tabulation of these results is presented in Appendix D.

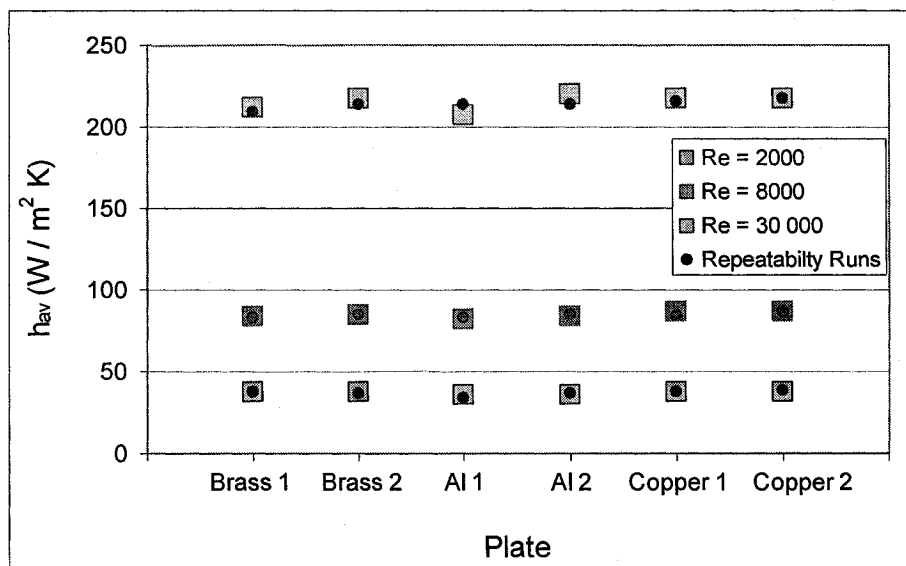


Figure 5.5: Sample results of repeatability tests.

## 5.6 AVERAGE HEAT TRANSFER COEFFICIENT

The final experimental runs to determine the average heat transfer coefficient were carried out with each of the six test plates shown in Figure 5.2, for nine different Reynolds numbers in the range 2 000 to 30 000. As was mentioned in Section 5.5, at least two sets of repeatability tests were undertaken for each test plate, for Reynolds number (nominal values) of 2 000, 8 000 and 30 000. The results are presented in Figure 5.6. *All* of the quantitative data that were used to prepare the graphical presentation of the average heat transfer versus Reynolds number results in Figure 5.6 are presented in tabular form in Appendix E.

Figure 5.7 shows the results obtained using measurements from the first copper test plate (test plate 5 in Figure 5.2). This copper plate provides the best results since it takes the longest to cool and is the one for which the LPA is most applicable. As was expected, the results in Figure 5.7 show that average heat transfer coefficient, and hence the corresponding Nusselt number, increases with the Reynolds number.

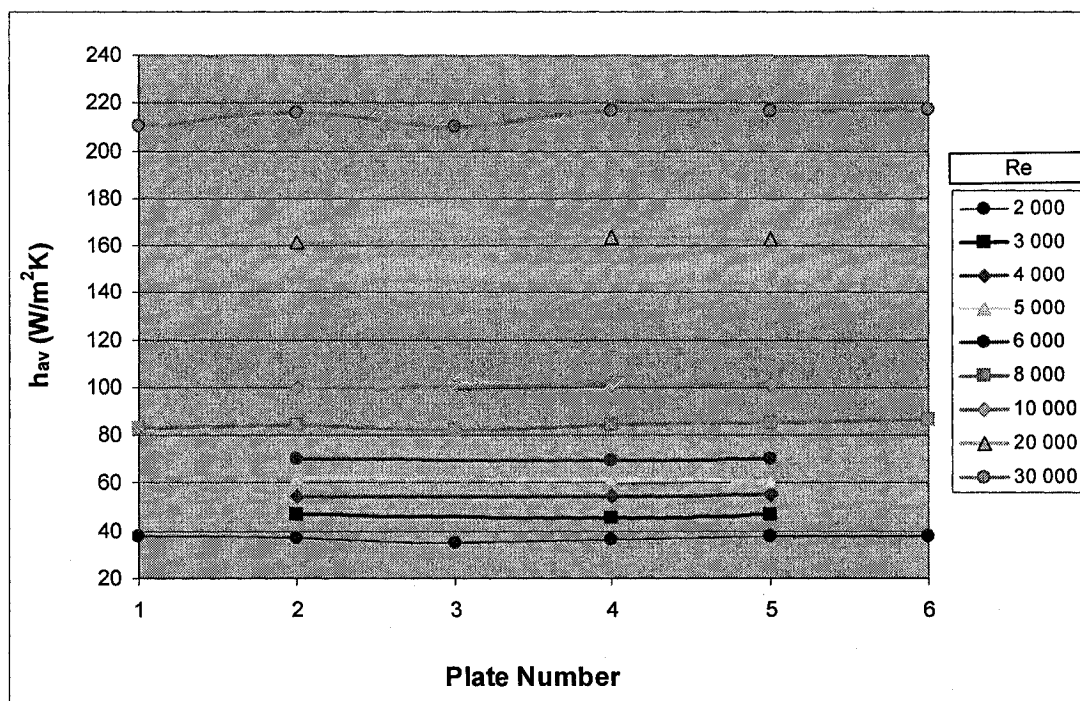


Figure 5.6: Average heat transfer coefficients obtained with six different test plates, for nine different values of Reynolds number.

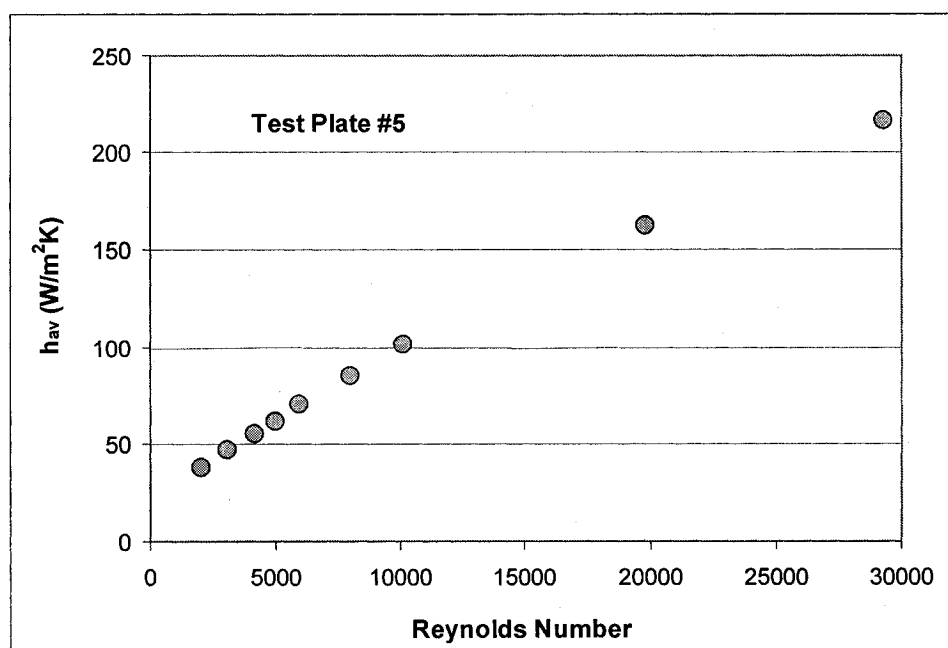


Figure 5.7: Variation of average heat transfer coefficient with Reynolds numbers – results obtained using measurements from the first copper test plate (see Figure 5.2).

## 5.7 CORRELATION FOR AVERAGE NUSSELT NUMBER

Tabular presentations of average Nusselt number results obtained using measurements from the six test plates (labelled test plates 1-6 in Figure 5.2) are provided in Appendix F. From the results obtained using the first copper plate (test plate 5 in Figure 5.2), a correlation was developed for the average Nusselt number as a function of the Reynolds Number (note that the Prandtl number remained essentially unchanged at about 0.7 in all of the experimental runs undertaken in this investigation).

$$\text{Nu}_{av} = (h_{av} D_h / k_{air}) = C * \text{Re}^m \quad (5.4)$$

Where,  $C = 0.25048$  and  $m = 0.6311$

As can be seen from the results given in Table 5.4, Eq. (5.4) correlates the experimental results within  $\pm 7\%$ . Figure 5.8 shows a comparison of the predictions of  $\text{Nu}_{av}$  given by Eq. (5.4) with the experimental results for the first five test plates (see Figure 5.2).

Table 5.4: Comparison of the average Nusselt number values obtained from the proposed correlation, Eq. (5.4), and the corresponding experimental results.

Re	Nu_correl	plate 2		plate 4		plate 5	
		Nu_exp	% diff	Nu_exp	% diff	Nu_exp	% diff
2058.053	30.90381	30.376	1.708	29.617	4.165	30.797	0.347
3057.02	39.67046	38.772	2.265	37.358	5.830	38.455	3.063
4137.991	48.02373	44.771	6.774	44.904	6.497	45.332	5.605
4962.283	53.85765	51.078	5.161	50.704	5.855	50.452	6.324
5946.362	60.37199	57.651	4.508	57.191	5.269	57.353	5.001
7964.013	72.59625	69.429	4.363	69.477	4.297	70.554	2.813
10135.61	84.52889	82.004	2.987	82.909	1.917	83.293	1.463
19799.41	128.9854	132.330	-2.593	135.331	-4.920	132.622	-2.819
29282.11	165.1209	175.492	-6.281	174.944	-5.949	176.671	-6.995

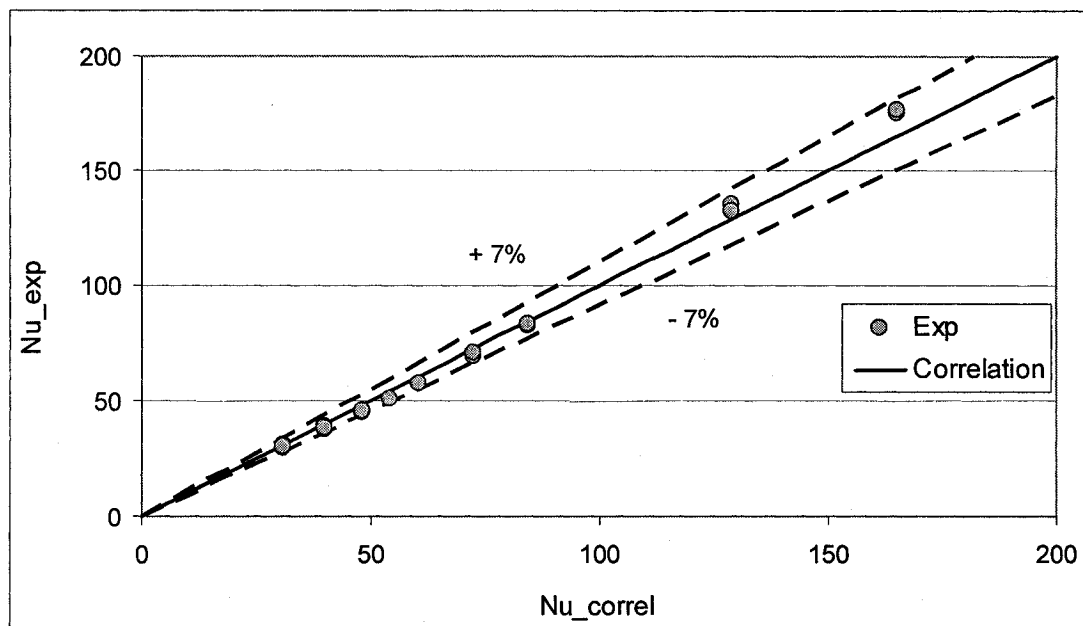


Figure 5.8: Comparison of the average Nusselt number values obtained from the proposed correlation, Eq. 5.4, and the corresponding experimental results.

## Chapter 6. Conclusion

This final chapter contains two main sections: first, the contents and contributions (highlighted by presenting the relevant text in *italics*) of this thesis are concisely reviewed; following that, some recommendations for extensions and improvements of this work are presented.

### 6.1 REVIEW AND CONTRIBUTIONS OF THE THESIS

In chapter 1, the motivation, overall goals, and specific objectives, as well as an overview of the experimental runs and results were presented. A review of published investigations relevant to this work was also given in this chapter.

Chapter 2 was dedicated to the presentation and discussion of the theoretical considerations that were used in the planning of the experimental set-up and the interpretation and presentation of the results. The assumptions used in this work as well as the equations that govern flows of Newtonian fluids, with constant density and viscosity, were introduced and explained. Following that, a short discussion of turbulent flows and their modelling was presented. This discussion pointed out the need for complementary experimental, theoretical, and computational studies to effect improvements of techniques and procedures used in the thermofluid design of interrupted-surface cores of compact heat exchangers. Then, the characteristics of velocity, static pressure, and temperature variations in the spatially-periodic fully-developed region of flows in interrupted-surface geometries were put forward, followed by dimensional analyses related to spatially-periodic fully-developed turbulent flows in straight rectangular ducts with interrupted-plate inserts. In addition, in Chapter 2, the different definitions of the dimensionless parameters that are employed in the literature to characterize spatially-periodic fully-developed turbulent flows akin to those investigated in this work were introduced, and the reasons for using the definitions proposed by Kays and London (1964, 1984) in this work were given.

In Chapter 3, a finite-volume method (FVM) for the simulation of unsteady three-dimensional heat conduction inside a composite solid bar, akin to the test plates used in this research work, was described concisely. The method was formulated by extending

ideas proposed by Patankar (1980). This numerical method was validated using an analytical solution for unsteady three-dimensional heat conduction in a bar of rectangular cross-section, subjected to forced convection on its boundary surfaces. The proposed FVM was used to assess the applicability of the lumped parameter analysis for calculating the average heat transfer coefficients for the experimental measurements. The strategy adopted for this assessment was described in Chapter 3. This FVM was also used to show that the effects of end losses from the central metal section to the plastic (ertalyte) end sections of the test plates were negligible. *For the aforementioned reasons, this FVM method and the proposed assessment strategy are considered to be one of the important contributions of this thesis.*

Descriptions of the experimental apparatus, techniques, and procedures used in this work were provided in Chapter 4. Special attention was given to the new parts and modifications to the original set-up built by McBrien (1986). Six new test plates were designed and constructed for the heat transfer measurements. The acrylic test section was also redesigned, with holes in the side walls and split-design plugs that allowed the thermocouples and heater wires of the test plates to pass through and thus facilitated the insertion of the test plates. *This redesigned acrylic test section as well as the design and construction of the suitably instrumented test plates for the heat transfer measurements are considered one of the key contributions of this work.*

In Chapter 5, the results obtained in this investigation were presented and discussed. A technique, based on the lumped parameter analysis (LPA), for processing the experimental data and obtaining the average heat transfer coefficient on the surface of the central metal section of the individual test plates was described. An assessment of applicability of this LPA technique was provided earlier in Chapter 3. First, in this chapter, it was demonstrated that the experimental set-up and procedures described in Chapter 4 produce results with the following characteristics: two-dimensionality over the central metal section of the test plates; negligible end losses from the ertalyte sections of the test plates; negligible effects of radiation heat loss; and repeatability. It was shown that the average heat transfer coefficients obtained individually with each of the six test plates (see Figure 5.2) are essentially the same for corresponding values of Reynolds number, thereby confirming that spatially-periodic fully-developed conditions

prevailed in the acrylic test section. Results for the average heat transfer coefficients and average Nusselt numbers for individual plates in the Reynolds number range from 2,000 to 30,000 were then presented and discussed. Then a correlation that gives the average Nusselt number as a function of Reynolds number was proposed. This correlation predicts the experimental data within 7%. Tabular presentations of all of the graphical results given in Chapter 5 are given in Appendices E and F, in order to enhance their usefulness as potential checks on (an aids for the refinements of) future mathematical models and numerical solution methods for computer simulations of turbulent flows and heat transfer in geometries similar to those encountered in compact heat exchangers.

*The results and the LPA-based technique presented in Chapter 5, and also the results presented in tables in Appendices E and F, together with the related discussions, are collectively considered the main contribution of this work.*

## **6.2 RECOMMENDATIONS FOR IMPROVEMENTS AND EXTENSIONS OF THIS WORK**

In this work, experiments were carried out for flows of air in a straight rectangular duct with interrupted-plate inserts with the following dimensionless parameters normalized with respect to the full height of the duct: width of the duct cross-section = 6.063; plate length = 1.001; plate thickness = 0.2526; and inter-plate spacing = 1.004. The Reynolds number, based on the Kays and London (1964, 1984) definition, ranged from about 2,000 to 30,000. The capacity of the air blower used in the present investigation limits the upper Reynolds number range to about 65,000, and the capability of the differential pressure transducer limits the lower Reynolds number range. It would be worthwhile to extend modify the apparatus and/or instrumentation to extend these limits, especially at the lower end of the Reynolds number range, so that laminar and transitional (laminar-turbulent) flows could be studied.

Additional work is also required to asses the influence of the geometric parameters on the heat transfer results. It would be useful to perform experiments to obtain results similar to those presented in this thesis, but with different values of the aspect ratio ( $b^*$ ) and nondimensional plate thickness ( $t^*$ ). Such an extension, together with the results

presented here, would enable the formulation of a reliable generalized correlation for the Nusselt number as a function of Reynolds number,  $b^*$ , and  $t^*$ .

Another logical extension would be to investigate spatially-periodic fully-developed heat transfer. In this context, it should be noted that the current experimental set-up allows for all six test plates to be heated and monitored simultaneously.

It would also be useful to study distributions of the heat transfer coefficient on the surface of the test plates. In this context, some of the techniques worth considering include the following: naphthalene sublimation [Cur and Sparrow (1978)]; thin gold film [Bernier and Baliga (1992)]; thermal paints [Jambunathan et al. (1987)]; and interferometry [Bahl and Liburdy (1991); Naylor (2003)].

Visualization of the temperature distribution on the surfaces of the test plates would be another desirable extension of this work, perhaps using liquid crystals sheets or paints. The work of Baughn (1995) would serve as a good starting point for such an extension.

It would also be useful to perform surface flow visualisation experiments. Preliminary surface flow visualization tests were undertaken by Candanedo (2003), using techniques similar to those employed by McBrien (1988) and Aboumansour (2001). However, the results obtained were not repeatable and reliable. Therefore, the aforementioned techniques would have to be improved to enable such an extension.

In closing, the author would like to express her hope that the results and discussions presented in this thesis will be useful in checking and refining mathematical models and numerical simulations of turbulent flows and heat transfer in interrupted-surface passages akin those encountered in compact heat exchangers, and also encourage other students and researchers to undertake some of the above-mentioned extensions.

## References

Aboumansour, E. (2001), "Investigation on Spatially Periodic Fluid Flows in Rectangular Interrupted Plate Ducts", *Honours Thesis*, Department of Mechanical Engineering, McGill University, Montréal, Québec.

Acharya, S., Myrum, T., Qiu, X., and Sinha, S. (1997), "Developing and Periodically Developed Flow, Temperature and Heat Transfer in a Ribbed Duct", *International Journal of Heat and Mass Transfer*, Vol. 40, pp-461-479.

Acharya, S., Dutta, S., and Myrum, T.A. (1998), "Heat Transfer in Turbulent Flow Past a Surface-Mounted Two-Dimensional Rib", *ASME Journal of Heat Transfer*, Vol. 120, pp. 724-734.

Ali, A.H., Kishinami, K., Hanaoka, Y., and Suzuki, J. (1998), "Experimental Study of Laminar Flow Forced-Convection Heat Transfer in Air Flowing Through Offset Plates Heated by Radiation Heat Flux", *International Communications in Heat and Mass Transfer*, Vol. 25, pp. 297-308.

Amon, C.H., and Majumdar, D., Herman, C.V., Mayinger, F., Mikic, B.B., and Sekulic, D. (1992), "Numerical and Experimental Studies of Self-Sustained Oscillatory Flows in Communicating Channels", *International Journal of Heat and Mass Transfer*, Vol. 35, pp. 3115-3129.

Anderson, D.A., Tannehill, J.C., and Pletcher, R.H. (1984), *Computational Fluid Mechanics and Heat Transfer*, New York, McGraw-Hill.

Atkinson, K.N, Drakulic, R., Heikal, M.R., and Cowell, T.A. (1998), "Two- and Three-Dimensional Numerical Models of Flow and Heat Transfer over Louvred Fin Arrays in Compact Heat Exchangers", *International Journal of Heat and Mass Transfer*, Vol. 41, pp. 4063-4080.

Bahl, S. and Liburdy, J.A. (1991), "Measurement of Local Convective Heat Transfer Coefficients using Three-Dimensional Interferometry", *International Journal of Heat and Mass Transfer*, Vol. 34, pp. 949-960.

Baughn, J.W. (1995), "Liquid-Crystal Methods for Studying Turbulent Heat-Transfer", *International Journal of Heat and Mass Transfer*, Vol.16, pp. 365-375.

Baliga, B.R. and Atabaki, N. (2006), "Control-Volume-Based Finite Difference and Finite Element Methods", in *Handbook of Numerical Heat Transfer*, W.J. Minkowycz, E.M. Sparrow, and J.Y. Murthy (Editors), 2<sup>nd</sup> Ed., Chapter 6, John Wiley & Sons, New York.

Batchelor, G.K. (1967), *An Introduction to Fluid Dynamics*, Cambridge University Press, Cambridge, U.K.

Bejan, A. (1984), *Convection Heat Transfer*, J. Wiley, New York (Second Edition, 1995).

Bernier, M.A. and Baliga, B.R. (1992), "Visualization of Upward Mixed-Convection Flows in Vertical Pipes Using a Thin Semitransparent Gold-Film Heater and Dye Injection", *International Journal of Heat and Fluid Flow*, Vol. 13, pp. 241-249.

Bird, R.B., Stewart, W.E., and Lightfoot, E.N. (1960), *Transport Phenomena*, J. Wiley, New York (Second Edition, 2002).

Candanedo, J.A. (2003), "Time-Mean Wall Static Pressure Distributions and Module Friction Factors for Spatially Periodic Fully Developed Flows in Interrupted-Plate Rectangular Ducts", *Master Thesis*, Department of Mechanical Engineering, McGill University, Montreal, Canada.

Candanedo, J.A., Aboumansour, E., and Baliga, B.R. (2003), "Time Mean Wall Static Pressure Distributions and Module Friction Factors for Fully Developed Flows in a Rectangular Duct with Spatially Periodic Interrupted-Plate Inserts", *Proceedings of the 2003 ASME International Mechanical Engineering Congress and Exposition*, Paper # IMECE2003-43969, pp. 1-10, Washington, D.C.

Cebeci, T. (2002), *Convective Heat Transfer*, Horizons Publications, New York.

Churchill, S.W. (1988), *Viscous Flows: the Practical Use of Theory*, Butterworths, Boston.

Cowell, T.A., Heikal, M.R., and Achaichia, A. (1995), "Flow and Heat Transfer in Compact Louvered Fin Surfaces", *Experimental Thermal and Fluid Science*, Vol. 10, pp.192-199.

Cur, N. and Sparrow, E.M. (1978), "Experiments on Heat Transfer and Pressure Drop for a Pair of Colinear, Interrupted Plates Aligned with the Flow", *International Journal of Heat and Mass Transfer*, Vol. 21, pp. 1069-1080.

Cur, N. and Sparrow, E.M. (1979), "Measurements of Developing and Fully Developed Heat Transfer Coefficients along a Periodically Interrupted Surface", *ASME Journal of Heat Transfer*, Vol. 101, pp. 211-216.

Currie, I.G. (1974), *Fundamental Mechanics of Fluids*, McGraw-Hill, New York (Third Edition, 2003).

Deissler, R.G. (1998), *Turbulent Fluid Motion*, Taylor & Francis, Philadelphia, PA.

Dejong, N.C. and Jacobi, A.M. (1997), "An Experimental Study of Flow and Heat Transfer in Parallel-plate Arrays: Local, Row-by-Row and Surface Average Behavior", *International Journal of Heat and Mass Transfer*, Vol. 40, p. 1365-1378.

- Dejong, N.C., Zhang, L.W., Jacobi, A.M., Balachandar S., and Tafti, D.K. (1998), "A Complementary Experimental and Numerical Study of the Flow and Heat Transfer in Offset Strip-Fin Heat Exchangers", *ASME Journal of Heat Transfer*, Vol. 120, pp. 690-698.
- Dubrovsky, E.V. and Vasiliev, V.Y. (1988), "Enhancement of Convective Heat Transfer in Rectangular Ducts of Interrupted Surfaces", *International Journal of Heat and Mass Transfer*, Vol. 31, pp. 807-818.
- Dubrovsky, E.V. (1995), "Experimental Investigation of Highly Effective Plate-Fin Heat Exchanger Surfaces", *Experimental Thermal and Fluid Science*, Vol. 10, pp. 200-220.
- Eckert, E.R.G. and Drake, R.M. (1971), *Analysis of Heat and Mass Transfer*, McGraw-Hill, New York.
- Fehle, R. and Klas, J. (1995), "Investigation of Local Heat Transfer in Compact Heat Exchangers by Holographic Interferometry", *Experimental Thermal and Fluid Science*, Vol. 10, pp. 181-191.
- Ferziger, J.H. and Peric, M. (1996), *Computational Methods for Fluid Dynamics*, Springer, New York (Second Edition, 1999).
- Fox, R.F. and McDonald, Alan (1985), *Introduction to Fluid Mechanics*, Third Edition, Wiley and Sons, New York (Fifth Edition, 1998).
- Frass, A.(1989), *Heat Exchanger Design*, Second edition, Wiley & Sons, Toronto.
- Grosse-Gorgemann, A., Weber, D., and Fiebig, M. (1995), "Experimental and Numerical Investigation of Self-Sustained Oscillations in Channels with Periodic Structures", *Experimental Thermal and Fluid Science*, Vol. 11, 226-233.
- Hachemi, A. (1999), "Experimental Study of Thermal Performance of Offset Rectangular Plate Fin Absorber-plates", *Renewable Energy*, Vol. 17, pp. 371-384.
- Hesselgreaves, J.E. (2001), *Compact Heat Exchangers: Selection, Design, and Operation*, Pergamon, New York.
- Hinze, J.O. (1975), *Turbulence*, McGraw-Hill, New York.
- Hu, S. and Herold, K.E. (1995a), "Prandtl Number Effect on Offset Fin Heat Exchanger Performance: Predictive Model for Heat Transfer and Pressure Drop", *International Journal of Heat and Mass Transfer*, Vol. 38, pp. 1043-1051.

Hu, S. and Herold, K.E. (1995b), "Prandtl Number Effect on Offset Fin Heat Exchanger Performance: Experimental Results", *International Journal of Heat and Mass Transfer*, Vol. 38, pp. 1053-1061.

*Hughes-Treitler website: <http://www.hughes-treitler.com/HXConstruct.htm>*

Incropera, F.P., and DeWitt, D.P. (2002), *Fundamentals of Heat and Mass Transfer*, Fifth Edition, Wiley and Sons, New York.

Jambunathan, K., Edwards, R.J., and Button, B.L. (1987), "Convective Heat-Transfer Coefficients: The Colour-Change Paint Technique", *Applied Energy*, Vol. 28, pp. 137-152.

Joshi, H.M. and Webb, R. (1987), "Heat Transfer and Friction in the Offset Strip-Fin Heat Exchanger", *International Journal of Heat and Mass Transfer*, Vol. 30, pp. 69-84.

Joyner, U.T. (1943), "Experimental Investigation of Entrance Region Heat Transfer Coefficients", NACA ARR 3K01.

Kakac, S. and Liu, H. (2002), *Heat Exchangers: Selection, Rating, and Thermal Design*, CRC Press, Boca Raton, Florida, Second Edition.

Kays, W.M. (1972), "Compact Heat Exchangers", *AGARD Lecture Series*, No.57 on Heat Exchangers, AGARD-LS-57-72, NATO, pp. 1-22.

Kays, W.M. and London, A.L. (1964), *Compact Heat Exchangers*, Second Edition, McGraw-Hill, New York (Third Edition, 1984).

Kays, W.M. and Crawford, M.E. (1993), *Convective Heat and Mass Transfer*, McGraw-Hill, New York, Third Edition.

Kays, W.M., and Perkins, H.C. (1985), *Handbook of Heat Transfer Fundamentals*, edited by W. M. Rohsenow, J. P. Hartnett and E. N. Ganic., McGraw Hill, New York.

Kelkar, K.M., and Patankar, S.V. (1989), "Numerical Prediction of Heat Transfer and Fluid Flow in Rectangular Offset-Fin Arrays", *Numerical Heat Transfer A*, Vol. 15, pp. 149-164.

Kilicastalian, I. and Sarac, H.I. (1998), "Enhancement of Heat Transfer in Compact Heat Exchanger by Different Type of Rib with Holographic Interferometry", *Experimental Thermal and Fluid Science*, Vol. 17, pp. 339-346.

Lamoureux, A., Camargo, L., and Baliga, B.R., "Strouhal Numbers and Power Spectrums for Turbulent Fully-Developed Flows in Rectangular Ducts with Spatially-Periodic Interrupted-Plate Inserts", Proc. Fifth International Conference on Enhanced, Compact

and Ultra-Compact Heat Exchangers: Science, Engineering and Technology, pp. 1-8, Whistler, British Columbia, Canada, September 11-16, 2005.

Landau, L.D. and Lifshitz, E.M. (1959), "Fluid Mechanics", translated from the Russian by J.B. Sykes and W.H. Reid, Pergamon Press, Oxford (Second Edition, 1987).

Launder, B.E. and Sandham, N.D. (2002), Closure Strategies for Turbulent and Transitional Flow, Cambridge University Press, Cambridge, U.K.

Lee, B.K. and Kwon, Y.K. (1992), "Flow and thermal field with relevance to heat transfer enhancement of interrupted-plate heat exchangers", *Experimental Heat Transfer*, Vol. 5, pp. 83-100.

London, A.L. (1983), "Compact Heat Exchangers – Design Methodology", *Low Reynolds Number Flow Heat Exchangers*, edited by Kakaç, S., Shah, R.K. and Bergles, A.E., Hemisphere Publishing Corporation, New York.

London, A.L. and Shah, R.K. (1968), "Offset Rectangular Plate-Fin Surfaces – Heat Transfer and Flow Friction Characteristics," *ASME Journal of Engineering for Power*, Vol. 90, pp. 218-228.

Lyman, A.C., Stephan, R.A., Thole, K.A., Zhang, L.W., and Memory, S.B. (2002), "Scaling of Heat Transfer Coefficients along Louvered Fins", *Experimental Thermal and Fluid Science*, Vol. 26, pp. 547-563.

Manglik, R.M. and Bergles, A. (1995), "Heat Transfer and Pressure Drop Correlations for the Rectangular Offset Strip Fin Compact Heat Exchanger", *Experimental Thermal and Fluid Science*, Vol. 10, pp. 171-180.

McBrien, R.K. (1986), "Pressure Measurements for Periodic Fully Developed Turbulent Flow in Rectangular Interrupted-Plate Ducts.", *M.Eng. Thesis*, Department of Mechanical Engineering, McGill University, Montréal, Canada.

McBrien, R.K. and Baliga, B.R. (1988), "Module Friction Factors and Intramodular Pressure Distributions for Periodic Fully Developed Turbulent Flow in Rectangular Interrupted-Plate Ducts", *ASME Journal of Fluids Engineering*, Vol. 110, pp. 147-154.

McBrien, R.K. (1989), "Fully Developed Turbulent Flow in Rectangular Interrupted-Plate Ducts", *Doctoral Thesis*, Department of Mechanical Engineering, McGill University, Montréal, Canada.

McDonald, C.F (1972), "Gas Turbine Recuperator Technology Advancements", *ASME Gas Turbine and Fluids Engineering and Products Show*, Paper No. 72-GT-32, San Francisco, March 26-30.

- McDonald, C.F. (2000), "Low-Cost Recuperator Concept for Microturbine Applications", *Proceedings of ASME TURBOEXPO 2000*, Paper No. 2000-GT-167, Munich, Germany, May 8-11.
- McDonald, C.F. (2003), "Recuperator Considerations for Future Higher Efficiency Microturbines", *Applied Thermal Engineering*, Vol. 23, Aug. 2003, pp. 1463-87.
- Michna, G. J., Jacobi, A. M., and Burton, R. L. (2005), "Air-Side Thermal-Hydraulic Performance of an Offset-Strip Fin Array at Reynolds Numbers up to 120,000," *Proceedings of the 5th International Conference on Enhanced, Compact and Ultra-Compact Heat Exchangers*, Whistler, British Columbia, Canada.
- Minkowycz, W.J., Sparrow, E.M., and Murthy, J.Y., and Pletcher, R.H., editors (2006), *Handbook of Numerical Heat Transfer*, Wiley and Sons, New York.
- Minkowycz, W.J. and Sparrow, E.M., editors (1997), *Advances in Numerical Heat Transfer, Vol. 1*, Taylor and Francis, Washington D.C.
- Minkowycz, W.J. and Sparrow, E.M., editors (2000), *Advances in Numerical Heat Transfer, Vol. 2*, Taylor and Francis, Washington D.C.
- Mochizuki, S. and Yagi, Y. (1987), "Transport Phenomena in Stacks of Interrupted Parallel-Plate Surfaces", *Experimental Heat Transfer*, Vol. 1, pp. 127-140.
- Mochizuki, S., Yagi, Y., and Yang, W.J. (1988), "Flow Pattern and Turbulence Intensity in Stacks of Interrupted Parallel-Plate Surfaces", *Experimental Thermal and Fluid Science*, Vol. 1, pp. 51-57.
- Moffat, R.J. (1985), "Using Uncertainty Analysis in the Planning of an Experiment", *ASME Journal of Fluids Engineering*, Vol. 107, pp. 173-182.
- Mukherjee, R. (2004), *Practical Thermal Design of Shell-and-Tube Heat Exchangers*, Begell House, New York.
- Mullisen, R.S. and Loehrke, R.I. (1986), "A Study of the Flow Mechanisms Responsible for Heat Transfer Enhancement in Interrupted-Plate Heat Exchangers", *ASME Journal of Heat Transfer*, Vol. 108, pp. 377-385.
- Muzychka, Y.S. and Yovanovich, M.M. (2001), "Modelling the f and j Characteristics of the Offset Strip Fin Array", *Journal of Enhanced Heat Transfer*, Vol. 8, pp. 261-277.
- Naylor, D. (2003), "Recent Developments in the Measurement of Convective Heat Transfer Rates by Laser Interferometry", *International Journal of Heat and Fluid Flow*, Vol. 24, pp. 345-355.

Okajima, A. (1982), "Strouhal Numbers of Rectangular Cylinders", *Journal of Fluid Mechanics*, Vol. 123, pp. 379-398.

Olsson, C.O. and Sunden, B. (1998), "Thermal and Hydraulic Performance of a Rectangular Duct with Multiple V-Shaped Ribs", *ASME Journal of Heat Transfer*, Vol. 120, pp. 1072-1077.

Panton, R.L. (1996), *Incompressible Flow*, Second Edition, J. Wiley, New York.

Patankar, S.V. (1980), *Numerical Heat Transfer and Fluid Flow*, McGraw-Hill, New York.

Patankar, S.V., Liu, C.H., and Sparrow, E.M. (1977), "Fully Developed Flow and Heat Transfer in Ducts Having Streamwise-Periodic Variations of Cross-Sectional Area", *ASME Journal of Heat Transfer*, Vol. 99, pp. 180-186.

Patankar, S.V. and Prakash, C. (1981), "An Analysis of the Effect of Plate Thickness on Laminar Flow and Heat Transfer in Interrupted-Plate Passages", *International Journal of Heat and Mass Transfer*, Vol. 24, pp. 1801-1810.

Pope, S.B. (2000), *Turbulent Flows*, Cambridge University Press, New York.

Ranganayakulu, Ch., Seetharamu, K.N and Sreevatsan, K.V. (1997), "The Effects of Longitudinal Heat Conduction in Compact Plate-Fin and Tube-Fin Heat Exchangers Using a Finite Element Method", *International Journal of Heat and Mass Transfer*, Vol. 40, pp. 1261-1277.

Reay, D.A., (2002), "Compact Heat Exchangers, Enhancement and Heat Pumps", *International Journal of Refrigeration*, Vol. 25, pp. 460-470.

Reddy, J.N. and Gartling, D.K. (1994), *The Finite Element Method in Heat Transfer and Fluid Dynamics*, CRC Press, Boca Ratón, Florida.

Roache, P.J., (1976), *Computational Fluid Dynamics*, Hermosa Publishers, Albuquerque, New Mexico.

Roache, P.J., (1998), *Fundamentals of Computational Fluid Dynamics*, Hermosa Publishers, Albuquerque, New Mexico.

Roadman, R.E. and Loehrke, R.I., (1983), "Low Reynolds Number Flow Between Interrupted Flat Plates", *ASME Journal of Heat Transfer*, Vol. 105, pp. 166-171.

Rouse, H. (1946), *Elementary Mechanics of Fluids*, Dover Publications Inc., New York, (Second Edition, 1978).

Saidi, A. and Sunden, B. (2001), "A Numerical Investigation of Heat Transfer Enhancement in Offset Strip Fin Heat Exchangers in Self-Sustained Oscillatory Flows", *International Journal of Numerical Methods for Heat and Fluid Flow*, Vol. 11, pp. 699-716.

Sara, O.N., Pekdemir, T., Yapici, S., and Yilmaz, M. (2001), "Heat-Transfer Enhancement in a Channel Flow with Perforated Rectangular Blocks", *International Journal of Heat and Fluid Flow*, Vol. 22, pp. 509-518.

Saunders, E.A.D. (1988), *Heat Exchangers: Selection, Design and Construction*, John Wiley and Sons, New York.

Schlichting, H. (1955), *Boundary Layer Theory (Translation of "Grenzschicht Theorie" by J. Kestin)*, McGraw Hill, New York (Second Edition, 1968; Third Edition, 1979).

Sebben, S. (1996), "Temporally and Spatially Periodic Flows in Interrupted-Plate Rectangular Ducts", *Ph.D. Thesis*, Department of Mechanical Engineering, McGill University, Montréal, Canada.

Sekulic, D. (1989), "Flow through Communicating Channels Compact Heat Transfer Geometry", *International Communications in Heat and Mass Transfer*, Vol. 16, pp. 667-679.

Shah, R.K. and London, A.L. (1978), *Laminar Flow Forced Convection in Ducts*, Advances in Heat Transfer, Supplement 1, Academic Press, New York.

Shah, R.K., Heikal, M.R., Thonon, B., and Tochon P. (2001), "Progress in the Numerical Analysis of Compact Heat Exchanger Surfaces", *Advances in Heat Transfer*, Vol. 34, pp. 363-443.

Sparrow, E.M., Baliga, B.R., and Patankar, S.V. (1977), "Heat Transfer and Fluid Flow Analysis of Interrupted-Wall Channels, with Application to Heat Exchangers", *ASME Journal of Heat Transfer*, Vol. 99, pp. 4-11.

Sparrow, E.M. and Liu, C.H. (1979), "Heat Transfer, Pressure Drop and Performance Relationships for In-Line, Staggered, and Continuous Plate Heat-Exchangers", *International Journal of Heat and Mass Transfer*, Vol. 22, pp. 1613-1625.

Sparrow, E.M. and Hajiloo, A. (1980), "Measurements of Heat Transfer and Pressure Drop for an Array of Staggered Plates Aligned Parallel to an Air Flow", *ASME Journal of Heat Transfer*, Vol. 102, pp. 426-432.

Streeter, V.L (1951), *Fluid mechanics*, McGraw Hill, Boston (Third Edition, 1962).

Suzuki, K., Hirai, E., Miyake, T., and Sato, T. (1985), "Numerical and Experimental Studies on a Two-Dimensional Model of an Offset-Strip-Fin Type Compact Heat

Exchanger used at Low Reynolds Number”, *International Journal of Heat and Mass Transfer*, Vol. 28, pp. 823-836.

Suzuki, K., Xi, G.N., Inaoka, K., and Hagiwara, Y. (1994), “Mechanism of Heat Transfer Enhancement Due to Self-Sustained Oscillation for an In-line Fin Array”, *International Journal of Heat and Mass Transfer*, Vol. 37, Suppl. 1, pp. 83-96.

Tennekes, H. and Lumley, J.L. (1972), *A First Course in Turbulence*, MIT Press, Cambridge, Mass.

Timmerhaus, K. D. and Flynn, T. M. (1989), *Cryogenic Process Engineering*, Plenum Press, New York.

Tinaut, F.V., Melgar, A., and Rahman Ali, A.A. (1992), “Correlations for Heat Exchanger and Flow Friction Characteristics of Compact Plate-Type Heat Exchangers”, *International Journal of Heat and Mass Transfer*, Vol. 35, pp. 1659-1665.

Valencia, A. (1999), “Heat Transfer Enhancement Due to Self-Sustained Oscillating Transverser Vortices in Channels with Periodically Mounted Rectangular Bars”, *International Journal of Heat and Mass Transfer*, Vol. 42, pp. 2053-2062.

Walter, F.M. (1969), “Hypersonic Research Engine Project – Phase IIA, Category I Test Report on Fin Heat Transfer and Pressure Drop Testing”, Data Item No. 63.02, AiResearch Manufacturing Co., Doc. AP-69-5348.

Wang, L.B., Jiang, G.D., Tao, W.Q., and Ozoe, H. (1998), “Numerical Simulation on Heat Transfer and Fluid Flow Characteristics of Arrays with Nonuniform Plate Length Positioned Obliquely to the Flow Direction”, *ASME Journal of Heat Transfer*, Vol. 120, pp. 991-998.

Wang, L.B., Tao, W.Q., Wang, Q.W., and Wong, T.T. (2001), “Experimental Study of Developing Turbulent Flow and Heat Transfer in Ribbed Convergent/Divergent Square Duct”, *International Journal of Heat and Fluid Flow*, Vol. 22, pp. 603-613.

Webb, R.L., and Joshi, H.M. (1982), “Friction Factor Correlation for the Offset Strip-Fin Matrix”, Heat Transfer, Proceedings of the International Heat Transfer Conference, pp. 257-262.

White, F.M. (1974), *Viscous Fluid Flow*, Second Edition, McGraw-Hill, New York (Second Edition, 1991).

White, F.M. (1979), *Fluid Mechanics*, Fourth Edition, McGraw-Hill, New York (Fifth Edition, 2003).

Wieting, A.R (1975), “Empirical Correlations for Heat Transfer and Flow Friction Characteristics of Rectangular Offset-Fin Plate-Fin Heat Exchangers”, *ASME Journal of Heat Transfer*, Vol. 97, pp. 488-490.

Wilcox, D. (1993), *Turbulence Modeling for CFD*, DCW Industries, La Cañada, California.

Wilkes, J.O. (1999), *Fluid Mechanics for Chemical Engineers*, Prentice Hall, Upper Saddle River, New Jersey.

Winternitz, F.A.L. and Fischl, C.F. (1957), "A Simplified Integration Technique for Pipe-Flow Measurement", *Water Power*, pp. 225-234.

Zelenka, R.L. and Loehrke, R.I. (1983), "Heat Transfer from Interrupted Plates", *ASME Journal of Heat Transfer*-, Vol. 105, pp. 172-177.

Zhang, L.W., Balachandar, S., Tafti, D.K., and Najjar, F.M. (1997), "Heat Transfer Enhancement Mechanisms in Inline and Staggered Parallel-Plate Fin Heat Exchangers", *International Journal of Heat and Mass Transfer*, Vol. 40, pp. 2307-2325.

# Appendices

## Appendix A

### Correlation for the Time-Mean Average Velocity

In this appendix, details of a correlation for determining the time-mean average velocity in the flow-measurement section of the experimental rig (see Figure 4.1), based on the measurement of the dynamic pressure at just point in a selected cross-section, is presented.

Winternitz and Fischl (1957) have provided a ten-point log-linear method for the determination of the time-mean average velocity in steady, incompressible, turbulent flow in a straight pipe of circular cross-section, based on the measurement of the dynamic pressure at 10 specified points in the pipe cross-section. Their method is based on the assumption that outside the laminar sublayer, the distribution along the diameter of the pipe of the time-mean axial velocity,  $W$ , can be represented by the following equation:

$$W = C + N \log(y^*/D) + M(y^*/D) \quad (\text{A.1})$$

where  $y^*$  is the distance from the wall of the pipe along a diameter;  $D$  is the inside diameter of the pipe; and  $C$ ,  $N$ , and  $M$  are constants which have dimensions of velocity. The cross-section of the flow tube is divided into four annular zones and one central circular zone, all of equal area. The ten measuring point ( $y^*$ ) are the positions at which the exact mean zone velocity occurs if the velocity distribution can be adequately represented by equation (A.1). The  $y^*$  coordinates of these measuring points are given by:

$$\begin{array}{ll} y_1^* = 0.019D & y_6^* = 0.639D \\ y_2^* = 0.077D & y_7^* = 0.783D \\ y_3^* = 0.153D & y_8^* = 0.847D \\ y_4^* = 0.217D & y_9^* = 0.924D \\ y_5^* = 0.361D & y_{10}^* = 0.981D \end{array} \quad (\text{A.2})$$

The average value of  $W$  in the cross-section of the flow tube is obtained by taking the arithmetic mean of its individual values measured at the ten  $y^*$  locations.

Winternitz and Fischl (1957) conducted an extensive study of log-linear methods and concluded that the ten-point log-linear traverse resulted in a mean-square error of about

0.5% for the flows that they investigated. Based on a review of their work, the ten-point log-linear method is expected to give similar accuracy for the flows investigated in this work.

In this work, an extension of the method of Winternitz and Fischl (1957) is proposed. This method works well for particular flow-measurement tubes and specific range of flow rates. It was fined-tuned and employed for the experiments undertaken in this investigation. In this method, first, the average value of  $\bar{W}$  was determined using the ten-point log-linear method of Winternitz and Fischl (1957) for duct Reynolds numbers, using the definition of Patankar and Prakash (1981), in the range 5, 000-24, 000 (nominal); and then a correlation that relates this average value to the value of  $W$  (obtained from the measurement of the corresponding dynamic pressure) at a single specified point in the cross-section was developed. In this work, Point number 5 (see equation A.2) was chosen (arbitrarily) as the single specific point. In all, flow rates corresponding to 17 different values of the duct Reynolds number in the aforementioned range of interest were used to develop and validate the proposed correlation. The following least-squares linear curve fit correlated the data very well:

$$\bar{W} = 9.182185548544E-01 * W_{y_5} - 2.229435234298E-01 \quad (\text{A.3})$$

Figure A.1 and Table A.1 shows the results.

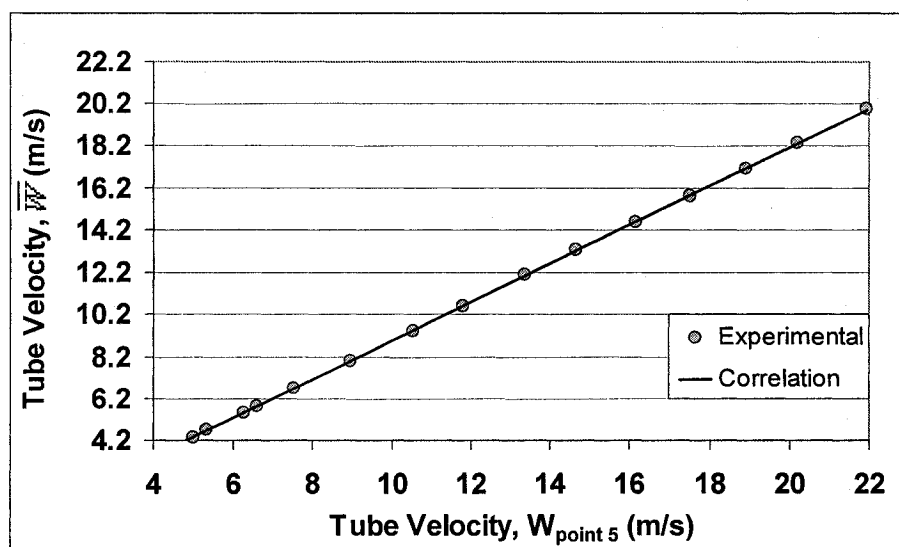


Figure A.1: Plot of  $\bar{W}$ , obtained using the ten-point log-linear method versus  $W_{\text{point 5}}$ .

Table A.1: Comparison of the  $\overline{W}_{10\text{-pointlog-linear}}$  and  $\overline{W}_{correl}$ .

Duct Re	$(2*\Delta P/\rho)^{1/2}$ at point 5	Tube Velocity (m/s)		% Error
		10-point log-linear rule	correlation	
5157.938	4.98	4.34	4.35	-0.233%
4741.914	4.57	3.99	3.97	0.315%
5614.511	5.34	4.69	4.68	0.353%
6584.131	6.27	5.52	5.53	-0.259%
7064.827	6.60	5.83	5.84	-0.072%
8075.449	7.52	6.69	6.68	0.185%
9641.901	8.94	8.00	7.98	0.189%
11357.56	10.53	9.44	9.45	-0.097%
12728.28	11.82	10.61	10.63	-0.218%
14396.85	13.37	12.05	12.05	0.022%
15773.45	14.65	13.25	13.23	0.116%
17346.71	16.17	14.60	14.62	-0.181%
19275.86	17.51	15.84	15.85	-0.082%
20854.89	18.91	17.13	17.14	-0.024%
22144.12	20.22	18.36	18.34	0.120%
24022.76	21.95	19.94	19.93	0.053%
15996.24	15.03	13.56	13.58	-0.143%

The error incurred in determining the average velocity using this above-mentioned correlation with  $W_{point\ 5}$ , obtained from just one measurement of the dynamic pressure at Point 5, as the input, with respect to average velocity obtained using the ten-point log-linear rule is defined as follows:

$$\% \text{ Error} = 100 \times \left( \left| \overline{W}_{10\text{-pointlog-linear}} - \overline{W}_{correl} \right| / \overline{W}_{10\text{-pointlog-linear}} \right) \quad (\text{A.4})$$

The average and maximum values of this error were 0.157% and 0.353%, respectively. Based on these results, it was decided to use the one-point measurement and the above-mentioned correlation to obtain the average velocity in all of the final experimental runs. This led to considerable reductions in the time that is needed to run each experiment. Thus, it was possible to undertake more experiments, with more care.

## **Appendix B**

### **Thermocouple Calibration**

In this appendix, the experimental procedure for the calibration of the thermocouples used in this work is described and the results obtained are presented. Twenty-three prefabricated chromel-constantan thermocouples (type E; AWG-36) from Omega were used in this work. These thermocouples were calibrated in the temperature range 5°C – 75°C in a constant-temperature water bath (Neslab RTE 221). The uncertainties in the temperature readings provided by the calibrated thermocouples were determined to be all less than  $\pm 0.02^\circ\text{C}$ .

The readings provided by a quartz thermometer (HP 2804 A) with a quartz probe (HP 18111 A / 2120A; 232 mm long) precisely calibrated ( $\pm 0.01^\circ\text{C}$ ) at the National Research Council Canada (NRC), in Ottawa, were used as reference values for the temperature measurements in this calibration procedure. A cylindrical block made of copper (7.5 cm diameter and 6.35 cm long), with one blind hole of 12.7 mm diameter at its center and eighty blind holes of 3.2 mm diameter radially distributed uniformly around the center, was used to hold the thermocouples and the quartz probe together. This assembly was submerged completely and rested on an empty upside down glass beaker at the center of the reservoir of the above-mentioned constant-temperature bath. With this set-up, the thermocouple beads and the quartz probe could be assumed to be essentially at the same temperature. A data acquisition control unit (HP 3497 A) was used to measure the temperatures. A personal computer was to record the thermocouple and quartz probe outputs, using a program written using VEE (software application program produced and marketed by Agilent Technologies). This program displays and records (saves) all the temperature readings in real-time.

The calibration procedure consists of the following steps:

1. All measurement systems and the PC are turned on (powered) at least two hours before starting the calibration procedure, to allow the electronic circuits to warm up and stabilize;
2. The constant-temperature water bath is turned on and set to the desired temperature (the initial set temperature is 5°C);

3. Readings of all data are then started and recorded, at time intervals of about 3 minutes;
4. The temperatures are monitored on the PC screen;
5. Once the difference in any two consecutive readings from the quartz probe becomes  $\leq 0.01^\circ\text{C}$  over an overall sampling period of 10 minutes, steady-state conditions are assumed to prevail, and data is acquired and saved on the hard disk of the PC for a period of 10 minutes, with a sampling time interval of about 6 seconds;
6. For each thermocouple, the temperature readings saved during this last 10-minute period are averaged and compared with the average of the temperature readings provided by the quartz probe during the same period of time;
7. The set temperature of the bath is increased by  $5^\circ\text{C}$  (nominal), and steps 3 to 6 are repeated; and this overall procedure is continued until the set temperature reaches  $75^\circ\text{C}$  (nominal);
8. For each thermocouple, the averaged temperature obtained during these measurements is plotted against the corresponding averaged temperature measured by the quartz probe. An example of such a plot is presented in Figure B.1;
9. Third-, fourth-, and fifth-order polynomials are then fitted to the calibration data for each thermocouple, using the least-squares procedure. These correlations have the following general form:

$$T_j = \sum_{i=0}^P b_{i,j} T_{read,j} \quad (P = 3, 4, \text{ and } 5) \quad (\text{B.1})$$

where  $T_{read,j}$  is the temperature read for thermocouple  $j$ ,  $T_j$  is the corresponding corrected temperature (in  $^\circ\text{C}$ ), and  $b_{i,j}$  are the coefficients in the polynomials. In this work, using the three correlations obtained from equation (B.1) for each thermocouple, the temperature data were reproduced and compared with the quartz probe readings: the best calibration correlation was found to be the fifth-order polynomial in all cases. Table B.1 presents the fifth-order polynomial correlations for each of the thermocouples ( $j = 1$  to 23).

10. The uncertainties in the temperature readings provided by the selected calibrated thermocouples were found to be all less than  $\pm 0.02^\circ\text{C}$ .

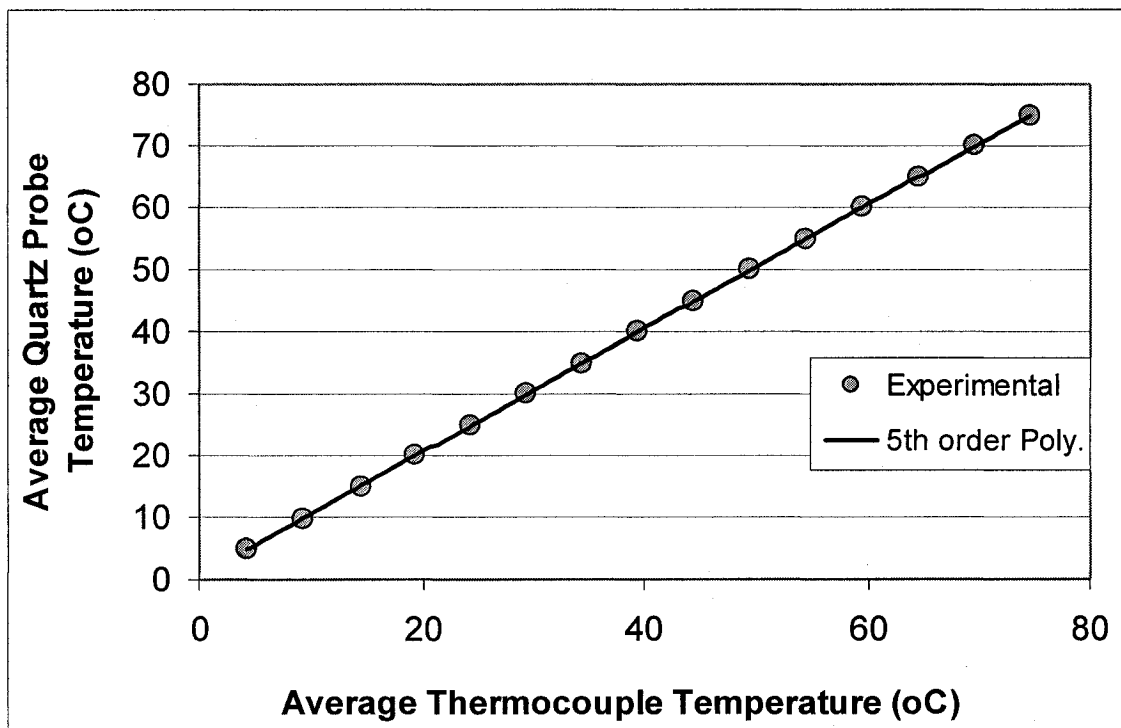


Figure B.1: Plot of the temperature reading provided by the quartz probe versus the temperature reading provided by thermocouple # 1.

Table B.1: Coefficients in the fifth-order polynomial calibration correlations for thermocouples 1 – 23.

TC	$b_0$	$b_1$	$b_2$	$b_3$	$b_4$	$b_5$
1	1.7803E-09	-3.3498E-07	2.4287E-05	-8.7706E-04	1.0131E+00	4.7929E-01
2	1.7123E-09	-3.2790E-07	2.4052E-05	-8.6993E-04	1.0128E+00	3.7764E-01
3	1.7123E-09	-3.2790E-07	2.4052E-05	-8.6993E-04	1.0128E+00	3.7764E-01
4	1.4069E-09	-2.8118E-07	2.1723E-05	-8.2501E-04	1.0128E+00	2.5134E-01
5	1.7654E-09	-3.4924E-07	2.6012E-05	-9.2090E-04	1.0129E+00	1.5635E-01
6	1.9417E-09	-3.8383E-07	2.8227E-05	-9.7031E-04	1.0133E+00	4.8677E-02
7	2.2702E-09	-4.4582E-07	3.2423E-05	-1.0982E-03	1.0158E+00	6.6570E-02
8	2.2442E-09	-4.4295E-07	3.2305E-05	-1.0899E-03	1.0146E+00	4.7012E-02
9	2.2220E-09	-4.3704E-07	3.1773E-05	-1.0687E-03	1.0142E+00	2.5224E-02
10	2.2042E-09	-4.3737E-07	3.2046E-05	-1.0854E-03	1.0148E+00	5.7357E-02
11	1.8961E-09	-3.8238E-07	2.8717E-05	-1.0030E-03	1.0137E+00	9.7043E-02
12	2.1359E-09	-4.2567E-07	3.1267E-05	-1.0541E-03	1.0140E+00	1.4521E-03
13	1.8921E-09	-3.7558E-07	2.7501E-05	-9.2778E-04	1.0126E+00	9.2639E-02
14	2.0598E-09	-4.0761E-07	2.9675E-05	-9.9138E-04	1.0127E+00	1.1776E-01
15	1.9102E-09	-3.7769E-07	2.7412E-05	-9.0904E-04	1.0112E+00	1.3192E-01
16	1.9244E-09	-3.7959E-07	2.7750E-05	-9.4480E-04	1.0122E+00	2.3806E-01
17	1.0653E-09	-2.2335E-07	1.7783E-05	-6.7594E-04	1.0094E+00	2.9549E-01
18	1.5315E-09	-3.0108E-07	2.2064E-05	-7.6553E-04	1.0097E+00	4.3111E-01
19	1.4134E-09	-2.8782E-07	2.2092E-05	-8.0261E-04	1.0105E+00	4.9678E-01
20	9.7181E-10	-2.0685E-07	1.6900E-05	-6.5550E-04	1.0091E+00	5.5829E-01
21	3.5239E-09	-7.1039E-07	5.2169E-05	-1.7216E-03	1.0221E+00	-1.4962E-01
22	3.0960E-09	-6.3824E-07	4.7981E-05	-1.6196E-03	1.0207E+00	-1.9048E-01
23	2.7613E-09	-5.7079E-07	4.2943E-05	-1.4462E-03	1.0185E+00	-1.2341E-01

## Appendix C

### Radiation Effects

Table C.1: Average heat transfer coefficients obtained using two different temperature ranges.

Re	Range for Unsteady Analysis	Plate #	$h_{av}$ (W/m <sup>2</sup> K)	% Difference in $h_{av}$ values
2058.05	62°C - 28°C	1	37.55	0.32
	45°C - 30°C		37.68	
	62°C - 28°C	2	36.66	-0.07
	45°C - 30°C		36.63	
	62°C - 28°C	3	34.99	0.13
	45°C - 30°C		35.03	
	62°C - 28°C	4	35.68	0.26
	45°C - 30°C		35.77	
	62°C - 28°C	5	37.44	0.35
	45°C - 30°C		37.57	
	62°C - 28°C	6	37.81	0.20
	45°C - 30°C		37.88	
7964.01	62°C - 28°C	1	83.46	0.15
	45°C - 30°C		83.58	
	62°C - 28°C	2	84.35	0.44
	45°C - 30°C		84.72	
	62°C - 28°C	3	81.66	0.29
	45°C - 30°C		81.90	
	62°C - 28°C	4	84.97	-0.11
	45°C - 30°C		84.87	
	62°C - 28°C	5	83.43	0.26
	45°C - 30°C		83.65	
	62°C - 28°C	6	86.08	-0.08
	45°C - 30°C		86.00	
29282.11	62°C - 28°C	1	211.00	0.36
	45°C - 30°C		211.77	
	62°C - 28°C	2	217.57	-0.03
	45°C - 30°C		217.52	
	62°C - 28°C	3	207.37	-0.27
	45°C - 30°C		206.82	
	62°C - 28°C	4	219.41	0.21
	45°C - 30°C		219.88	
	62°C - 28°C	5	217.08	0.12
	45°C - 30°C		217.33	
	62°C - 28°C	6	217.48	0.03
	45°C - 30°C		217.56	

## Appendix D

### Repeatability Checks

Table D.1: Repeatability checks conducted at Re nominal = 2 000; 8 000; and 30 000.

Re_avg	Repeatability Run#	Plate #	$h_{av}$ (W/m <sup>2</sup> K)	% Difference in $h_{av}$ values
2058.05	1	1	37.68	-1.00
	2		37.30	
	1	2	37.46	-2.21
	2		36.63	
	1	3	35.03	-3.02
	2		33.98	
	1	4	35.77	1.79
	2		36.41	
	1	5	37.52	0.14
	2		37.57	
	1	6	37.52	0.97
	2		37.88	
7964.01	1	1	83.58	-0.77
	2		82.94	
	1	2	84.14	0.68
	2		84.72	
	1	3	81.90	0.64
	2		82.42	
	1	4	83.51	1.64
	2		84.87	
	1	5	86.04	-2.78
	2		83.65	
	1	6	86.00	0.36
	2		86.32	
29282.11	1	1	211.77	-1.13
	2		209.38	
	1	2	217.52	-1.65
	2		213.92	
	1	3	206.82	3.43
	2		213.91	
	1	4	219.88	-2.82
	2		213.69	
	1	5	217.33	-0.71
	2		215.78	
	1	6	217.56	-0.04
	2		217.48	

## Appendix E

### Average Heat Transfer Coefficients: Inputs and Results

Table E.1: Geometry of the test section.

b (mm)	2H (mm)	L (mm)	2t (mm)	s (mm)
152.67	25.18	25.21	6.36	25.59

$D_h$ (mm)	$\lambda =$ b/2H	$L^* =$ L/2H	$t^* =$ 2t/2H	$s^* =$ s/2H
21.32	6.063	1.001	0.252	1.004

Table E.2: Effective values of (Mass \* Specific Heat).

#### Plate 1 - Brass

	m (g)	cp (J/g-°C)
Metal plate	97.706	0.380
Screws	0.450	0.461
Pins	0.074	0.461
sum(m*cp)	37.880	

#### Plate 3 - Al

	m (g)	cp (J/g-°C)
Metal plate	31.001	0.875
Screws	0.434	0.461
Pins	0.074	0.461
sum(m*cp)	27.870	

#### Plate 5 - Copper

	m (g)	cp (J/g-°C)
Metal plate	103.220	0.385
Screws	0.430	0.461
Pins	0.074	0.461
sum(m*cp)	40.482	

#### Plate 2 - Brass

	m (g)	cp (J/g-°C)
Metal plate	97.853	0.380
Screws	0.432	0.461
Pins	0.074	0.461
sum(m*cp)	37.927	

#### Plate 4 - Al

	m (g)	cp (J/g-°C)
Metal plate	31.149	0.875
Screws	0.436	0.461
Pins	0.074	0.461
sum(m*cp)	28.001	

#### Plate 6 - Copper

	m (g)	cp (J/g-°C)
Metal plate	102.598	0.385
Screws	0.436	0.461
Pins	0.074	0.461
sum(m*cp)	40.245	

#### Paste

$A_{c.s.}$ (cm <sup>2</sup> )	0.013
Length (cm)	16.203
Vol. (cc)	0.204
rho (g/cc)	2.530
m (g)	0.517
cp_silicone(J/g-oC)	1.967
cp_paste(J/g-oC)	0.987
m*cp	0.510

#### Neglected

	m (g)	cp (J/g-°C)
Ni wire	0.132	0.444
Insl.	0.235	0.840
TC		

length of fiberglass and heating wire (in)  
11.535433



## Appendix F

### Average Nusselt Number: Inputs and Results

Table F.1: Average Nusselt number for test plates 2, 4, and 5.

Re ↓	Plate →	2	4	5
3057.02	$T_{\text{air}}$	297.7478	298.0205	297.9861
	$k_{\text{air}}$	0.02590	0.02592	0.02592
	$h$	47.10426	45.42118	46.75089
	$NU_{\text{av}}$	38.772	37.358	38.455
4137.991	$T_{\text{air}}$	298.1048	298.2349	298.2108
	$k_{\text{air}}$	0.02593	0.02594	0.02594
	$h$	54.44713	54.62899	55.14609
	$NU_{\text{av}}$	44.771	44.904	45.332
4962.283	$T_{\text{air}}$	298.0114	298.3731	298.0509
	$k_{\text{air}}$	0.02592	0.02595	0.02592
	$h$	62.10139	61.71009	61.34673
	$NU_{\text{av}}$	51.078	50.704	50.452
5946.362	$T_{\text{air}}$	298.3652	298.6404	298.9101
	$k_{\text{air}}$	0.02595	0.02597	0.02599
	$h$	70.16257	69.65767	69.90802
	$NU_{\text{av}}$	57.651	57.191	57.353
10135.61	$T_{\text{air}}$	297.6802	298.0655	298.3395
	$k_{\text{air}}$	0.02590	0.02593	0.02595
	$h$	99.60717	100.8168	101.3625
	$NU_{\text{av}}$	82.004	82.909	83.293
19799.41	$T_{\text{air}}$	298.9747	299.2131	299.1825
	$k_{\text{air}}$	0.02599	0.02601	0.02601
	$h$	161.3281	165.0979	161.7792
	$NU_{\text{av}}$	132.330	135.331	132.622

Table F.2: Average Nusselt number for test plates 1 – 6.

Re ↓	Plate →	1	1_R	2	2_R	3	3_R	4	4_R	5	5_R	6	6_R
2058.053	$T_{air}$	298.7899	299.0088	298.9697	299.1944	298.8824	298.9217	298.9629	298.6147	299.2777	298.6953	299.3405	298.9793
	$k_{air}$	0.02598	0.02599	0.02599	0.02601	0.02599	0.02599	0.02599	0.02597	0.02601	0.02597	0.02602	0.02599
	$h$	37.67569	37.29948	37.45806	36.62879	35.03373	33.97659	35.76806	36.40719	37.51951	37.57314	37.51951	37.88274
	$Nu_{av}$	30.920	30.592	30.726	30.026	28.744	27.874	29.340	29.894	30.749	30.844	30.744	31.073
7964.013	$T_{air}$	298.8299	299.2631	298.597	299.2844	298.5531	299.3635	298.5581	299.6906	299.0773	299.5403	298.3929	298.4905
	$k_{air}$	0.02598	0.02601	0.02596	0.02601	0.02596	0.02602	0.02596	0.02604	0.02600	0.02603	0.02595	0.02596
	$h$	83.58433	82.94113	84.14422	84.71776	81.89629	82.41971	83.5054	84.87271	86.03976	83.64615	86.00433	86.31506
	$Nu_{av}$	68.588	67.977	69.093	69.429	67.256	67.531	68.576	69.477	70.554	68.502	70.662	70.897
29282.11	$T_{air}$	299.1525	299.1178	299.1759	298.9299	298.7299	299.0472	299.8739	299.6552	299.6517	299.6258	299.2791	299.591
	$k_{air}$	0.02601	0.02600	0.02601	0.02599	0.02597	0.02600	0.02606	0.02604	0.02604	0.02604	0.02601	0.02604
	$h$	211.765	209.3801	217.515	213.9216	206.8195	213.9096	219.8825	213.6905	217.3317	215.7825	217.5587	217.4824
	$Nu_{av}$	173.614	171.675	178.316	175.492	169.762	175.424	179.902	174.944	177.927	176.671	178.300	178.080

Note: the “R” suffix denotes repeatability tests